Toward the Construction of a Vascularized, Hydrogel-Based Lymph Node Model for *In Vitro* and *In Vivo* Therapeutic Applications

A THESIS

SUBMITTED TO THE FACULTY OF THE

UNIVERSITY OF MINNESOTA

BY

Caleb Harff

IN PARTIAL FULFILLMENT OF THE REQUIREMENTS

FOR THE DEGREE OF

MASTER OF SCIENCE

Dr. Angela Panoskaltsis-Mortari, Adviser

April 2021

Acknowledgements

I am exceedingly grateful for my adviser, Dr. Angela Panoskaltsis-Mortari, without whose patience, direction, and expertise this research and report would not have been possible. I would like to thank my lab managers, Carolyn Meyer and Haylie Helms, for their advice and assistance with a wide variety of procedures and experiments. My colleagues Fanben Meng, Caleb Vogt, Ifeolu Akinnola, and Zachary Galliger provided me with a wealth of knowledge concerning various aspects of tissue engineering, and their insights contributed greatly to the progress of this research. Michael Ehrhardt of the Cytokine Reference Laboratory at the University of MN kindly performed multiple assays to provide me with important data on cytokines. The Visible Heart Laboratory at the University of MN graciously provided me with porcine lymph node tissue for decellularization and analysis. The laboratory of Dr. Brenda Ogle provided me with access to and training for their microplate reader. The laboratories of Dr. Jeffrey Miller, Dr. Bruce Blazar, and Dr. Keli Hippen, at the University of MN, each generously provided me with the central component of my research, peripheral blood mononuclear cells, at different stages of my research.

Abstract

Clinical trials for drugs and vaccines often suffer from the use of culture or animal models that do not accurately recreate the microenvironment of human tissues, including the lymph nodes. Furthermore, insufficient immune function resulting from genetic deficits, cancer or auto-immune disease, and the loss of lymph nodes due to surgical resection or radiation therapy may benefit from the implantation of therapeutic immune cells. These needs could be served through the development of a biocompatible, vascularized, 3D hydrogel scaffold that supports leukocytes and recreates lymph node function by providing a biomimetic microenvironment. While other lymph node models exist, their complexity and function are limited in that they incorporate few of the bioactive molecules from the lymph node microenvironment and do not contain vasculature.

Preliminary viability studies were performed to determine the optimal choice of hydrogel type and density for the 3D culture of peripheral blood mononuclear cells (PBMCs). Fibrin hydrogels were found to better maintain PBMC viability over three days compared to gelatin methacrylate hydrogels. The inclusion of ECM from decellularized porcine lymph nodes into fibrin hydrogels was met with technical challenges with regard to solubilization and peripheral blood cell (PBC) viability assessment, indicating that additional steps or different approaches were required. However, successful decellularization was demonstrated by the sufficient removal of DNA content as determined by DNA quantification and histological staining. Cytokine and growth factor analysis showed significant depletion of many of the analytes but retention of IFNα2, IL-3, IL-9, IL-13, IL-17A, and VEGF. To construct a perfusable model, pin molds were used to create channels that would undergo eventual endothelialization and angiogenesis. Few of these channels maintained structural integrity. While continued experimentation is required to implement all of the features desired for the construction of a biomimetic and functional human lymph node model, these results indicate that it is feasible to improve upon previous designs by incorporating decellularized ECM and introducing vascularization in fibrin hydrogels.

Table of Contents

List of Figures

List of Tables

1. Introduction

The purpose of the lymphoid system is to defend the body from pathogens while maintaining tolerance of the body's own tissues and avoiding adverse reactions to non-pathogenic external sources of antigens (i.e., commensal bacteria, food, etc.). The requisite functions for the achievement of this purpose are divided between different subsets of immune organs. The primary lymphoid organs, namely the thymus and bone marrow, are the sites for production and differentiation of hematopoietic progenitors into lymphoid and myeloid cells which provide the adaptive and innate branches of the immune response. They also provide an environment conducive to the selection of the lymphocytes, which are functional yet do not display pathogenic autoreactivity. The secondary lymphoid organ subsystem is comprised of the spleen, lymph nodes, tonsils, Peyer's patches, adenoids, and other lymphoid formations which are found in a variety of tissues and referred to as the mucosa-associated lymphoid tissues[1]. These organs survey the body (primarily through the lymphatics) for antigens and are responsible for mounting an adaptive immune response by selectively activating B and T cells whose receptors are specific to the threat. Alternate forms of the antigen-specific receptors on B cells are secreted as antibodies. Tertiary lymphoid organs form in tissues experiencing chronic inflammation and perform many of the same functions as secondary lymphoid organs. Finally, the lymphatic vasculature, although not placed in any of these three categories, plays a vital role in the transportation of immune cells and pathogens. In addition, the lymphatic endothelial cells of the vasculature support secondary lymphoid organs by enabling immune cell chemotaxis and antigen presentation[2]. Within the lymphatic organs, lymphocytes are supported by a variety of stromal cells which provide them with signals needed for survival, growth, development, and migration.

1.1 Lymph node structure and function

The peripheral lymphatic system includes the spleen and lymph nodes as well as other mucosa-associated lymphoid tissues, such as the tonsils and Peyer's patches, which

are distributed throughout the body[3]. The purpose of these organs and tissues is to enhance immune surveillance by filtering extracellular fluids, providing an environment for effective antigen capture and presentation, and facilitating adaptive immune responses[3]. Extracellular fluid called lymph drains from tissue and flows into the lymph nodes via afferent lymphatic vessels. It brings antigens that are produced by infection or malignancy (see Fig. 1.1)[3]. Lymph flow also transports inflammatory mediators generated by the innate immune response at the site of infection, such as interleukin-1β (IL-1β) and tumor necrosis factor α (TNFα)[4,5]. Furthermore, antigen-bearing dendritic cells (DCs) are carried by the lymphatic vasculature and actively recruited to the lymph nodes by chemokine gradients[5]. The primary chemokines which mediate the migration from the lymphatic vasculature to the lymph nodes are C-C motif chemokine ligand 21 (CCL21) and C-C motif chemokine ligand 19 (CCL19) (see Fig 1.1)[6]. CCL21 is produced by the endothelial cells of the high endothelial venules (HEVs) and both chemokines are secreted by fibroblastic reticular cells (FRCs)[6,7]. These molecules also promote the entry of naive T cells into the lymph nodes, while B cell integrin activation and subsequent migration are also dependent on the chemokines C-X-C motif chemokine ligand 12 (CXCL12) and C-X-C motif chemokine ligand 13 (CXCL13)[6,8].

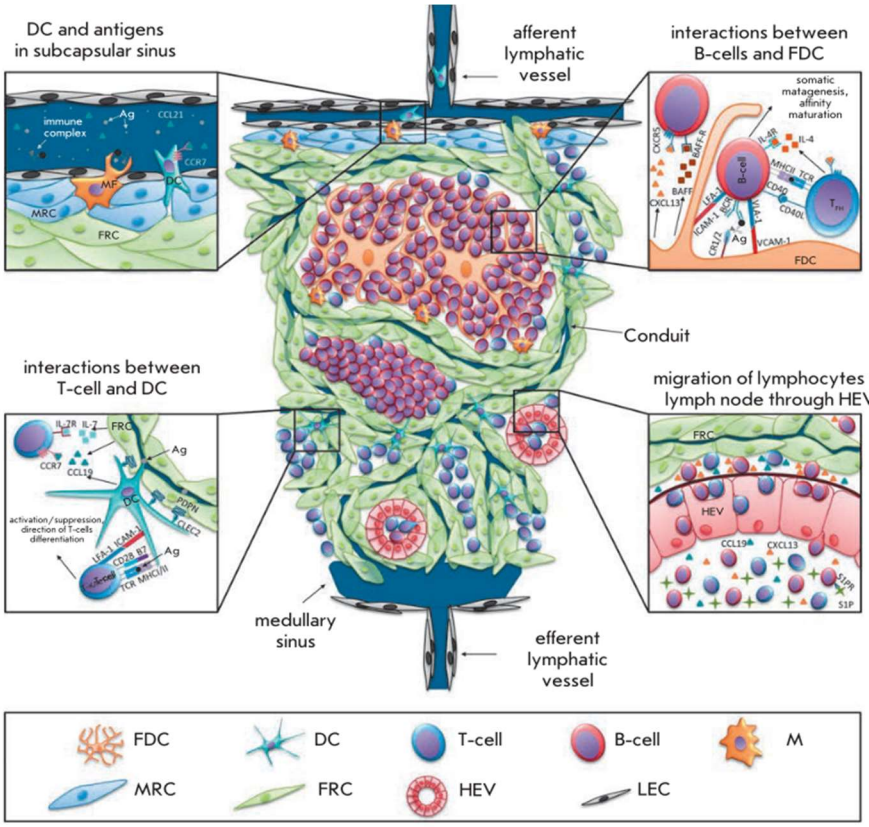

Figure 1.1 The lymph nodes facilitate interactions between stromal cells and lymphocytes which allow activation and the progression of the adaptive immune response. Adapted from Nosenko et al.[9]. Reproduction is permitted under the terms of the Creative Commons Attribution 4.0 International license.

DCs in the lymph nodes can either be resident cells or migratory cells which are recruited from the peripheral tissues after their activation in response to inflammation[7]. DC motility is promoted by the upregulation of chemokine receptor C-C chemokine receptor 7 (CCR7) and lectin CLEC-2, upon activation[7]. Resident DCs can acquire soluble antigens which flow into the lymph node and some can even process viruses and bacteria which arrive by the same conduits and end up in the subcapsular sinus (SCS)[7]. Furthermore, DC signaling can promote the expansion of the lymph node's vascular and stromal networks in response to infection in order to remodel and enlarge the organ to improve capacity and function[7].

Although DCs are the primary antigen presenting cells (APCs) in the lymph node, macrophages can also present antigens to T cells as well as B cells and DCs[10]. Lymph

node macrophages are distinct from those that arise from monocytes and are present as a resident population[10]. They fall into a number of distinct subtypes which are localized to the SCS, medullary sinus, medullary cords, or interfollicular regions[10,11]. Furthermore, lymph node macrophages are susceptible to viral infection, which may allow them to enable viral replication for the purpose of creating enough viral antigen to promote an adaptive immune response[10].

B and T lymphocytes are present in designated, separate areas in the lymph node[3]. The lymph node lobule, its basic functional unit, is separated from the outer, fibrous capsule of the lymph node by the SCS (see Fig. 3.8 panel **a,** solid arrow), into which lymph flows from afferent vessels (see Fig. 3.8 panel **b,** dashed arrow)[4]. Further subdomains contain specific populations of cells and enable their function. The superficial cortex contains the follicles and interfollicular cortex[4]. B cells are primarily found in the follicles and this is where germinal center (GC) formation and activity occur (see Fig. 3.8 panel **a,** solid circle)[4]. T cells interact with DCs in the interfollicular cortex and the deeper paracortex (see Fig. 3.8 panel **a,** dashed circle). The latter region is where they proliferate after activation[4]. The medulla contains the medullary sinuses and medullary cords and contains activated B cells, or plasma cells, which produce antibodies[4,12]. Medullary sinuses converge on the efferent vessel through which lymphocytes can exit the lymph node[4]. T cell localization to their zones is maintained by the action of chemokines CCL19 and CCL21. B cells are similarly attracted to the follicles by CXCL13[3]. The colocalization of DCs and T cells enables high rates of antigen presentation to facilitate the adaptive immune response[3].

Upon activation, T cells migrate to the edges of their zones to encounter B cells and provide helper signals to activate them[3]. This is performed primarily through the cell-surface expression of CD40L and secretion of interleukin 21 (IL-21), which promote B cell survival, proliferation, and differentiation. Activated lymphocytes proliferate and differentiate in the lymph node and leave via the efferent vessels to perform their effector functions. The exit of T cells from the lymph node through the cortical sinuses, to the medullary sinuses, and finally out of the efferent vessel is mediated by a gradient of

sphingosine 1-phosphate (S1P). Activated T cells express fewer of the receptors for this lipid molecule in order to remain within the lymph node until they are ready to fulfill their effector function[3]. Aside from T helper cells, there are a variety of effector T cells. Cytotoxic CD8+ T cells promote viral immunity by killing virally infected cells, while T_H1, T_H2, and T_H17 cells mediate immunity against intracellular pathogens, parasites, and bacteria, respectively[3]. Activated B cells can become plasma cells which produce antibodies that enhance immunity by neutralizing pathogens through a variety of means[3]. A subset of activated B cells become memory B cells which are maintained over a longer period of time to provide a faster adaptive immune response against future infection by the same or similar pathogens[3].

B cell zones are home to the GC reaction, a key process which results in B cell antibody class switching and affinity maturation[12]. GCs are temporary structures that form in response to B cell activation from T cell-dependent signaling[12]. A subset of these B cells undergoes phenotypic changes and enter the center of the follicle where they proliferate rapidly and experience somatic hypermutation, a B cell receptor (BCR)-changing process which results in a population of B cells that can produce higher-affinity antibodies[12]. Class switching diversifies the repertoire of antibodies that can be produced by changing the immunoglobulin (Ig) gene to provide isotypes with specialized function[3].

Stromal cells in the lymph nodes provide support to leukocytes by forming structures and secreting soluble chemical signals[11]. FRCs are present in the paracortex and, as previously mentioned, secrete CCL19 and CCL21[11]. FRCs also form the reticular network in conjunction with reticular fibers, bundles of basement membrane-covered collagen, which they produce[4]. Lymphocytes migrate along this network by binding to FRC-expressed adhesion ligands and are simultaneously exposed to the conduits within the network which allow the transport of antigen and inflammatory signals[4]. Follicular dendritic cells (FDCs) are present in the follicles alongside B cells and produce both CXCL13 and B-cell activating factor (BAFF), which promote B cell localization and survival, respectively[3,11]. Marginal reticular cells (MRCs), found in the subcapsular sinus, also produce BAFF and CXCL13[13].

In addition to stromal cells, lymphatic endothelial cells (LECs) play an important role in delivering cells, cytokines, and antigen to the lymph nodes. They also directly enable transmigration of leukocytes across the vessel wall by expressing hyaluronic acid receptor LYVE-1, adhesion molecules ICAM-1 and VCAM-1, and chemokine CCL21[14]. Furthermore, LECs produce interleukin 7 (IL-7) which promotes lymphocyte expansion during an immune response[15]. Finally, LECs play a role in regulating T cell tolerance by acquiring or delivering antigens to or from DCs for presentation to CD4+ T helper cells and expressing peripheral antigens for presentation to CD8+ cytotoxic T cells[15]. LECs undergo proliferation and migration primarily in response to lymphangiogenic growth factor vascular endothelial growth factor C (VEGF-C), which can be provided by a variety of cells including macrophages and B cells[15,16].

Lymphocytes interact with ECM proteins in the lymph nodes that can impact their migration, survival, and proliferation[17]. Many of these proteins are found within the basement membranes of the lymph node vasculature and the reticular network. The latter contains collagens I, III, and IV which provide structural strength and adhesion ligands[18]. Collagen IV is found in basement membranes and reticular fibers alongside laminins, trimeric proteins which contain adhesion ligands and are named after their combination of α, β, and γ subunits, in that order. Laminins 332, 411, and 511 are found in the reticular fibers and promote lymphocyte migration[17]. Moreover, laminin 511 promotes T cell proliferation[17]. Laminins 411 and 511 are found in the basement membranes of the lymph node vasculature and it has been shown that the ratio of their abundance may have an impact on the strength of immune responses[19,20]. Laminins in the lymph nodes are thought to primarily be secreted by FRCs but some studies have indicated that lymphocytes may also produce laminins 411 and 511[19]. Fibronectin is an adhesion ligand-containing protein that is also associated with the reticular network in lymph nodes and promotes T cell migration[18,21].

1.2 Tissue engineering

The design of biomimetic constructs or models, grounded in an understanding of biology and engineering principles, has made significant contributions to the field of regenerative medicine and resulted in a supply of commercially available products that are used to develop approaches to replace injured or dysfunctional tissues. This endeavor, known as tissue engineering, makes use of cells, scaffolds, and a variety of chemical or physical signals to replicate the structure and function of natural tissues (see Fig. 1.2). For the purposes of immune tolerance, it is often most efficacious to use autologous cells from the intended recipient of a tissue engineered construct[22]. These cells may be taken from a patient to be expanded and seeded in scaffold *ex vivo* or they may simply be recruited to a site of implantation of such a scaffold to be incorporated into a design *in vivo*. Stem cells are another useful resource since they are self-renewing and capable of differentiation. The term scaffold refers to a variety of three-dimensional structures, which can be used to contain and provide signals to cells. These may be derived from natural materials or from synthetic sources and generally have pores or channels which allow the movement and interaction of one or more cell types within the construct. It is imperative that these materials not be cytotoxic and that, if they are intended to be implanted, display full biocompatibility with the recipient animal model or human patient.

Signals which are used in tissue engineered designs may include chemical signals such as growth factors, cell adhesion peptides, chemokines, and other relevant molecules that promote viability, proliferation, migration, or specific functions of a target cell population. Physical signals may be provided by the material used for scaffolding, as is the case for factors such as stiffness or surface topography. External physical signals such as fluid flow, tensile or compressive loading, and even electrical stimulation can play an important role in the development of an intended cellular phenotype or function.

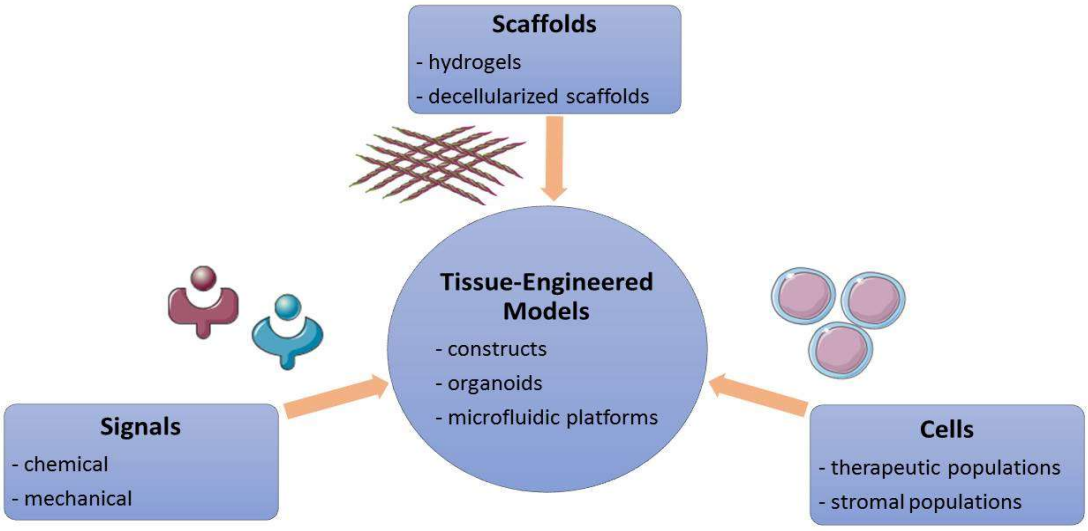

Figure 1.2 Tissue engineering design often utilizes a combination of scaffold materials, cell types, and environmental signals to replicate natural function and achieve desired outcomes. Reproduction of the artwork: "Ligand", "Receptor", "Lymphocyte", and "Collagen" by Servier Medical Art at https://smart.servier.com/ is permitted under the terms of the Creative Commons Attribution 3.0 Unported license.

The design of a tissue engineered construct generally falls into one of a set of distinct approaches. One standard approach involves the seeding of cells into a porous scaffold. Such a design may be constructed by the casting or bioprinting of a polymeric material or hydrogel. Hydrogels are comprised of hydrophilic, crosslinked polymers which form a 3D network that absorb and swell with water[23]. These characteristics provide a porous, aqueous environment that allows the diffusion of nutrients, oxygen and various chemical signals[23]. They can often be formulated or modified to achieve desirable mechanical properties and incorporate adhesion ligands or other bioactive molecules, allowing them to mimic the microenvironment of various tissues[23]. One major concern regarding the choice of materials with which to assemble an appropriate hydrogel is cytocompatibility, as the cells of therapeutic interest need to maintain high viability and function[23]. Another is the potential for vascularization, a process that enables better transport of relevant cells and signals throughout the scaffold. Vascularization of tissue engineered constructs remains one of the most significant challenges to the field[23]. One

popular choice of hydrogel is that which is made from gelatin methacrylate (GelMA). GelMA is a combination of the natural, polymeric material, gelatin, and methacrylic anhydride[24]. It can be crosslinked with the aid of a photoinitiator and ultraviolet (UV) light source. GelMA contains cell-binding RGD peptide motifs. It is mechanically and chemically tunable, biodegradable (due to sites recognizable by matrix metalloproteinases), and bioprintable[24]. Fibrin is another widely used hydrogel. It is formed by the cleaving and subsequent polymerization of a natural monomer, fibrinogen, which occurs due to the action of thrombin[25]. In the body, fibrin plays an important role in blood clotting and wound healing. It has been used for its angiogenic potential and, as a natural scaffold, is highly biocompatible[25].

Hydrogels and other 3D culture scaffolds can be assembled in a variety of ways and with or without additional supporting structures. Bioprinting provides a means of creating a complex spatial organization that may not be possible with simpler methods but requires the use of materials whose properties allow them to be effectively printed[26]. When stem cells are placed in 3D clusters that self-organize and differentiate into requisite somatic cell types, it is known as organoid formation[27]. This approach is often supported by placement of the cells within a scaffold material, but it is also possible for these cells to secrete their own ECM. To provide cells within a tissue engineered construct that is maintained *in vitro* with nutrients and waste removal, scaffolds are often placed within a perfused housing known as a bioreactor. Bioreactors can also be used to provide chemical or physical signals with or without temporal variation. Alternatively, a construct can be implanted into an animal model for *in vivo* maturation or designed to simply exert its effect directly upon implantation within a patient, as is the case with many injectable scaffold approaches. Advances in microfluidic technology have led to its combination with 3D cell culture to create organ-on-a-chip models. An advantage of this approach is the high degree of control over architecture and perfusion which it imparts[28].

Another technology, which permits use of the body's own structural design, is decellularization: removal of cellular content from an organ or tissue leaving behind the natural scaffold provided by its ECM. This is most often achieved by use of surfactants,

acids/bases, enzymes, or a combination of these methods[29]. Surfactants disrupt the lipid bilayer of cells in the sample to lyse them and remove their nuclear material[29]. Some commonly used surfactants include Triton X-100, sodium dodecyl sulfate (SDS), sodium deoxycholate, and 3-[(3-cholamidopropyl) dimethylammonio]-1-propanesulfonate (CHAPS)[29]. SDS is highly effective at removing nuclear material but tends to damage the ECM of the tissue[29]. CHAPS, sodium deoxycholate, and Triton X-100 can be used to preserve the ECM to a greater degree[29, 30]. However, CHAPS and sodium deoxycholate tend to be less effective at total removal of nuclear material and may need to be used in multiple cycles or with additional agents[29]. Acids and bases disrupt the membrane through solubilization[29]. These have been found to be damaging to certain components of the ECM[31]. Finally, enzymatic agents such as trypsin-ethylenediaminetetraacetic acid (EDTA), pepsin, and DNase I can be used to supplement these approaches. Trypsin-EDTA and pepsin break bonds between the ECM and cell, while DNase I can be used to degrade DNA segments[29,31]. Trypsin-EDTA and pepsin need to be used with care, as overexposure to the tissue may break down the ECM[31].

In addition to consideration of the scaffold type and method used, the material itself is an important factor. Many synthetic materials are easily and consistently producible and can be modified with natural peptides or other bioactive molecules to impart biological function[32]. These modifications can often be forgone if a naturally derived material is chosen but these are generally harder to manipulate and process, and can be more vulnerable to batch variability[32,33].

1.3 Objectives of lymphoid tissue engineering

Lymphatic bioengineering involves the use of cells and biological factors in an appropriate medium or scaffold to reconstruct or mimic the function of some part of the lymphoid organ system. This endeavor has the potential to provide the medical sector with a variety of services. For example, it could better establish the efficacy and safety of pharmaceutical drugs that can be limited by their interaction with the immune system and

the resultant, potentially immunotoxic, response. The advent of highly biomimetic, three-dimensional engineered models of each organ of the immune system could provide the industry with a reliable, reproducible, cost-effective, and ethical alternative to the pre-clinical trials which are performed on animal models and whose results often translate poorly to the clinical phase[28,34,35]. Some other, experimentally related concerns with the use of animal models include the presence of fundamental differences in the immune systems of different species and the inability to fully measure or control the complex cellular interactions in a test subject[27,28]. Additionally, *in vitro* models provide a multitude of experimental benefits including the ability to manipulate signaling pathways, engineer tissue niches, and introduce epigenetic or genomic alterations to cell lines[36]. Of these, the ability to recreate the appropriate, 3-dimensional tissue niche in terms of ECM components, chemical gradients, scaffold stiffness, and other mechanical gradients is especially vital for immune cell function, giving a bioengineered tissue model an advantage over oversimplified, 2-dimensional culture systems[28,36]. Furthermore, *in vitro* models provide an improved system for imaging or performing molecular analyses at multiple timepoints in an experiment, thereby allowing observation of temporal dynamics[27,37]. Finally, bioengineered models have the potential to encapsulate individual specificity within therapeutic screening tests by isolating, expanding, and seeding the patient's own cells in the scaffold or construct. This could serve to capture the traits of their specific disease by using affected cell populations, avoid adverse immune responses to allogeneic cells, and characterize their personalized reaction to a drug or immunotherapy[28,35,38].

Alongside providing *in vitro* systems for drug and immunotherapy screening, bioengineered lymphatic tissue models can provide a means of studying the dynamics of auto-immune disease and cancer within an organ-specific microenvironment[9,34]. This could elucidate the evolution of these pathologies and give insight on potential immunotherapeutic approaches based on the interactions of diseased cells with surrounding immune cells.

Another beneficial outcome of the progression of lymphatic tissue engineering would be the implantation of secondary lymphoid organ constructs to replace or bolster inadequate natural immune function. Such an approach could be used as a vehicle for immunotherapy by implanting immune cells in a physiologically and pathologically relevant location. These cells could be pre-primed against an antigen particular to the infectious disease vector or to the cancer type of interest. They can also be provided with the appropriate microenvironment by the scaffold they are seeded in, allowing *in vivo* expansion and improved viability. Furthermore, this tactic could be used to combat pathological inflammation and auto-immune disease by providing a population of regulatory immune cells to control these adverse immune responses[38]. Additionally, the negative effects of genetic disorders involving an inhibition of lymphatic organ development or lack of function such as DiGeorge syndrome or Fanconi anemia could be circumvented by implantation of an appropriate lymphatic tissue construct to restore function. As a final application, the implantation of a tissue-engineered secondary lymphoid organ construct (alongside engineered lymphatic vasculature, as needed) could be used as a direct tissue replacement to treat inherited or acquired lymphedema, the accumulation of interstitial fluid resulting from insufficient lymphatic drainage. Acquired lymphedema is often a result of radiation therapy or tumor removal[39]. Another benefit of such a replacement would be the restoration of immune surveillance provided by the lost lymphatic organs and vasculature.

1.4 Current strategies for tissue engineering lymph nodes

Many of the lymph node tissue-engineering studies of the last two decades have been focused on either the production of a GC reaction (using only B cells) or on the formation of more efficient immunological synapses (T cells and APCs) in 3D. Of the former, studies by Purwada et al. show promising results. In the first of these publications, a gelatin and silicate nanoparticle hydrogel was used to incubate B cells in the presence of a transgenic stromal cell line and exogenous IL-4[40]. The stromal cells in this study produced CD40L and BAFF to replicate the function of the T follicular helper

(TFH) cells and FDCs found naturally in the lymph node. The latter study replaced the modified gelatin matrix with a polyethylene glycol (PEG)-maleimide scaffold conjugated with adhesion peptides and was able to achieve GC-like B cell phenotypes, antibody class switching, and the production of antigen-specific B cells[41].

With regard to those studies focused on the formation of immunological synapses and T cell activation, microfluidic devices provide a highly controllable format with which to study specific behaviors, as demonstrated by Rosa et al. in a study that looked at T cell and DC interactions under controlled flow conditions[42]. The use of artificial APCs for the activation of T cells in 3D culture conditions has been recently investigated by research groups out of Barcelona and Harvard and found to have an advantage over traditional 2D culture approaches[43,44]. The study by Cheung et al. found success in the complementary use of soluble mitogenic signals and liposome membrane-bound T cell receptor (TCR) stimulation ligands co-delivered by matrix-forming silica microrods to achieve rapid expansion of T cells[44]. Finally, injectable gels have proven their use in the delivery and expansion of T cells in vivo. This was accomplished using an alginate gel functionalized with GFOGER peptide, and through a polyisocyanopeptide hydrogel functionalized with GRGDS[45,46]. This approach can be applied to the immunotherapeutic treatment of cancer by delivering and expanding T cells that can recognize tumor-specific antigens at the location of a tumor or tumor resection site[45]. These studies included an integrin-binding peptide to enable cell migration and egress from the gel into the site of interest[45,46].

Of the studies that involve both T and B lymphocytes, long term research by Giese et al. has resulted in a bioreactor with RGD-Dextran gel discs that is able to support a lymphocytic immune response to protein aggregates, and maintain separated T and B cell zones, mimicking secondary lymphoid organ structure[47]. While this series of publications focused on in vitro functionality, other studies implemented in vivo recruitment of immune cells to seed implanted collagen sponges supported by thymus-derived stromal cells[48,49]. These efforts resulted in the induction of distinct B and T cell areas, antigen-specific antibody production, and even some evidence of a secondary

immune response upon further stimulation. There have also been recent attempts to utilize decellularized lymph nodes as a scaffold for the in vivo production of potentially therapeutic cell populations. One example is the work of Lin et al. demonstrating the use of this approach to produce anti-tumor DCs in a biologically relevant microenvironment[50].

For a comprehensive review of lymphoid tissue engineering, please see appendix section A.3. This review has been submitted to the Journal of Immunology and Regenerative Medicine and is currently in revision.

For the purposes of creating a lymph node model construct that is highly biomimetic with applicability *in vitro* as well as *in vivo*, it is important to choose an approach which allows an ease of manipulation and control with clinically and physiologically relevant size and complexity. Hydrogels are a prime candidate for this, as they can be relatively easily produced, have the potential to be utilized in rapid manufacturing practices such as 3D bioprinting, and contain base materials which can be tuned, modified, and supplemented to implement target characteristics. These characteristics include parameters such as stiffness, degradation time, density and distribution of cells and chemical signals, and size. However, since the complexity of ECM composition and microstructure can be very difficult to replicate, it may prove useful to implement decellularized ECM from native tissue. An additional key foresight lies in the choice of method for supplying the construct with a continual source of nutrients and means of waste removal. Designs lacking this feature may be limited in their functional duration. Bioreactors fit this description but do not guarantee complete diffusion of nutrients and waste products through the entirety of the construct. A sufficient degree of vascularization might accomplish this goal and add important cell-cell interactions through the incorporation of endothelial cells. A vascularized hydrogel scaffold with the appropriate cell populations, chemical and ECM supplementation, and means of perfusion could meet the needs for a versatile and effective tissue engineered lymph node model construct.

2. Methods

2.1 PBMC/PBC isolation and hydrogel seeding

PBMCs were obtained [with natural killer (NK) cells removed] from the Dr. Jeffrey Miller lab (University of Minnesota, Minneapolis). The cells were attached to microbeads when received. These cells were incubated overnight at 37°C and 5% CO_2 in a 150 cm^2 flask (Corning, Corning, NY) with X-VIVO^{TM} 15 cell medium (Lonza, Basel, Switzerland) to allow them to detach from the beads. The next day, the cells were used in 3D hydrogel culture assays. Discarded normal donor peripheral blood cells (PBCs) [Angela Panoskaltsis-Mortari] were provided by the Cytokine Reference Laboratory (University of Minnesota, Minneapolis). The layer containing hematopoietic cells was drawn from the tubes and placed in an ammonium chloride RBC (red blood cell) lysis solution (07850, Stemcell Technologies, Vancouver, Canada) at a 1:9 ratio. Cells were mixed by tube inversion and placed on ice for 10 minutes to lyse RBCs. PBCs were washed in AIM V medium (ThermoFisher Scientific, Waltham, MA) and PBMCs/PBCs were counted using a hemocytometer (Hausser Scientific, Horsham, PA) and Nikon Labophot microscope (Nikon, Tokyo, Japan).

GelMA (gelatin methacrylate) solutions were prepared by mixing 10%, 16%, 20%, or 24% w/v stock solutions of GelMA, which was provided by the University of Minnesota 3D Bioprinting Facility, with 1% w/v lithium phenyl-2,4,6-trimethylbenzoylphosphinate (LAP) (UV crosslinking agent, Allevi, Philadelphia, PA) in culture medium. All solutions containing LAP were prepared in the dark and wrapped in aluminum foil until they were combined with cell suspensions and crosslinked. These solutions were diluted by a factor of two when mixed with an equal volume of a cell suspension. Fibrinogen solutions were prepared by mixing human plasma fibrinogen (341576, MilliporeSigma, Burlington, MA) at concentrations of 10, 20 or 40 mg/mL in the culture medium. This solution was combined with cell suspensions of equal volume and a 10 U/mL stock solution of human plasma thrombin (605190, MilliporeSigma). Cells were seeded at $250x10^3$/mL, $10x10^6$/mL, or $20x10^6$/mL in well-mixed suspensions. In some experimental conditions, laminin 411 (BioLamina AB, Sundbyberg, Sweden)

and laminin 511 (BioLamina AB) were added to the fibrinogen solution at a final concentration of 10 µg/mL. In cases where processed porcine lymph node ECM was included, fibrinogen was added to AIM-V medium containing 10 mg/mL of the ECM.

Fibrinogen solutions were mixed with cell suspensions in a 24 or 48 well plate (CELLTREAT, Pepperell, MA) in sterile conditions. Thrombin, at a 10 U/mL stock concentration, was thawed and kept on ice then added to the wells to reach a final concentration of 1 U/mL. Each well's contents were mixed thoroughly with a pipette and then the plate was allowed to incubate for 30 minutes at 37°C and 5% CO_2 to allow the fibrinogen to crosslink and form a fibrin hydrogel. GelMA stock solutions were mixed thoroughly with cell suspensions in a 48 well plate (CELLTREAT) and then crosslinked for 70 seconds, at a distance of 13 cm from a 405 nm light source provided by an INKREDIBLE 3D bioprinter (Cellink). After crosslinking, hydrogels of either type were covered in 400 µL of culture medium (see Fig. 2.1).

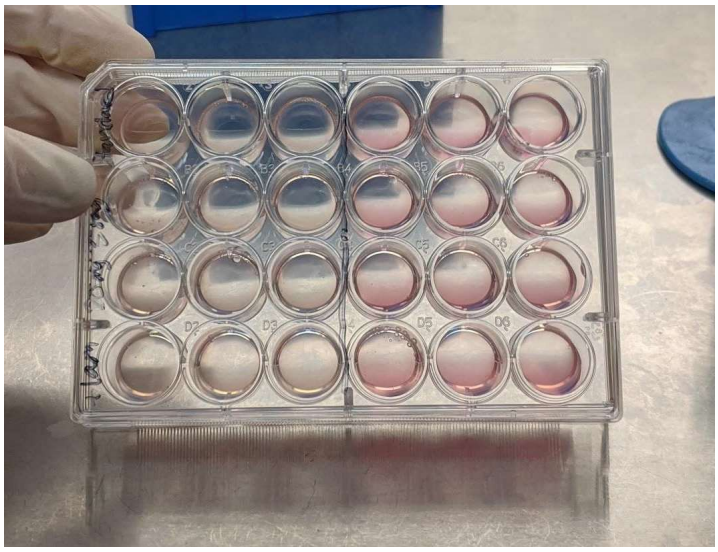

Figure 2.1 220 µl fibrin gels containing PBCs. The gels in the left half of the plate had already been imaged and were not covered with culture medium at the time this picture was taken. The gels in the right half of the plate had yet to be imaged and were covered in culture medium.

Figure 2.2 Close-up of the hydrogels in wells D3 and D4 shown in Figure 2.1.

2.2 PBMC/PBC 3D culture and imaging

Cell-containing gels were incubated at 37°C and 5% CO_2 for either 24 or 72 hours. In later experiments, the culture medium covering the gels was replaced every day for each of the 72 hour trials. At the end of the incubation period, the culture medium covering the gels was aspirated and replaced with 200 μL of LIVE/DEAD® Viability Assay reagent (L3224, Invitrogen, Carlsbad, CA) containing calcein acetoxymethyl (AM) and ethidium homodimer-1. The reagent was incubated with the hydrogels for 1 hour. At that point, the remaining reagent was aspirated from the surface of the gels. An Evos FL Auto 2 microscope (Invitrogen) was used to image gels in green and red fluorescence channels to determine the number of live and dead cells, respectively. Z-stacks were compiled from images that began at the lowest focal plane that contained in-focus cells and ended at the highest focal plane that contained in-focus cells. This depth ranged from 0.2 to 1 mm, depending on the gel. Z-stacks were taken in the middle of each gel to avoid edge effects and provide sampling consistency.

2.3 Quantification of viability

Upon obtaining Live/Dead (L/D) fluorescent images of PBMC/PBCs, grid systems were overlaid on them to improve the efficiency and accuracy of manual cell

counting. A tally of live and dead cells was kept for every other row in the grid in each sample image. Cells falling on the right and upper boundaries of a given grid square were included in its count, and those on the left and lower boundaries were not, so as to avoid double-counting. Row totals were added together to obtain the final count for each image. Viability was calculated as the percentage of live cells within a given number of total cells. For each experimental condition where multiple trials were performed, mean viability and standard error were calculated.

2.4 Obtaining lymph nodes

Porcine mesenteric lymph nodes were obtained from waste carcasses from the Visible Heart Laboratory (University of Minnesota, Minneapolis, MN). Fatty connective tissue was removed from the tissue samples using tweezers and dissecting scissors. Lymph nodes were flash frozen whole for use in histology or further dissected into ~2-5mm pieces for decellularization (see Fig. 2.2). Additional samples were likewise dissected into smaller pieces and used in dsDNA or soluble protein content analysis. A human lymph node which had come with lungs that previously been purchased from the International Institute of the Advancement of Medicine (Edison, NJ) and frozen whole in O.C.T. was used to create sections for positive IHC controls.

2.5 Decellularization and digestion of porcine lymph nodes

Decellularization of porcine lymph nodes was performed using studies by Galliger et al. for tracheal decellularization and Skolasinki et al. for lung decellularization as a basis[51,52]. Dissected porcine mesenteric lymph nodes were placed in 140 mL of deionized water in a beaker along with a stir bar (see Fig. 2.3). They were then soaked for 1 hour on a stir plate. The deionized water was drained and replaced with 140 mL of 0.1% v/v Triton X-100 (Sigma-Aldrich, St. Louis, MO). This mixture was stirred for 18 hours. The Triton X-100 solution was subsequently replaced with 140 mL of 2% w/v sodium deoxycholate for an additional 18 hours. Tissue samples were then stirred in 1 M

sodium chloride (NaCl) for 2 hours, followed by a solution containing 30 μg/mL porcine pancreatic DNase (Roche Diagnostics, Basel, Switzerland), 1.3 mM magnesium sulfate, and 2 mM calcium chloride for another 2 hours. Finally, the samples were rinsed in phosphate-buffered saline (PBS) for 5 minutes by the same method. All steps occurred at 4°C. A stir plate (PC-353, Corning) was used at a medium speed setting. Samples were either used immediately or stored in PBS at -80°C.

Decellularized tissue which was intended to be incorporated into hydrogels was lyophilized for 48 hours using a Freezone 6 freeze dryer (Labconco, Kansas City, MO). An electric coffee grinder (Bodum, Triengen, Switzerland) was used to grind the ECM into small pieces. These pieces were digested in 0.01 N HCl with 1 mg/mL pepsin from porcine gastric mucosa (Sigma-Aldrich, P6887). The solution was stirred on a stir plate (Corning) for 2 days at room temperature. The solution was neutralized using 0.1 N NaOH and then drained. The tissue was washed in PBS (see Fig. 2.3) and frozen overnight at -80°C. The tissue was then lyophilized a second time for 48 hours and ground down to a powder using the coffee grinder. Before use in 3D culture, the ECM was vortexed in warmed (37°C) AIM-V culture media.

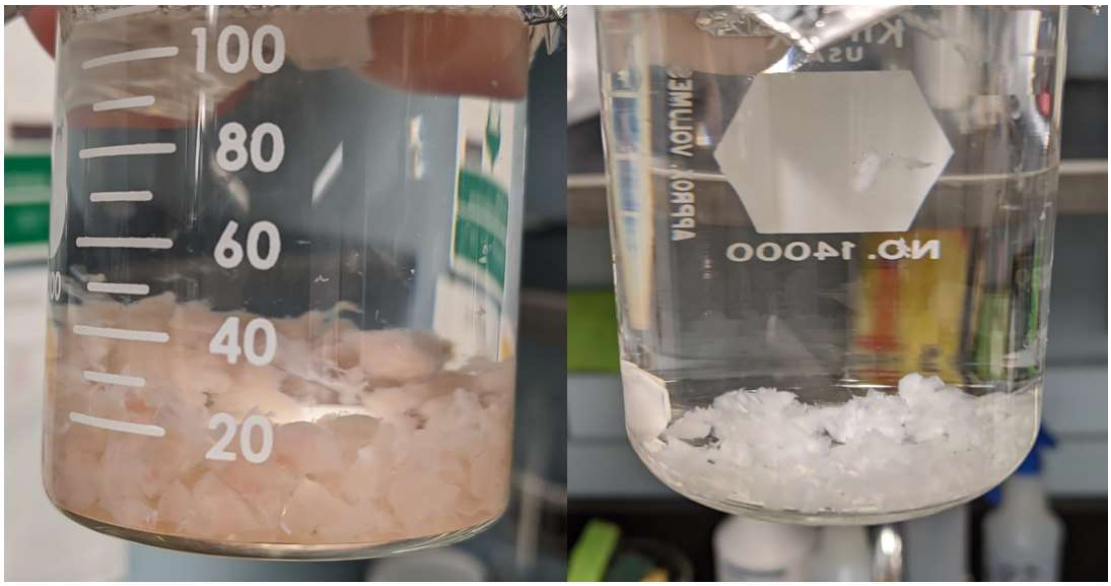

Figure 2.3 Porcine mesenteric lymph nodes were cut into 2-5 mm pieces and rinsed in deionized water for 2 hours to remove extraneous material before the decellularization process began (see left panel). Porcine mesenteric lymph node pieces were visibly more translucent and smaller in size at the end of the decellularization process (see right panel).

2.6 Histology

2.6.1 Freezing tissue blocks

Whole porcine lymph nodes with all connective tissue removed or decellularized porcine lymph node tissue pieces were placed in cylindrical aluminum foil molds containing Tissue-Tek O.C.T (optimal cutting temperature) compound (Sakura Finetek USA, Torrance, CA). These samples were flash frozen in liquid nitrogen and the resultant blocks were stored at -80°C until sectioning.

2.6.2 Sectioning

O.C.T blocks containing tissue samples were allowed to equilibrate to -16°C inside of a Leica CM1900 cryostat (Leica Biosystems, Buffalo Grove, IL) for 20 minutes prior to sectioning. Blocks were sectioned into 6 μm slices between -16°C and -18°C, depending on the consistency of the sample. Cryostat temperature adjustments were made

based on section quality during the cutting process. A human lymph node block was used to provide a positive control for primary antibody selection (see section on immunofluorescent staining). Sections were adhered to Fisherbrand ProbeOn Plus microscope slides (Thermo Fisher Scientific, Waltham, MA) and stored at -80°C or used immediately for staining.

2.6.3 Hematoxylin & Eosin

After sectioning, slides were immersed in a coplin jar containing hematoxylin dye (Sigma-Aldrich) for 5 minutes. Slides were then rinsed in distilled water for 2 minutes. From there, slides were dipped once in acid alcohol (1% HCl in 70% ethanol) and rinsed in distilled water for another 5 minutes. Then, slides were dipped 5 times in bluing solution (0.2% sodium bicarbonate, 1% magnesium sulfate), 10 times in 2 changes of distilled water, immersed in 70% ethanol for 2 minutes, and dipped twice in Eosin Y dye (Sigma-Aldrich). Slides were dehydrated in 70%, 95%, and 100% ethanol and cleared in xylene. Coverslips (Thermo Scientific) were affixed using a permount medium (Fisher Scientific) and imaged using an Evos FL Auto 2 microscope on a brightfield setting at 4x, 10x, and 20x magnification.

2.6.4 Masson's Trichrome

After sectioning, slides were immersed in a coplin jar containing Weigert's iron hematoxylin dye (Sigma-Aldrich) for 10 minutes. Slides were rinsed for 10 minutes in warm, running water from the tap then dipped in distilled water 10 times each. Then, slides were immersed in Biebrich scarlet-acid fuschin dye (Sigma-Aldrich) for 10 minutes followed by 10 dips in distilled water. At this point, slides were immersed in phosphomolybdic-phosphotungstic acid (Sigma-Aldrich) for 10 minutes and aniline blue dye (Sigma-Aldrich) for 10 minutes. Slides were then washed in glacial acetic acid for 5 minutes, dipped 10 times in distilled water, and dehydrated in 95% and 100% ethanol. Slides were cleared in xylene. Coverslips (Thermo Scientific) were affixed using a

permount medium (Fisher Scientific) and the sections were imaged using an Evos FL Auto 2 microscope on a brightfield setting at 4x, 10x, and 20x magnifications.

2.7 Immunofluorescence staining

After their removal from storage at -80°C, slides were allowed to thaw for 30 minutes. Acetone that had been chilled to a temperature of -20°C was pipetted onto sections and let sit for 10 minutes. At this point, the acetone was poured off the slides that were then rinsed with PBS after an additional 15 minutes was given for the acetone to fully evaporate. A hydrophobic slide marker (MilliporeSigma) was used to draw barriers around each section to avoid run-off. Each section was blocked with a normal serum blocking solution (927503, BioLegend, San Diego, CA) for 1 hour at room temperature. Then, primary antibody dilutions were applied to the appropriate sections. Slides were placed on racks in a tin foil-wrapped box with damp paper towels to ensure a dark, humid atmosphere. These conditions were maintained at 4°C overnight. The next day, primary antibody solutions were removed and the slides were rinsed with PBS. Secondary antibody dilutions were pipetted onto each section and the slides were allowed to incubate in the dark for 2 hours at room temperature. The secondary antibody solutions were discarded, the slides were rinsed again with PBS, and coverslips were affixed to each slide using a 4′,6-diamidino-2-phenylindole (DAPI) anti-fade mounting medium (H-1500, Vector Laboratories, Burlingame, CA). Slides were dried for 15 minutes then placed in a slide book and kept at 4°C overnight. Control slides containing no stain or secondary-only stains were incubated with PBS in place of primary or primary and secondary antibody dilutions to prevent dehydration. Images were taken at 4x, 10x, or 20x magnification on the Evos FL Auto 2 microscope. The background signal of each channel was visually minimized, and the resultant gain was maintained throughout the imaging process. Nuclear DAPI was detected using the Evos FL Auto 2 microscope's DAPI channel.

2.7.1 Laminin

As a primary antibody for immunohistochemical staining (IHC), an anti-laminin rabbit polyclonal IgG (ab11575, Abcam, Cambridge, UK), was chosen to target multiple isoforms of laminin, most likely including laminins 411 and 511 (see section 3.5). This antibody was diluted 1:250 in the serum block, and reacted with a DyLight 594-conjugated donkey anti-rabbit secondary antibody (711-515-152, Jackson ImmunoResearch Laboratories). The secondary antibody was diluted 1:500 in the serum block. The Evos FL Auto 2 microscope's red fluorescent protein (RFP) channel was used to detect DyLight 594 fluorescence.

2.7.2 Fibronectin

An anti-human fibronectin rabbit polyclonal IgG (H-300, Santa Cruz Biotechnology, Dallas, TX) was used as the primary antibody to detect fibronectin. This antibody was diluted 1:250 in serum block and reacted with a DyLight 488-conjugated goat anti-rabbit polyclonal IgG (35552, Invitrogen, Carlsbad, CA) acting as a secondary antibody. The secondary antibody was diluted 1:500 in the serum block. The Evos FL Auto 2 microscope's green fluorescent protein (GFP) channel was used to detect DyLight 488.

2.8 Quantification of dsDNA

A Quant-iT (Invitrogen) PicoGreen dsDNA kit was used to quantify dsDNA content in native and decellularized porcine lymph node samples. The 20X TE (tris-EDTA) buffer (Invitrogen) was diluted to a 1X working solution using sterile, distilled, nuclease-free water (Qiagen, Hilden, Germany). The Quanti-iT PicoGreen dsDNA reagent (Invitrogen) was diluted to a working volume using the 1X TE buffer and kept wrapped in aluminum foil to avoid photodegradation. It was used within a few hours of dilution. The lambda DNA standard solution (Invitrogen) was diluted to 2 μg/mL in TE

buffer. This stock solution was further diluted to 0, 2, 10, 20, 100, or 200 ng/mL using TE buffer to provide a standard curve. These samples were further diluted by a factor of 2 when combined with 1 mL of reagent to produce final dsDNA concentrations of 0, 1, 5, 10, 50, and 100 ng/mL. Native or decellularized porcine lymph node pieces were massed on a scale (ED124S, Sartorius AG, Göttingen, Germany). These values ranged from 5 to 8 mg. A PRO200 tissue homogenizer (PRO Scientific) was used for 2 minutes at a medium power setting to release dsDNA from the tissue samples within 1.2 mL of TE buffer. Decellularized samples were homogenized first, and the homogenizer was cleaned in sterile, distilled, nuclease-free water between samples to avoid introduction of DNA from one sample to another. A clamshell mini microcentrifuge (USA Scientific, Ocala, FL) was used to spin down samples for 2 minutes and 1 mL of the supernatant was collected for analysis. All samples and standard curve solutions were allowed to incubate with the reagent for 5 minutes prior to data collection. Native tissue samples were in buffer by a factor of 100 to ensure that all read values fell within the standard curve. After mixing, 200 μL of each solution was transferred to a 96-well plate (CELLTREAT) and fluorescence was measured by a Cytation 3 microplate reader (BioTek, Winooski, VT) at an excitation wavelength of 480 and emission wavelength of 520. “Blank” wells containing only TE buffer and reagent provided a means of determining the background signal. Multiple trials were performed at once to minimize the effect of differing incubation times. Native and decellularized tissue samples were prepared in triplicate. Additional native and decellularized tissue samples were weighed, frozen at -80°C in PBS overnight, lyophilized using a Freezone 6 freeze dryer (Labconco) for 24 hours, and weighed again to normalize fluorescence values by the dry weight of the tissues.

2.9 Isolation and quantification of soluble protein

Lyophilized and native porcine lymph node tissue samples were placed on a scale and each adjusted to a mass of 900 mg. A lysate buffer was prepared with 100 mM Tris base (Fisher Scientific), 1 mM ethylenediaminetetraacetic acid (EDTA) (Sigma-Aldrich), 0.1% w/v Triton X-100, 0.5% w/v sodium deoxycholate, 150 mM NaCl, and cOmplete

Mini protease inhibitor cocktail (Roche Diagnostics). The pH of the buffer was adjusted to 7.4 by adding hydrochloric acid (HCl) (Sigma-Aldrich) and measuring with Hydrion pH test strips (Micro Essential Laboratory, Brooklyn, NY). Tissue samples were homogenized in the lysate buffer for 5 minutes using a homogenizer (PRO Scientific, Oxford, Connecticut) on its high-power setting. The final concentration of tissue in the buffer after blade rinses was 15 mg/mL. The mixtures were aliquoted and centrifuged at 4000 rotations per minute (RPM) for 30 minutes. The supernatant was collected and kept at -80°C until analysis. The samples were delivered to the Cytokine Reference Laboratory). A Bradford protein assay was performed to determine the amount of total protein and a Luminex platform-based (R&D Systems) multiplex immunoassay was used to determine the type of soluble protein in each sample. The full list of analytes is present in appendix A.1. This assay was performed as 4 trials for both decellularized and native tissue.

The standard error of each set of native or decellularized samples for a given analyte was calculated using Microsoft Excel. MATLAB was used to calculate the p value of a one-tailed t-test comparing the means of the two sets of data. The alternative hypothesis used for each test was that the mean of the decellularized tissue sample data set was lower than the mean of the native tissue sample data set. The distributions were not assumed to have equal variance. A critical value of $\alpha = 0.05$ was considered for the determination of statistical significance. The low number of data points in each set ($n \leq 4$) contributed to a high degree of variability for the distributions of many analytes. In cases where some of the data points in a set were below the lower limit of quantification (LLOQ) of the immunoassay, these samples were omitted from statistical calculations. In cases where one of the experimental conditions (native tissue or decellularized tissue) produced values above the LLOQ but the other did not, no t-test was performed. Each sample data set was checked for outliers. To do so, Excel was used to check for data points that fell outside of 3 standard deviations from the mean and MATLAB was used to check for data points that fell outside of 3 median absolute deviations from the mean.

2.10 Channel molding

Incubation chamber constructs were 3D-printed using room temperature-vulcanizing (RTV) silicone (American Sealants, Fort Wayne, IN) on a Cellink BioX printer (Cellink). Silicone was printed out of a 27-gauge nozzle (Nordson EFD, Westlake, OH) attached to a 2 mL printing tube (Nordson EFD) at 180 kPa. At 50% completion, the print was paused to place a needle (1.5 cm long, 300 μm outer diameter) across two walls of the construct using tweezers. The needle was slightly impacted into the layer below and the print was finished. The silicone was cured overnight. The middle chambers of the constructs were filled with 48 μL of 10 mg/mL fibrinogen in AIM-V cell medium combined with 12 μL of 10 U/mL thrombin. The gels were incubated overnight at 37°C. At this point, the needles were carefully removed from the gels by pulling them horizontally through the walls of the construct, leaving behind a channel. 2 μL of Trypan blue dye was injected into one end of each channel and pulled through by capillary action. Gels were imaged by phone camera and assessed for patency (see Fig. 2.4).

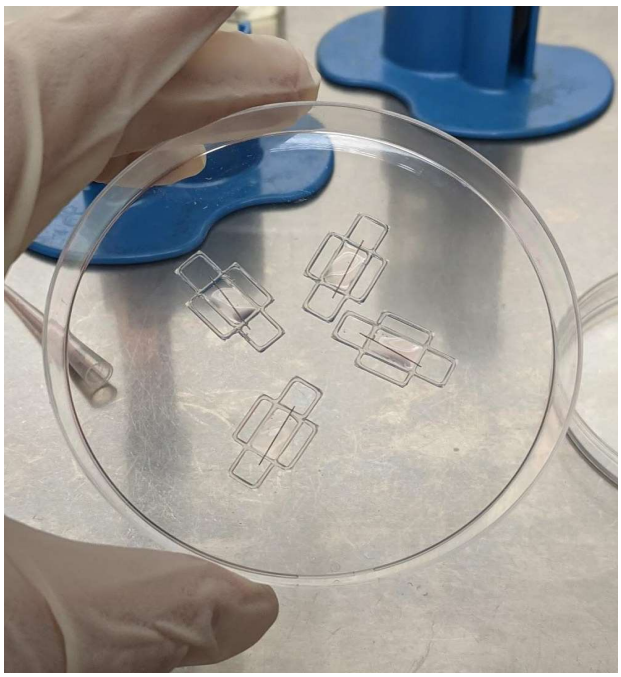

Figure 2.4 60 μl fibrin gels were cast around pins set into the walls of 3D printed silicone constructs. These constructs had a height of 1 mm. The dimensions of the central chamber were 9 mm x 5 mm. The end and side chambers, seen above, were intended for introduction and collection or to supply the gel with a source of additional culture media.

2.11 Statistical analysis

In cases where only two groups of data were compared, a two-sample, one-tailed, independent t-test was performed. The one exception to this was the comparison of PBC viability in fibrin hydrogel cultures with added exogenous laminins to viability in the standard fibrin hydrogel culture without added exogenous laminins (see Fig. 3.3). In this case because the data distributions were overlapping, a two-sample, two-tailed, independent t-test was performed. When comparing a data set to a fixed reference value, a one-sample, one-tailed, independent t-test was performed. When comparing multiple groups of data to each other, a one-way ANOVA was performed to determine whether there existed a significant difference between them. When a significant difference was found, a post-hoc Tukey's honest significant difference (HSD) test was performed to determine which of the data sets were different from each other, by pairwise comparison. Each of the previously described tests were performed using MATLAB. All data points were assessed to be within three standard deviations and three median absolute deviations from the mean and therefore not considered to be outliers. P-values less than 0.05 were considered significant.

3. Results

3.1 PBMC/PBC viability in 3D culture

It has been found that 3D culture often improves the function of cells within tissue-engineered constructs by providing a more biomimetic microenvironment than 2D culture[53]. Hydrogels provide a porous, hydrated material with which to build these constructs and are commonly used in a variety of tissue engineering approaches. With this knowledge in mind, a 3D culture assay was developed with L/D staining to determine which of two commonly used hydrogels, GelMA and fibrin, would better sustain PBMC viability. Cell viability in 10mg/mL fibrin gels was compared to viability in 8%, 10%, and 12% w/v GelMA. It was at first qualitatively determined that fibrin yielded better viability and so an assay comparing fibrin and 5% GelMA was performed. A lower density of GelMA was chosen because qualitative inspection had indicated lower viability in higher density GelMA. Fibrin continued to provide better results and was used as the hydrogel for all future 3D cultures. Another experiment was performed in which the concentration of fibrin gels was varied to determine whether a higher or lower concentration would have a favorable impact on PBC viability.

ECM proteins can be included in 3D cultures to improve viability and function by providing biochemical cues and adhesion peptides. Laminins 411 and 511 are the two predominant laminin isoforms found in the lymphatic vasculature of lymph nodes and ECM and play an important role in cell adhesion and migration[17,19]. These proteins were added to fibrin gels and compared to a laminin-free control. In another attempt to incorporate ECM proteins into 3D culture, porcine lymph node tissue was decellularized, processed, and included in fibrin gels.

As seen in Fig. 3.1, a comparison of the effect of fibrin gel at a concentration of 10mg/mL to GelMA at varied concentrations on the viability of PBMCs in 3D culture revealed that fibrin gel produces better results at both 1 and 3 days. This difference is especially visible after a longer duration of culture. However, due to a lack of multiple trials in all conditions except fibrin and 8% GelMA at the 3-day time point, these were the only two that could be statistically compared. A two-sample, one-tailed, independent

t-test showed that the mean viability of PBMCs in fibrin after 3 days was significantly higher than that of PBMCs in 8% GelMA at the same time point ($p = 0.0028$). Example images of PBMCs in this experiment that were stained and imaged for L/D status can be seen in Fig. 3.4.

Fig. 3.2 displays the result of PBMC viability in 3D culture in fibrin (10 mg/mL) and 5% GelMA at 1 and 3 days. It was determined that mean viability was higher in fibrin at the 3-day time point than in 5% GelMA, per a two-sample, one-tailed independent t-test ($p = 0.0016$). Due to an experimental error, only one 5% GelMA trial could be imaged at 3 days, and so no statistical comparison could be made with fibrin at the same time point. However, the mean viability of PBMCs in fibrin was higher than the viability of PBMCs in 5% GelMA in that trial. Similar to the previously discussed experiment, it appears that the difference in PBMC viability as a consequence of gel choice increases over time. Images of L/D PBMCs can be seen in Fig. 3.5.

Additional studies were done to attempt to improve the viability of PBCs in fibrin 3D cultures, as the generally accepted value for good viability in 3D bioprinted, hydrogel constructs for tissue engineering is 80%. Processed ECM was included, as previously described, but the ECM itself became stained by the ethidium homodimer-1 and obscured large segments of each image (see Fig. 3.7). For this reason, this assay was discontinued, and no viability data was collected. The results that were produced by varying fibrin gel concentration and adding soluble laminin proteins (laminins 411 and 511) are displayed in Fig. 3.3. Adding laminins to 10 mg/mL fibrin gels decreased viability at both 1- and 3-day time points, counter to its expected effect. A t-test confirmed that the mean viability of PBCs in gels with laminin was significantly less than those without after 1 day of culture ($p = 0.0019$), although the difference was not significant after 3 days ($p = 0.4608$). A one-way ANOVA was chosen to determine whether changing fibrinogen concentrations in fibrin gels had a significant effect on PBC viability. It was found that this was the case in gels that were imaged after 1 day of culture. Post-hoc analysis using Tukey's HSD test revealed that the highest concentration (20 mg/mL) produced a significantly lower mean viability than the standard and lower concentrations (10 mg/mL ($p = 0.0102$) and 5 mg/mL ($p = 0.0028$), respectively). There was no significant

difference in mean viability between standard and low concentrations ($p = 0.4210$) One-way ANOVA did not detect a significant difference from varied concentration after 3 days of culture ($p = 0.1136$), which may be due to a higher variance in viability in these trials. Fig. 3.6 contains example images of L/D stained PBCs for this experiment.

Other parameters were changed over the course of viability experimentation that were not directly tested with controlled comparisons but may have led to an increase in PBC viability. Earlier experiments had a lower seeding density than later ones (from 250,000/mL in the fibrin vs. varied GelMA concentration assay to 20 mil/mL in the assay with varied fibrinogen concentration and addition of laminins), which could have resulted in the overall improvement of viability that can be seen in Fig. 3.6. Additionally, the method of obtaining cells changed from separating left-over PBMCs from microbeads to separation of PBCs directly from peripheral blood that had been drawn only hours before use of these cells. The lower time in between isolation and use could have caused less stress to these cells and improved their viability in culture. Furthermore, the assay in which fibrinogen concentration was varied was performed using the same volume as previous experiments but in a 24 well plate instead of a 48 well plate. This resulted in a thinner gel, effectively reducing the distance of diffusion for media-based nutrients to reach the cells. Finally, in this last experiment, the culture media was changed every 24 hours to avoid the depletion of nutrients in the culture over time.

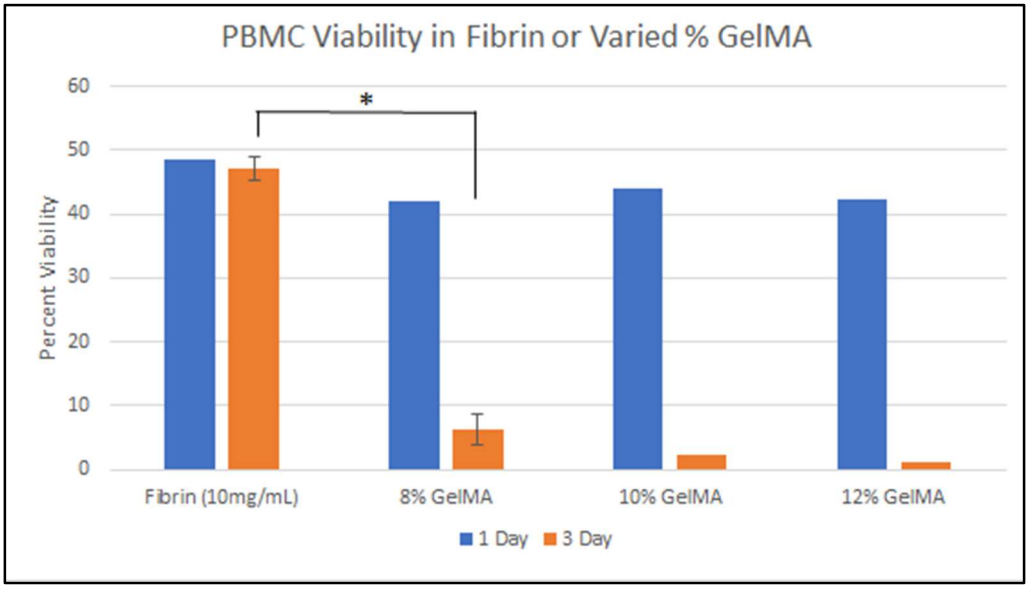

Figure 3.1 PBMC viability mean values after 1 or 3 days in fibrin gels or gelatin methacrylate gels of varied density. The 3-day viability means for fibrin and 8% GelMA were different to a statistically significant degree, with fibrin producing higher viability. Group bars without error bars contained only one sample, n = 2 for all other groups.

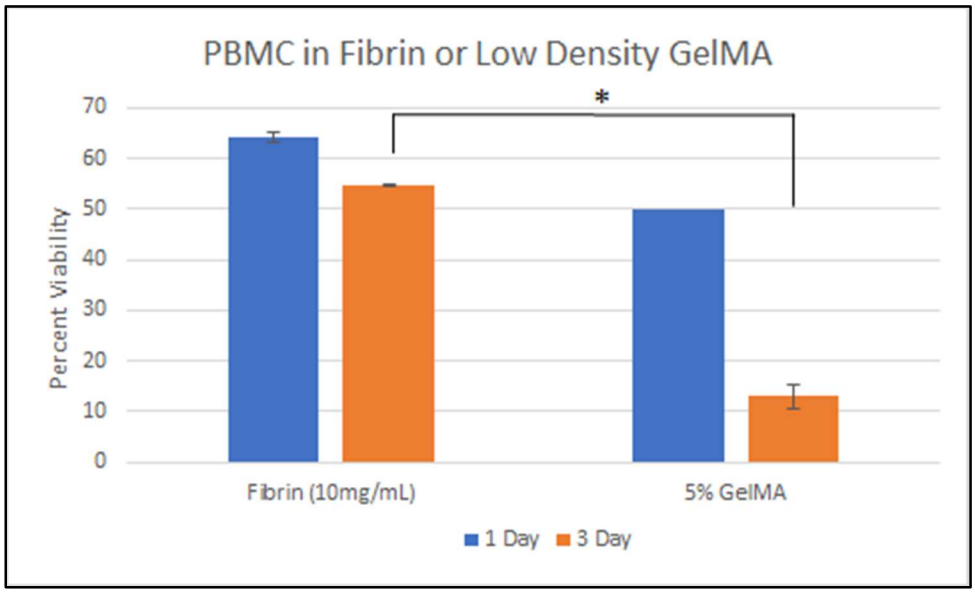

Figure 3.2 PBMC viability mean values after 1 or 3 days in fibrin gels or 5% gelatin methacrylate gels. The 3-day viability means for fibrin and 5% GelMA were different to a statistically significant degree, with fibrin producing higher viability. Group bars without error bars contained only one sample, n = 2 for all other groups.

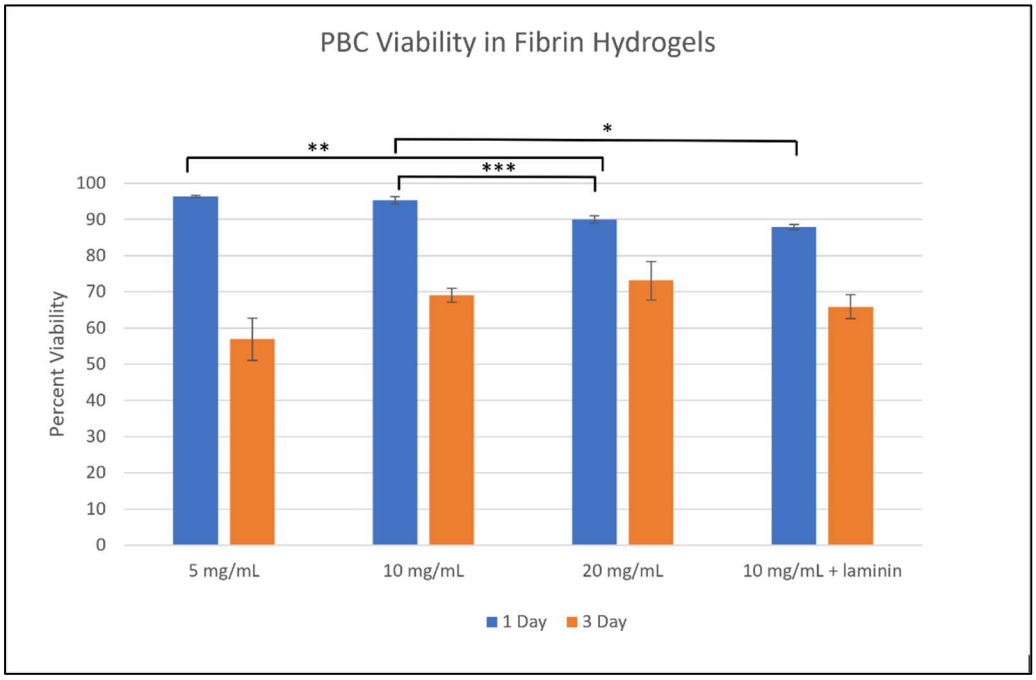

Figure 3.3 PBC viability mean values after 1 or 3 days in fibrin gels of varied concentrations and with or without the addition of exogenous laminins 411 and 511. Brackets with stars indicate viability means that are different to a statistically significant degree. All group bars represent the mean viability of multiple trials (n=3).

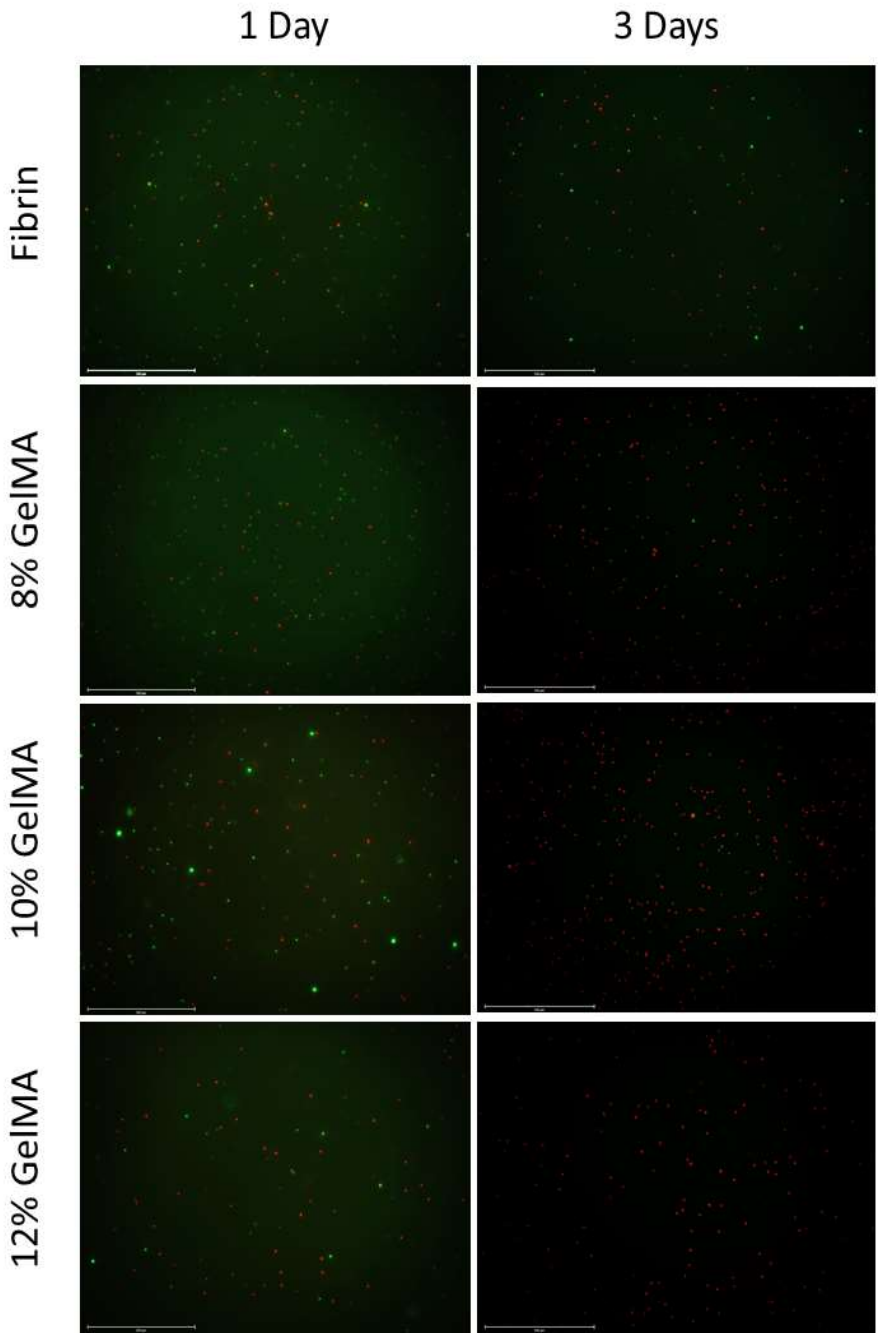

Figure 3.4 PBMCs in fibrin gels or gelatin methacrylate gels of varied concentration. Stained and imaged for L/D (green = live cells, red = dead cells) after 1 or 3 days of culture. Scale bars = 500 μm.

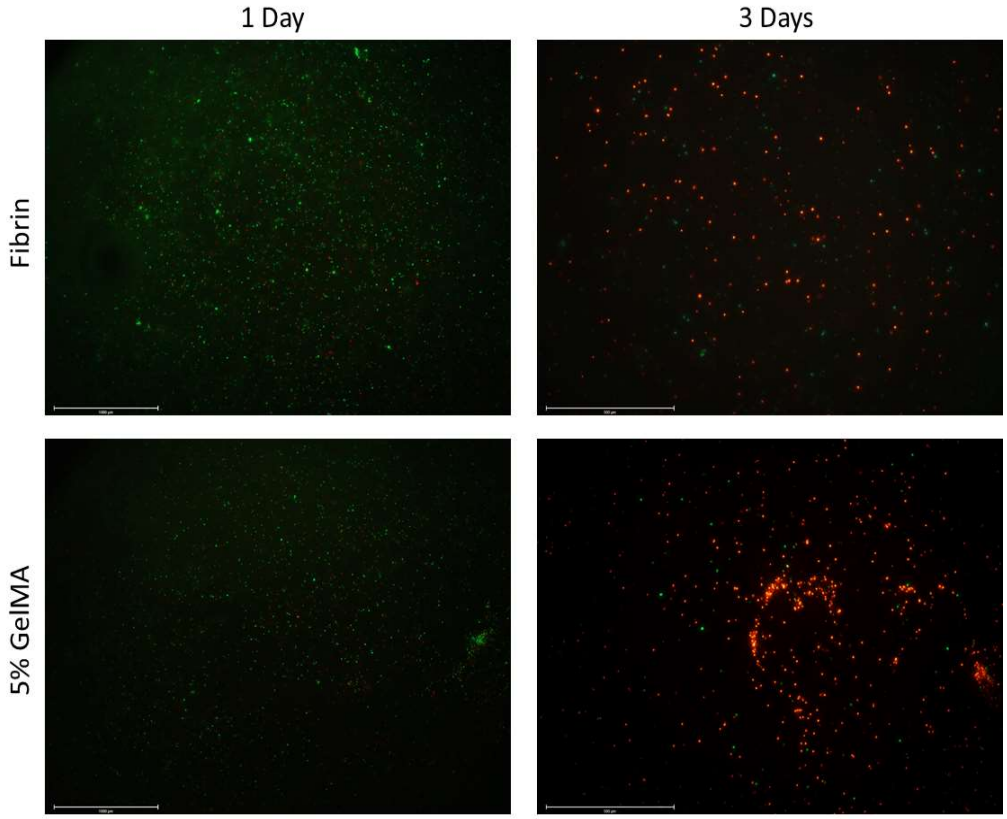

Figure 3.5 PBMCs in fibrin or gelatin methacrylate gel. Stained and imaged for L/D (green = live cells, red = dead cells) after 1 or 3 days of culture. Scale bars = 500 μm.

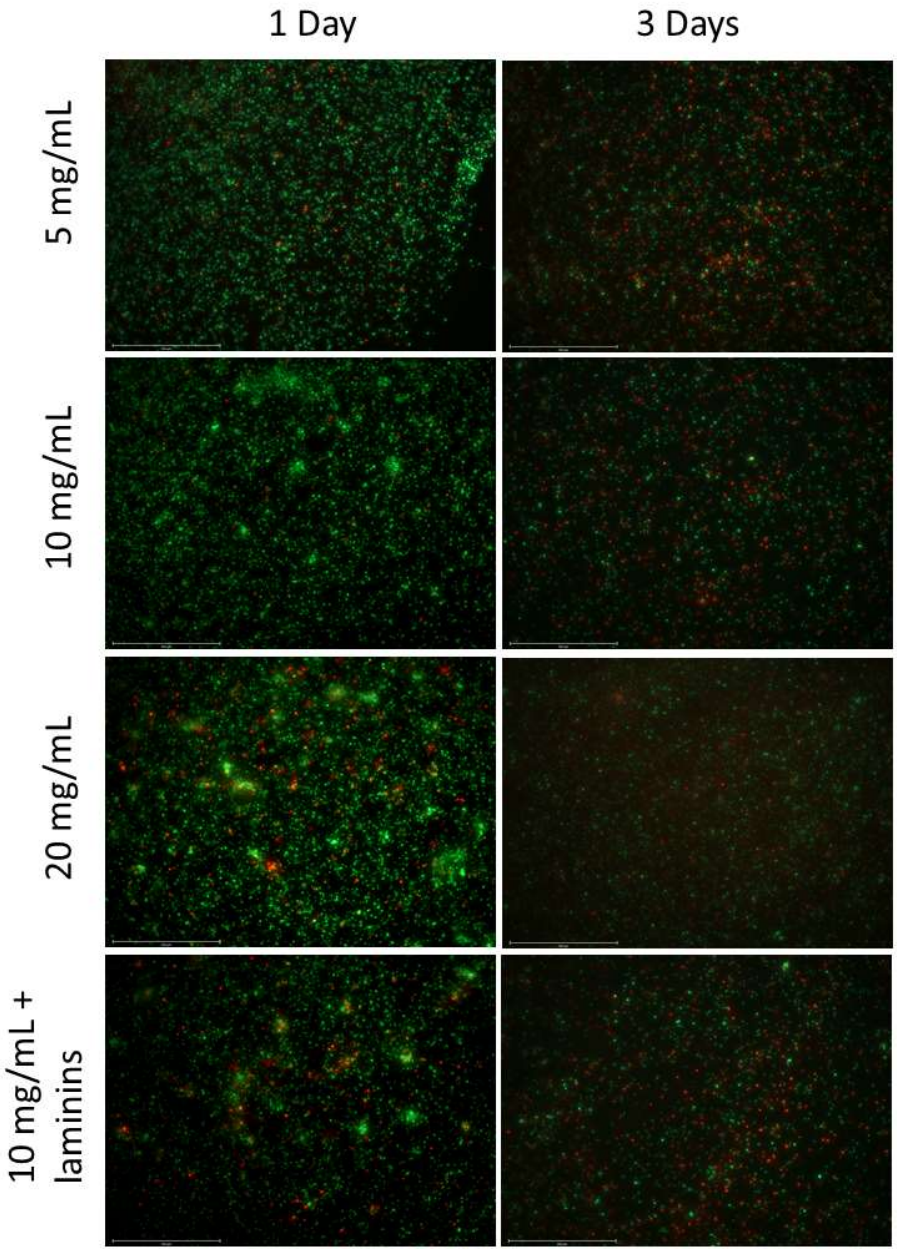

Figure 3.6 PBCs in fibrin gel of varied concentration, with or without the addition of exogenous laminins (411 & 511). Stained and imaged for L/D (green = live cells, red = dead cells) after 1 or 3 days of culture. Scale bars = 500 μm.

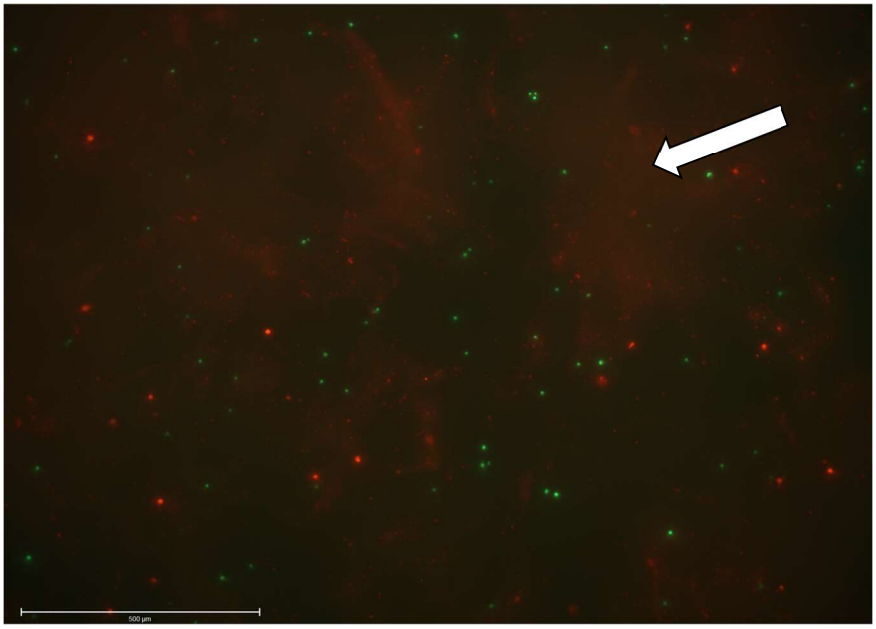

Figure 3.7 PBCs in fibrin gel containing decellularized, processed porcine lymph node ECM. Stained and imaged for L/D (green = live cells, red = dead cells) after 1 day of culture. Lymph node ECM is visible as faint, diffuse, red areas surrounding PBCs (see arrow). Scale bar = 500 μm.

3.2 Quantity of dsDNA in native and decellularized tissues

To avoid immunorejection, it is important to remove xenogeneic genetic material from tissues that are intended to be used as part of a tissue-engineered construct that is intended for *in vitro* use with human cells or for implantation[29]. In this case, porcine genetic material needed to be removed from porcine lymph node ECM that could then be included in a lymph node model containing human immune cells. The decellularized ECM provides key biomechanical and biochemical signals that can be difficult or expensive to obtain from other sources. Among the widely accepted criteria that define sufficient decellularization is the requirement that the decellularized tissue contain less than 50 ng of dsDNA per mg (dry weight) of ECM[29]. For these reasons, the dsDNA content of decellularized porcine lymph node tissue was quantified using a PicoGreen assay. Native porcine lymph node tissue samples provided a positive control for this experiment.

The assay was performed multiple times using the standard, a blank well with no reagent, three decellularized tissue samples, and three native tissue samples. The standard ladder was changed to include the following concentrations of dsDNA: 100 ng/mL, 50 ng/mL, 10 ng/mL, 5 ng/mL, 1 ng/mL, and 0 ng/mL. Furthermore, in subsequent analysis of the data, the fluorescence output of the 0 ng/mL standard well (essentially, the background signal) was subtracted from all output values in each trial. Due to concerns about contamination of decellularized samples due to carryover from the homogenizer, a cleaning procedure was developed to be performed in between the processing of each sample (see section 2.8). Lyophilization of another decellularized sample was performed to determine the dry weight of the ECM as compared to its wet weight.

The 0 ng/mL fluorescence output was subtracted from each fluorescence value for the standard and samples. The standard values were plotted in Excel (fluorescence vs. known concentration of dsDNA) with a linear fit ($R^2 = 0.9997$). The linear function was used to calculate the dsDNA concentration of all samples. The mass of the tissue from which each sample was extracted was converted to a concentration (mg/mL) based on the constant solvent volume used for each extraction. The concentration of dsDNA was divided by the tissue concentration to produce a value with units of ng/mg (nanograms of dsDNA per milligram of wet tissue). The mean value and standard error for each condition was calculated and a two-sample, one-tailed, independent t-test determined that the native tissue samples contained significantly more dsDNA than the decellularized tissue samples (see Table 1). The ratio of wet weight to dry weight for decellularized tissue, determined by lyophilization, was used to convert each decellularized sample's units to nanograms of dsDNA per milligram of dry ECM. The mean and standard error of these values were calculated. A one-sample, one-tailed t-test found that the decellularized samples contained significantly less dsDNA than the accepted maximum limit of 50 ng/mg (dsDNA to dry weight ECM), indicating that this criterion for decellularization was met. These results are displayed in Table 2.

Table 1. Mean DNA Content of Tissue Samples

Native Porcine Lymph Node	156.5 ± 48.9* (ng dsDNA/mg tissue [wet weight])
Decellularized Porcine Lymph Node	1.0 ± 0.2* (ng dsDNA/mg tissue [wet weight])

* It was determined that the value in the upper row is significantly greater than the value in the lower row by using a one-tailed, independent, two-sample t-test. The result of this test was that $p = 0.0049$ ($\alpha = 0.05$).

Table 2. Mean DNA Content of Decellularized Tissue Sample Compared to the DNA Content Reference Criteria for Tissue Decellularization

Maximum DNA Content Criteria	50.0* (ng dsDNA/mg tissue [dry weight])
Decellularized Porcine Lymph Node	9.0 ± 1.9* (ng dsDNA/mg tissue [dry weight])

*It was determined that the value in the upper row is significantly greater than the value in the lower row by using a one-tailed, one-sample t-test. The result of this test was that $p = 1.9222 \times 10^{-6}$ ($\alpha = 0.05$).

3.3 Collagen and cellular content in native and decellularized tissues

The process of decellularization, while necessary to remove native genetic material to avoid immunorejection, has the potential to degrade ECM proteins. As mentioned previously, these proteins provide important biochemical and biomechanical signals to cells that can aid in maintaining viability and function. In particular, collagen forms a structural basis for the lymph node and contains bioactive domains that enable cellular adhesion and migration. For these reasons, it was decided that hematoxylin and eosin (H&E) as well as Masson's trichrome staining would be used to evaluate the matrix integrity and presence of collagen in native and decellularized porcine lymph node tissue sections. Furthermore, the hematoxylin used in H&E and the Weigert's hematoxylin that

was a part of the chosen formulation of Masson's trichrome were used to visualize the presence of cells in these sections.

H&E and Masson's trichrome staining were done on O.C.T.-embedded tissue samples. Whole, native porcine lymph node sections were used to provide a positive control to compare visually with decellularized sections. Imaging was done at multiple magnifications to observe tissue structures of various sizes and to determine whether the impact of decellularization had spatial variation.

Images were visually compared for the quantity and density of collagen, which was stained pink in H&E slides and blue in Masson's trichrome slides. In Fig. 3.8, it is apparent from panel **d** that collagen of significant quantity and density is present in decellularized porcine lymph node tissue. Cells can be observed in panels **a** and **c,** which correspond to the native lymph node section at different magnifications. Comparing this with the two panels on the right, it is clear that decellularization thoroughly removed cells from the ECM, as intended. These findings are corroborated by Fig. 3.9, in which cells are also visible (in dark brown dye) in the left two panels that display native tissue but are not present in the decellularized tissue displayed on the right. Furthermore, the collagen fibers that are shown (in blue) in panels **b** and **d** are dense and intertwined. It is difficult to determine whether the overall amount and density of collagen fibers is decreased by decellularization, but it is apparent that decellularized porcine lymph node tissue retains a significant amount of this ECM. This is consistent with what has been reported by our lab for the decellularization of porcine lung tissue[30]. It should be noted that the eosin component of H&E (the light pink dye) can also stain elastic fibers, which are present in the lymph node ECM, although in lesser abundance than collagen[54]. It should also be noted that these stains do not identify specific types of collagen, and that an analysis of the impact of decellularization on them separately would require a different approach.

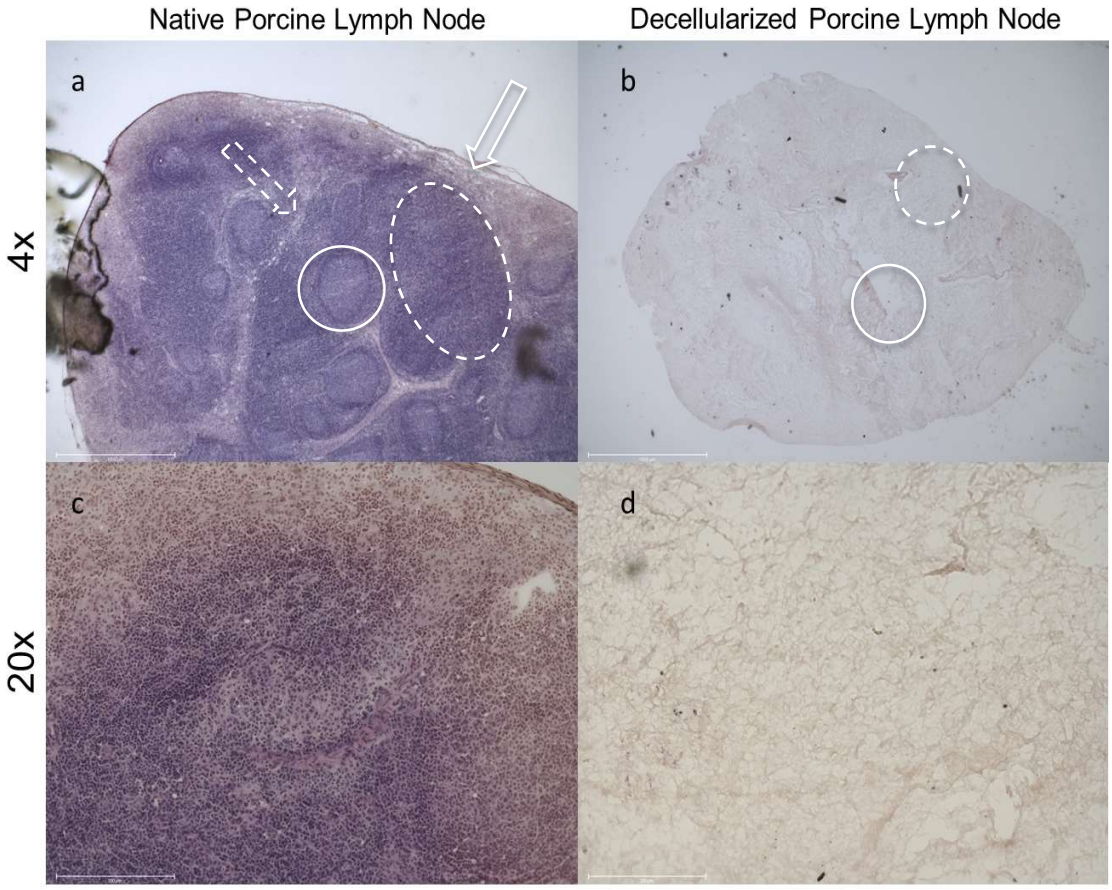

Figure 3.8 Brightfield images of tissue sections stained with H&E. In panel **a,** solid circle shows follicle, dashed circle shows paracortex, solid arrow shows capsule and SCS, and dashed arrow shows trabecula (afferent vasculature). In panel **b,** sold circle shows the central vein and dashed circle shows an arteriole. Tissue type and magnification are displayed on the top and left sides of the figure. For 4x, scale bars = 1000 µm; for 20x, scale bars = 200 µm.

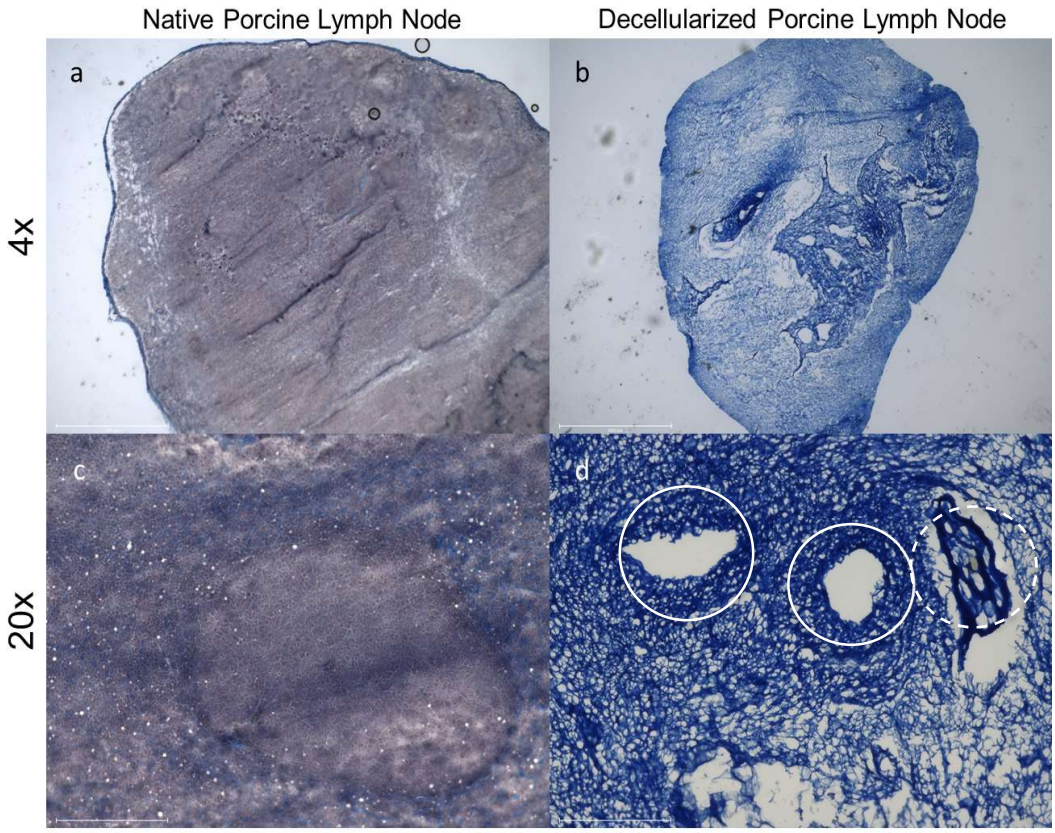

Figure 3.9 Brightfield images of tissue sections stained with Masson's Trichrome. Collagen and connective tissue are in blue and cells are in dark gray. Tissue type and magnification are displayed on the top and left sides of the figure. Solid circles indicate vessels and dashed circle indicates artery. For 4x, scale bars = 1000 µm; for 20x, scale bars = 200 µm.

3.4 Laminin and fibronectin in native and decellularized tissues

For reasons mentioned in section 3.4, it is ideal to preserve ECM proteins while decellularizing tissue. Several isoforms of laminin are found in lymph node ECM and have been shown to impact immunological function. Isoforms 332, 411, and 511 are among the most prevalent of these. To determine whether laminin content and structure was preserved in decellularized porcine lymph node tissue, IHC staining was performed on tissue sections. Initially, three different primary antibodies were selected to detect the presence of different laminin isoforms, most notably laminins 332, 411, and 511.

Due to poor fluorescent signals from the antibodies that were selected to detect laminin alpha chains α3 and α4, the results of those experiments are not shown. It is likely that the dilution of the primary and/or secondary antibodies would need to be optimized to provide better results. It should be noted that the immunogen from which the anti-laminin rabbit polyclonal IgG used to detect laminin isoforms in this experiment was produced (see section 2.8.1) was laminin from basement membrane tissue of Engelbreth Holm-Swarm (EHS) mouse sarcoma. The laminin isoform purified from EHS sarcoma is laminin 111, which, although distinct from other isoforms in its entire structure, shares β and γ chains with some of them (notably 411 and 511, but not 332)[55]. For this reason, these antibodies have the potential to bind to a variety of laminins, but not necessarily all that are important to the function of immune cells within the lymph node[55]. In future studies, specific isoforms of laminin could be detected by using and optimizing the dilution of primary antibodies that bind to specific alpha chains.

Product information for the primary antibody showed that it has been validated as having species reactivity with human laminins but not porcine laminins. As the tissue being decellularized and analyzed was porcine, it was decided that to determine whether or not there was a loss in signal due to differences in species reactivity, human lymph node sections were to be used as a positive control. Sections stained with only secondary antibodies and unstained sections were used as negative controls to detect non-specific staining and autofluorescence, respectively.

Fibronectin was chosen as another key ECM component to detect via IHC due to its prevalence in lymph node tissue and roles in promoting cellular adhesion and migration. The anti-human fibronectin rabbit polyclonal IgG primary antibody that was chosen to detect fibronectin was validated for use in IHC, according to product information. It is specific to human fibronectin and therefore warranted the use of a similar comparison with human lymph node tissue. Similar negative controls were used.

From the tissue sections that were stained with primary antibodies reactive to laminins of multiple isoforms (see Fig. 3.10), a clear fluorescent signal was obtained in human, native porcine, and decellularized porcine lymph node sections. There does not appear to be a loss of signal due to interspecies differences or due to decellularization. In

fact, the signal obtained by imaging decellularized tissue appears to be stronger than in the other cases. It may be that decellularization exposes laminin domains that are bound to cells in native tissue, resulting in a greater total number of bound antibodies and a stronger signal. A look at Fig. A.2.1 in Appendix A.2 to compare this result with its negative controls confirms that the fluorescent signal is highly specific.

Fig. 3.10 also displays the results of incubating human, native porcine, and decellularized porcine tissue sections with antibodies against human fibronectin. Here, it is clear by comparing panels **a** and **b** that there is a significant difference in signal strength between human and porcine samples, indicating that the primary antibody used for this assay has higher affinity for human fibronectin. Even so, it can be observed by comparing panels **b** with the negative control images in Fig. A.2.2, Appendix A.2, that there is a specific signal associated with native porcine tissue. This signal is mostly lost in decellularized sections, indicating that this process results in a loss of binding sites for this antibody.

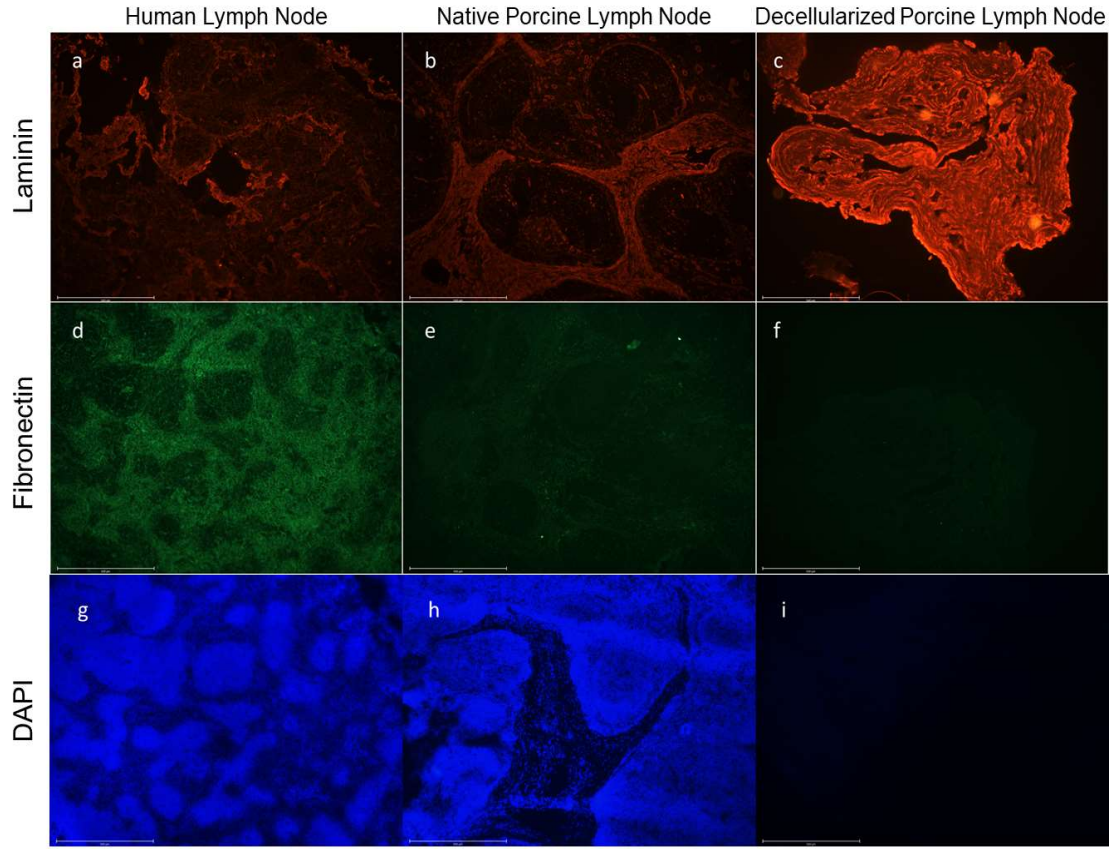

Figure 3.10 Fluorescence images resulting from IHC antibody staining to detect laminin and fibronectin, and DAPI counterstaining to detect nuclear material. The type of tissue section is displayed at the top of each panel column. All scale bars = 500 μm.

3.5 Nuclear material in native and decellularized tissues

In addition to the criterion that decellularized tissue contains less than 50 ng of dsDNA per mg of dry ECM, it is accepted that nuclear material should not be visible in decellularized tissue sections when subjected to a DAPI stain[29]. DAPI is a popular nuclear stain due to its ability to bind to adenine-thymine regions of dsDNA and emit a fluorescent signal[56].

During the process of detecting specific ECM proteins in native and decellularized porcine lymph node tissue through IHC, each section was also imaged to observe the presence of nuclear material via DAPI counterstain. In Fig. 3.10, it can be

seen that the native porcine section contains bright blue dots distributed throughout the tissue, indicating the presence of cells. On the other hand, the decellularized section lacks specific DAPI staining and, by extension, significant cellular content. This upholds additional criteria for sufficient decellularization of these tissues.

3.6 Cytokines in native and decellularized tissues

Soluble growth factors and cytokines that are sequestered in porcine lymph node tissue could serve to improve leukocyte viability and function in an *in vitro* human lymph node model. A protein extraction assay was performed to determine whether certain porcine growth factors and cytokines remained within porcine lymph node tissue after decellularization. Soluble protein content in decellularized samples was compared to that of "native" (not decellularized) porcine lymph node tissue to observe changes due to decellularization. A panel of human analytes was used to perform a Luminex multiplex immunoassay in the Cytokine Reference Laboratory. Although the proteins contained in the tissue samples were porcine in origin, it was decided that they might have a suitable degree of homology to the equivalent human sequences to be detected by the immunoassay and provide beneficial signals to human leukocytes in 3D culture. A Bradford assay yielded the total protein concentration in each sample while the immunoassay determined specific analyte concentrations in each sample. In some cases, the concentration of a specific protein in the sample was too low for detection. The analytes included in the panel are listed in appendix A.1.

The total protein values from the Bradford assay were used to normalize the analyte concentration results in each sample (see Tables 3 and 4). Four samples of both decellularized and native tissue were prepared to assess variability and develop more reliable statistics.

In general, it appears that decellularization of porcine lymph node tissue decreases the relative amount of growth factors and cytokines present (see Table 3). In many cases, a given analyte was detectable before decellularization but not after. In others, namely

fibroblast growth factor 2 (FGF2), the beta subunit of interleukin 12 (IL-12p40), interleukin 1 beta (IL-1β), and interferon gamma-induced protein 10 (IP-10), the decrease in relative amount of the protein after decellularization was statistically significant. The comparison of the other analytes displayed in Table 3 did not indicate a statistically significant decrease in concentration from decellularization. The single exception to the categories previously mentioned is the case of the relative amount of vascular endothelial growth factor (VEGF). The data indicate that an amount of VEGF that exceeded the detection limit was present in decellularized samples but not in native ones. It should be noted that, in cases in Table 3 where standard error is not displayed with the mean values, there was only one sample with a result that was above the LLOQ.

Table 3. Bradford Assay Results for Total Protein in Native and Decellularized Porcine Lymph Node Tissue Samples

Mean Total Protein Concentration in Native Tissue Samples	Mean Total Protein Concentration in Decellularized Tissue Samples
0.12 ± 0.03 mg/mL	0.26 ± 0.07 mg/mL

Table 4. Luminex Multiplex Immunoassay Results for Analyte Concentration in Native and Decellularized Lymph Node Tissue Samples

Analyte	Native Tissue Sample Mean Concentration (pg/mg total protein)	Decellularized Tissue Sample Mean Concentration (pg/mg total protein)	T-test P value (α=0.05)
FGF-2	61677.27 ± 14570.99	2771.95 ± 555.19	0.0034
TGF-α	23.00 ± 6.88	<LLOQ	n/a
FLT-3 ligand	567.23 ± 180.06	<LLOQ	n/a
GM-CSF	11.88	<LLOQ	n/a

IFNα2	24558.86 ± 14161.22	266.99 ± 48.96	0.0685
IL-10	10.19 ± 3.43	<LLOQ	n/a
IL-12p40	346.65 ± 95.06	115.14 ± 29.65	0.0295
IL-13	31031.60 ± 16514.19	115.11 ± 38.83	0.0552
IL-15	28.47 ± 8.13	<LLOQ	n/a
IL-17A	14.40 ± 4.12	7.47 ± 2.06	0.1790
IL-9	31.29 ± 8.21	17.78 ± 3.79	0.0928
IL-1β	18.48 ± 4.27	6.81 ± 1.71	0.0222
IL-2	5.50 ± 2.39	<LLOQ	n/a
IL-3	2.34 ± 0.85	2.04 ± 0.54	0.3842
IL-6	7.10	<LLOQ	n/a
IL-7	13.91 ± 9.29	<LLOQ	n/a
IL-8	6.49 ± 1.14	<LLOQ	n/a
IP-10	62.18 ± 13.65	29.24 ± 3.04	0.0500
VEGF	<LLOQ	2511.87 ± 497.80	n/a

3.7 Channel development in hydrogels for vascularization

LECs form the lining of lymphatic vessels and perform a variety of signaling functions that enable the migration of immune cells and the uptake of pathogenic antigens. A functional human lymph node model requires lymphatic vasculature both for biomimetic functionality and as a way of introducing molecules or cells for experimentation. In a study by Meng et al., published in 2019, channels were created for subsequent endothelialization by pulling pins from a fibrin hydrogel-containing silicone structure[57]. Endothelial cells were introduced to the space left behind via injection and capillary action[57]. Furthermore, VEGF was placed within the hydrogel to promote vessel sprouting and thereby vascularize the 3D culture for improved viability and function[57].

This same approach could be used to vascularize an *in vitro* lymph node model using LECs.

Silicone constructs were printed as previously described in section 2.10. The model was designed based on dimensions used in the study by Meng et al., but modified for the desired application by changing the configuration of the chambers. Optimal printing parameters were chosen by varying print speed, infill density and pattern, and layer height and visually observing the structural integrity of the resultant constructs. Varying volumes of fibrinogen were pipetted into these constructs to determine the minimum volume that would provide even coverage of the space. This was determined to be 60 μL. The initial concentration of thrombin used in these gels was 0.5 U/mL. The mixture was pipetted thoroughly and incubated at 37°C for 30 minutes. The gels were inspected at this time and found to still be liquid at their centers, with a crosslinked, firmer shell around them. They were allowed to incubate for an additional 90 minutes, without significant changes. The concentration of thrombin was changed to 1 U/mL or 2 U/mL for an additional two sets of gels. These were incubated overnight. It was observed that the 1 U/mL gels still failed to solidify sufficiently. The 2 U/mL gels appeared to be much firmer and were selected to have the pins were removed from them. It is unclear why the initial concentration of thrombin (0.5 U/mL) did not gel sufficiently or why a much longer incubation period was required, because the reference study used this concentration and observed rapid gelation with it[57]. One possibility is batch variation in thrombin, but solutions from two different shipments were used in this screening test, and there was no obvious difference in gelation time. Figure 3.11 displays the result of the attempt to perfuse the channels with Trypan blue, per the method described in section 2.10. Trypan blue was chosen for its high color contrast with the fibrin gel, allowing clear visualization of the degree of perfusion and patency of the channels.

Of the four gels that were prepared, only one contained a fully perfusable, well-defined channel (see Figure 3.11, circled). The others contained channels that partially collapsed. It was observed that in some of these cases, the action of pulling the pin from the construct appeared to apply stresses to the gel itself that pulled it away from the

silicone walls and possibly caused tearing within the gel itself. This may have left spaces for dye to flow into, without following the course of the channel. A visual indication of this result may be the sections of gel in which the dye is not contained in a well-defined space and appears to have “bled” into other portions (see Figure 3.11, arrow). It is worth noting that when perfusion was not achieved from injection of the dye at one end of the channel, it was attempted from the other end, resulting in the presence of dye at both channel openings.

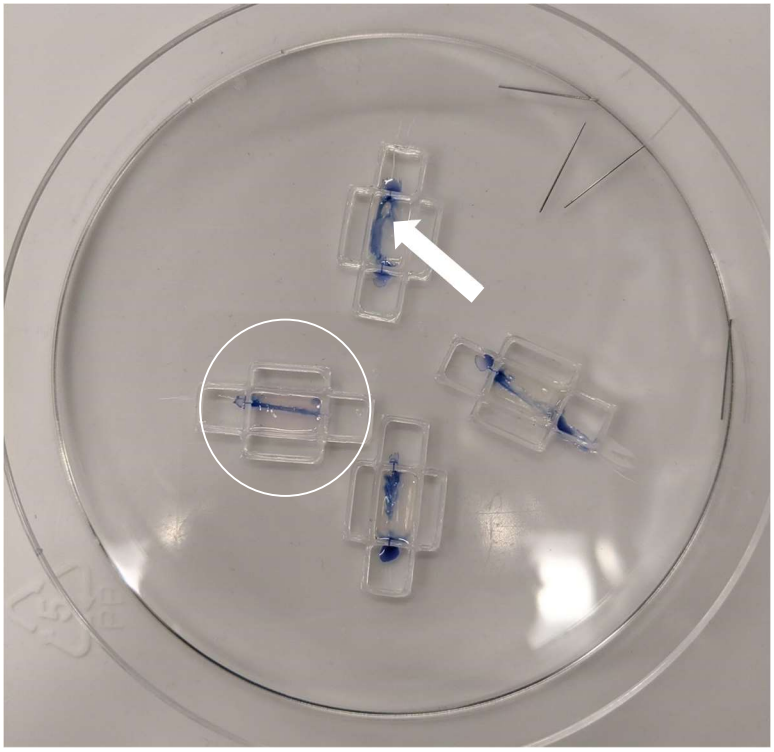

Figure 3.11 Silicone constructs containing fibrin gels from which pins have been removed and the resultant channels perfused with Trypan blue dye. The circled construct contains a well-defined, fully perfused channel. The white arrow indicates a section of gel with diffuse dye distribution that lacks well-defined borders.

4. Discussion

4.1 Fibrin hydrogels provide a promising 3D scaffold for PBMC/PBC culture but can be further optimized

As previously stated, hydrogels provide an effective means of 3D culture in the form of a porous, hydrated, and modifiable microenvironment. Comparisons of PBMC viability in fibrin and GelMA hydrogels after 1 and 3 days were made to determine which material would better support an *in vitro* lymph node model. Viability analysis was somewhat limited in that cell counting was performed manually and was therefore subject to a degree of human error. An initial attempt to use ImageJ to automate the process and limit bias failed due to L/D stain background noise, dense cell clustering, and the irregularity of apparent cell size from imaging out-of-focus cells whose focal planes were not included in the chosen z-stack. These issues could be partially addressed in future studies by casting thinner gels of more consistent thickness and optimizing the duration of L/D stain incubation to limit background noise while brightly staining cells.

It was determined that fibrin maintains PBMC viability better than GelMA of any of the chosen concentrations, especially at longer culture durations (see Figs. 3.1 and 3.2). While the difference is only statistically significant at 3 days when comparing fibrin to 5% and 8% GelMA, this is likely due to experimental errors that resulted in single trials of certain conditions such that no population variance could be assessed. To strengthen these results, it would be necessary to repeat these experiments with several trials of each condition and time point. However, the stark differences that do exist between the viabilities assessed for each gel type after 3 days of culture indicate that fibrin is more capable of supporting PBMCs. This may be due to the engagement of fibrin with leukocyte integrin Mac-1, expressed by monocytes, dendritic cells, NK cells, and some subsets of B and T lymphocytes[58,59]. CD11d, another leukocyte integrin that is similar to Mac-1 and expressed by monocytes, NK cells, B cells, and some T cells, also binds to fibrin[60]. These binding events, in addition to cellular surface integrin interactions with the RGDS and γ-chain AGDV binding motifs contained in fibrin, may impart fibrin with an overall greater bioactivity with regard to PBMCs[61]. While fibrin has not been a

popular choice of hydrogel in studies regarding attempts to engineer lymph nodes or other peripheral lymphoid organs (see section 1.4), Ferreira et al. used fibrin gels to support the proliferation of hematopoietic stems cells and multiple other studies have shown that fibrin gels can support significant lymphangiogenesis with LECs[62,63,64,65].

After deciding on fibrin as the base hydrogel material for continued assays, an experiment was conducted to assess the effect of varied fibrinogen concentrations on PBC viability. The addition of laminins 411 & 511 was also compared to a control as these were expected to improve viability by providing binding motifs and key signals to the lymphocytes within. PBCs within 20 mg/mL fibrin gels had significantly lower average viability after 1 day of culture than those in 5 and 10 mg/mL fibrin gels (see Fig. 3.3). Despite this, PBCs in the higher concentration gels maintained a higher average viability over 3 days of culture. This difference was not significant, likely due to the higher variance in viability after 3 days. This experimentation could be repeated with more trials to achieve higher statistical power and possibly detect significant differences. While the trends remain mostly unclear, the lower viability in high concentration gels after 1 day of culture may be due to decreased diffusion of nutrients through the gel and this disadvantage may be removed over time due to ECM remodeling. In opposition to expectations, the PBCs in fibrin gels that were supplemented with laminins had a significantly lower average viability after 1 day of culture (see Fig. 3.3). In addition to laminin 511 promoting adhesion and migration in lymphocytes, both isoforms also play a role in T cell proliferation and activation[19]. It is possible that increased T cell proliferation in these hydrogels was not sufficiently supported by the nutrient supply, leading to pockets of cell starvation and death. To better understand the dynamics of leukocyte proliferation and death in fibrin gels, a combination 3-(4,5-dimethylthiozol-2-yl)-2,5-diphenyltetrazolium bromide (MTT) and lactate dehydrogenase (LDH) assays (see section 4.4 for more detail) could be performed. Alternatively, hydrogels could be fixed, sectioned, and subjected to anti-Ki67 IHC, as this protein is a marker of cell proliferation and has been used to detect the proliferation of lymphocytes[66]. Finally, the hydrogels could simply be subjected to L/D staining multiple times over the culture duration, and imaged in specific, consistent locations to detect proliferation and cell

death. One concern with this approach is the need to accurately track cells, requiring an imaging location with set boundaries to distinguish between the contribution of migration and proliferation to cell counts. It is also possible that imaging would have to be performed more often to identify migratory and proliferative behavior. It should also be noted that the change from using PBMCs to using PBCs during experimentation introduced new cell populations, namely granulocytes. Because cell viability was assessed as a whole, it is not clear whether some cell populations were better maintained than others over time or with changes in hydrogel type and density. Future studies would benefit from assays in which cells are separated by phenotype after culture and population viabilities are assessed individually (see section 4.6 for more detail).

Some changes were made between viability assays that were not strictly controlled for or directly compared, but which may have made a positive impact on leukocyte survival. For one, higher seeding densities were implemented in later assays due to changes in PBMC/PBC acquisition methods that led to higher cell numbers. This may have resulted in the relatively higher viability of PBCs in Fig. 3.3, as opposed to Figs. 3.1 and 3.2, due to cell-cell signaling that promotes survival. On the other hand, a high seeding density can lead to an oxygen consumption rate that exceeds the transport of oxygen through the hydrogel and leaves some areas hypoxic[67]. To be sure that this change improved viability, further tests would need to be performed in which all other conditions are held constant while seeding density is varied. Furthermore, this experiment used the same volume (220 μL) as previous assays, but in a 24-well plate instead of a 48-well plate. This resulted in thinner gels with lower diffusion distances for nutrients from culture media. Again, this change would be to be directly compared to thicker gels to confirm its impact. One assay (not presented here) was done with 22 μL gels, but these small volumes were deposited as droplets with radii that did not appear significantly smaller than the thickness of larger volume gels that spread across the well. Furthermore, qualitative inspection of PBC viability after 1 day of culture did not reveal obvious improvements, and so this approach was not continued in later assays because larger volumes were easier to work with and facilitated a more even distribution of PBCs. It is clear from observing the results of these viability experiments that all conditions suffer

serious decreases in leukocyte viability over time. Purwada et al. maintained B cells for 6 days in 10 μL static gel culture whereas Sardi et al. maintained lymphocytes for 21 days in a perfusion bioreactor[41,68]. For this reason, future studies would likely need to find a way to implement far smaller volumes or the use of a bioreactor to ensure sufficient nutrient transport. As stated before, vascularization of these hydrogels would provide an even better and more biomimetic means of accomplishing this goal.

4.2 Porcine lymph node tissue can be decellularized but needs further characterization of remaining nuclear material

As previously mentioned, cells and nuclear material must be removed from allogeneic tissues that are intended to be used with human cells or implanted to avoid immunorejection[29]. The method used to produce the decellularized porcine lymph node tissue analyzed in this study uses the surfactants triton X-100 and sodium deoxycholate in conjunction with DNase I to lyse cells and degrade DNA. The benefit of this choice of reagents is that they are known to cause minimal damage to the tissue ECM. Sodium deoxycholate can be less effective at full decellularization but, in this case, is combined with triton X-100 to provide multiple wash cycles. This method was modified slightly from that which was published by Galliger et al. for the decellularization and digestion of tracheal tissue for use in GelMA hydrogels[51]. While this combination of reagents has been previously used to decellularize lung tissue by perfusion, Galliger et al. adapted it to the decellularization of small pieces of tracheal tissue intended for additional processing and hydrogel incorporation for 3D cell culture[51,52]. Other researchers have compared the use of SDS, CHAPS, or Triton X with deoxycholic acid for the decellularization of lymph nodes and found that SDS provided full decellularization while maintaining collagen and reticular fibers, thereby deeming it the best option[69]. However, SDS treatment is known to denature proteins in the ECM and while fiber structures may have been maintained, as ascertained by histology, it was not clear whether this approach would destroy important bioactive molecules and binding sites[31,69]. Furthermore, the authors mentioned that SDS may have been more effective in decellularization of whole lymph nodes due to the density of their fibrous capsule; in the studies described here the

lymph nodes were cut into smaller pieces, effectively disrupting the capsule and its resistance to diffusion[69]. Similarly, Lin et al. compared the efficacy of a variety of acids on the decellularization of whole lymph nodes[50]. While they found that formic acid delivered sufficient decellularization and preserved collagen and glycosaminoglycans (GAGs), this finding is directly in conflict with other studies that have found that acid treatment tends to damage collagen and GAG content[31]. Lin et al. provided a similar explanation, suggesting that formic acid effectively permeates the fibrous capsule of whole lymph nodes[50].

Assessment of dsDNA content via PicoGreen assay found that porcine lymph node tissue that was decellularized by the methods described in this paper contained significantly less dsDNA than the accepted upper limit of 50 ng/mg ECM (dry weight)[29]. One potential caveat to this result is that time of homogenization (to release dsDNA), while kept the same between decellularized and native tissue samples, was not varied to determine whether there was a significant effect of duration on dsDNA detection. For validation purposes, future studies could look at the effect of homogenization duration on dsDNA concentration and determine what the minimum time to release nearly all of the dsDNA from tissue samples would be. This could be decided by observing at what point the additional time of homogenization no longer resulted in significant changes to dsDNA release.

Staining of decellularized porcine lymph node tissue sections with DAPI did not result in any clearly visible nuclear material (see Fig. 3.10). The last addition to experimentation to fully meet the requirements of sufficient decellularization would be to verify that any remaining dsDNA fragments are less than 200 bp in length. Flow cytometry can detect dsDNA lengths down to about 125 bp by staining the dsDNA with fluorescent, intercalating dyes whose total output is linearly dependent on the fragment length[70]. Gel electrophoresis could also be used to ensure that the criteria are fully met in future studies.

4.3 Decellularized porcine lymph node tissue maintains some ECM proteins and relevant cytokines

The ECM of the lymph nodes contains diverse proteins with bioactive and structural functions that can be incorporated into 3D hydrogel scaffolds to support encapsulated leukocytes. To determine whether decellularization removed key proteins from the ECM, histology and IHC were performed on native and decellularized lymph node tissue. To determine whether soluble cytokines and chemokines remained sequestered in the ECM after decellularization, a Luminex multiplex immunoassay and Bradford assay were performed on the same tissues.

A visual analysis of collagen content in H&E and Trichrome-stained tissues in Figs. 3.8 and 3.9 reveals a dense network of the protein even after decellularization. Collagen contains the cell binding motif, GFOGER, and is a key structural component of the ECM[71]. Lin et al. and Cuzzone et al. both looked at the collagen content of decellularized lymph nodes, histologically, before using them as scaffolds for therapeutic immune cells[50,69]. The primary drawback to detecting collagen using H&E or Trichrome is a lack of specificity since distinct collagen subtypes are not identifiable this way. Further studies would benefit from using IHC with antibodies against the primary collagen subtypes that are present in the lymph nodes.

Comparing native and decellularized porcine lymph node tissue sections in Fig.3.10, it can be seen that there was no loss of signal from antibodies with a general specificity for laminin as a consequence of decellularization. In fact, these decellularized sections actually appear brighter; this may be due to the uncovering of laminin binding sites through the loss of cells that would have otherwise occupied them. Antibodies that were specific to laminin chains α3 and α4 had been used in experimentation, but those results are not shown due to weak signals across each condition that do not reveal significant differences. This may be a consequence of an over-dilution of primary or secondary antibodies, and future studies could home in on their ideal concentrations to yield more usable results. These findings would be impactful, as laminins 332 and 411 have significant and distinct interactions with immune cells that would ideally be incorporated into the scaffold[19]. Furthermore, it would also be worthwhile to perform

IHC with antibodies against laminin chain α5, as this could detect the equally important 511 isotype.

The observation of lymph node sections stained for fibronectin, visible in Fig. 3.10, reveals that there is a loss of specific signal in porcine lymph nodes as a result of decellularization. This indicates that the fibronectin binding sites that the antibody recognizes have been lost or altered and may indicate that there is an overall loss or alteration of fibronectin due to decellularization. However, this is not necessarily true, as the epitope against which the primary antibody was produced is at the C-terminal of the protein, whereas fibronectin contains cell-binding motifs in its central regions[72]. It is also notable that there is a significant interspecies difference in primary antibody binding. Since the antibody was produced using human fibronectin, it has more affinity for human lymph node tissue and produces a stronger fluorescent signal. While human and porcine fibronectin are highly homologous (93%), this would indicate a difference in C-terminal peptide sequences[73]. It is not clear whether porcine fibronectin would be similarly less effective at binding human leukocytes. Theodore et al. found that porcine PBMCs bind to human fibronectin but did not perform the reverse experiment[74].

From Table 3, it can be seen that relatively few cytokines that were detectable in native tissue remained so in decellularized tissue. The presence of several important interleukins, including IL-2, IL-6, IL-7, and IL-15, was significantly decreased in decellularized samples. Several analytes in the panel were not detectable in either native or decellularized tissue samples, including chemokine CXCL1 and B-cell activating molecule CD40L. Future studies could increase the time of tissue sample homogenization to potentially release more cytokines from the ECM, similar to the method described in section 4.2. There are several key cytokines and chemokines that have a large impact on lymph node functionality that were not included in this panel. CCL19 and CCL21, whose functions are described in detail in section 1.1, have been used in a microfluidic platform and a collagen-PEG hydrogel, respectively, to study T cell migration and activation[75,76]. CXCL12 and CXCL13 also contribute to lymphocyte migration and could be included in an expanded, future panel. IL-21 and BAFF support B cell survival. Engineered stromal cells that secrete BAFF were used by Purwada et al. to support B cell survival and GC

formation in hydrogels[41]. Finally, IL-4, though not included in this panel, induces proliferation of activated B cells, and was also used by Purwada et al. to achieve these goals[41]. One interesting observation is that there was more detectable VEGF in decellularized samples than native ones. This observation is consistent with other studies of cytokine content in decellularized renal and vascular tissue[77,78]. It is likely that VEGF, which is bound too tightly to native ECM to be detected by the assay, was released by degradation of its binding sites by some step of the decellularization process.

One limitation of this experiment was the high degree of variance found in the data. Increasing the number of trials per condition would allow an improved statistical detection of differences and make the results more accurate and meaningful. Another aspect to consider is that a panel for human analytes were used in the immunoassay. Differences in human and porcine homology may have contributed to some cytokines not being detected. On the other hand, those that were detected likely have closer homology and therefore may be more recognizable by human immune cells such that they impart the desired bioactivity.

To achieve a sufficient level of functionality in a tissue engineered lymph node model, it may be necessary to supplement fibrin-encapsulated leukocytes with exogenous soluble cytokines or to co-culture them with cytokine-producing stromal cells. While much of this role is filled by lymph node stromal cells, namely FRCs and FDCs, *in vivo*, these cell lines are difficult to isolate, such that some research groups have chosen to develop custom stromal cell lines[79]. While many studies have relied on exogenous supplementation, Purwada et al. engineered a custom stromal cell line to produce BAFF and CD40L, and Sardi et al. differentiated mesenchymal stromal cells (MSCs) into a stromal line with similarities to lymph node stromal cells to recreate the signaling provided by those cells[41,68]. The continuation of the studies presented here would potentially require the selection or creation of a stromal cell line to support leukocyte culture in fibrin hydrogels.

4.4 Incorporating decellularized tissue into hydrogels requires additional experimentation

As stated before, decellularized ECM can contain a wide variety of adhesion ligands and sequestered cytokines. The complexity of signals present in the ECM of the lymph nodes would be difficult to fully recapitulate *in vitro* from base materials. A number of studies in the literature that used hydrogels to culture immune cells and achieve peripheral lymphoid organ function used collagen (containing the GFOGER cell binding motif) or another polymer modified with a single cell binding sequence. Sardi et al. modified dextran with RGD peptides, while Purwada et al. functionalized maleimide-polyethylene glycol hydrogels with RGD or GREDV peptides[41,68]. While inclusion of a single binding motif is an improvement over hydrogels with none present, the ECM of the lymph node contains several proteins with a variety of binding motifs. This complexity could be relatively easily obtained by incorporating decellularized, processed lymph node ECM into fibrin hydrogels. This was attempted by including 10 mg/mL of ECM that had been decellularized, ground, and digested with pepsin into fibrinogen solutions that were used to form hydrogels for 3D PBC culture. This did not produce small enough ECM fragments, as they could not be fully solubilized in 10 mg/mL fibrinogen despite being subjected to warming at 50 °C and thorough mixing. This resulted in an uneven distribution of ECM in the gels (see Fig. 3.7). In future studies, the ECM could be ground into significantly smaller fragments via cryomilling.

The idea behind pepsin digestion and mechanical grinding was to reduce the ECM into fragment sizes that can be solubilized into the fibrinogen solution without destroying binding motifs and sequestered bioactive molecules. While the duration of pepsin digestion was limited, further studies would likely need to verify that said proteins were not degraded. This could be done by a variety of methods, including performing an extraction method to detect soluble proteins and mass spectrometry to identify binding motifs, after processing and before use in culture. Alternatively, hydrogels could be frozen, sectioned, and subjected to IHC to detect key proteins.

Another potential roadblock that presented itself after gels with ECM were imaged is that the ECM itself binds to the ethidium homodimer-1 in the L/D stain (see

Fig. 3.7). This event obscures live and dead cells and makes an accurate count difficult to obtain. To circumvent this, viability could instead be measured using a colorimetric assay, such as the MTT and LDH assays that can be used to measure the number of live and dead cells, respectively[80]. The MTT assay measures metabolic activity and is used to determine cell proliferation while the LDH assay measures the rate of cell death. When used together and in conjunction with an initial viability count before encapsulation, these assays have been shown to be effective at estimating the viability of hydrogel-encapsulated cells[80]. Alternatively, fibrin gels could be degraded using the serine protease, nattokinase, due to its fibrinolytic activity[81]. Leukocytes could be recovered from the degraded scaffolds and their viability measured by imaging. This method has already been used to effectively release MSCs from fibrin gels without any significant damage to them, and the authors of the study suggest that this approach could be utilized with other cell types[81].

4.5 Vascularization of hydrogels requires improved pin molding followed by LEC seeding and lymphangiogenesis

Tissue engineered structures of a physiologically and clinically relevant size (~1 mm to 10 cm), contain distances too great for effective transport of nutrients and waste products by diffusion[82]. For most tissues in the body, the maximum distance between cells and the vasculature is about 200 μm[82]. Areas in tissue engineered constructs that exceed this distance from the supply medium are prone to hypoxia and loss of cellular phenotype, function, and viability[82]. For these reasons, *in vitro* vascularization is one of the tissue engineering field's greatest and most pressing challenges.

As previously mentioned, the lymphatic vasculature and LECs that form it bring antigens, inflammatory cytokines, and migratory immune cells to and from the lymph nodes and facilitate their migration into them. LECs also support antigen presentation, peripheral tolerance, and lymphocyte expansion.

Inspiration for the pin molding technique presented in this thesis comes from the work of Meng et al., who used it to form patent, endothelialized channels in fibrin gels and then induced directional, human umbilical vein endothelial cell (HUVEC)

angiogenesis with VEGF gradients, among other functional outcomes[55]. These gradients were implemented by rupturing VEGF-containing capsules with a laser, to one side of the endothelialized channel. Cancer cells were able to migrate through this induced network and into the main channel[55]. This approach could potentially be applied with both endothelial and lymphatic endothelial cells to produce vasculature of both kinds within the fibrin hydrogel. Some research groups have already attempted to produce blood and lymphatic capillaries in hydrogels. Helm et al. encapsulated blood endothelial cells (BECs) and LECs in fibrin-collagen gels with covalently bound VEGF and induced BEC and LEC angiogenesis by subjecting them to interstitial flow by use of a flow chamber[63]. While they found that BEC vessel formation was dependent on collagen content, other studies have achieved this without collagen. Knezevic et al. co-cultured BECs and LECs with adipose-derived stromal cells (ASCs) in fibrin gel supplemented with soluble VEGF-C[64]. They found that ASCs provided critical signals for blood vessel formation, while VEGF-C was needed for lymphangiogenesis[65]. Marino et al. similarly seeded LECs and BECs in collagen or fibrin with VEGF-A or VEGF-C and provided stromal support with human fibroblasts[65]. They found that lymphangiogenesis was dependent on fibroblast signaling and that both VEGF-A and VEGF-C supplementation enhanced it[63]. No significant difference was imparted by the choice of hydrogel[65]. Given all of these findings, future studies would likely need to experiment with stromal cell support and VEGF-A/C supplementation to achieve the best outcomes.

A silicone mold was 3D printed to place a pin between its walls and provide a central chamber for the fibrin gel. Side and end chambers were also included to hold culture media for nutrient diffusion and humidity. The 10 mg/mL fibrinogen solution placed in the central chamber failed to gel within 30 minutes at 1 U/mL of thrombin added. Incubation times were increased to 3 hours and overnight, but full gelation still did not occur. Finally, the thrombin concentration was increased to 2 U/mL and the solution was allowed to gelate overnight. This experiment produced hydrogels that were visibly solidified and from which pins were removed (see Fig. 3.11). Even so, the removal of pins from this batch of hydrogels only resulted in one patent channel in four attempts, as determined by pipetting Trypan blue dye into one end of the channel and allowing

capillary action to perfuse it through. The mechanical strength of the gel appeared lacking, as some of the gels separated from the silicone walls and tore as the pin was slowly removed. In one of the gels, this separation did not appear to occur, but the channel collapsed and was not perfusable. This may be due to continued gelation issues. Thrombin from multiple shipment batches was compared to determine if expiration or batch variability presented a problem, but gels made from either one of them displayed slow and partial gelation. It could also be that the plasma fibrinogen batch was at fault, but this was not tested due to time constraints. Future studies would need to ensure that all reagents were functional, and if the fibrin gels made from them still failed to hold their shape and allow channel formation, modification of hydrogels would be considered. One option for strengthening fibrin hydrogels is by covalently crosslinking the fibrin polymers with factor XIIIa, a transglutaminase that performs its function in the presence of calcium ions[83]. Fibrin polymers can be chemically crosslinked and strengthened further by introducing genipin, a naturally derived crosslinking molecule that displays good cytocompatibility[84]. These actions can also improve the long-term stability of fibrin hydrogels, alongside the addition of aprotinin, an enzymatic inhibitor that has been shown to slow fibrinolysis[25].

Once patent channels could be consistently formed in fibrin hydrogels, LECs and BECs could be introduced to endothelialize pin mold channels, as Meng et al. demonstrated by injecting HUVECs at the channel opening[55]. Channel coverage can be easily monitored by fluorescence imaging without sectioning or whole mount immunostaining, given that fluorescent protein-expressing cell lines could be acquired[55]. Vessel patency can be demonstrated by perfusing the channel with fluorescent microbeads and subsequent imaging[55]. While Meng et al. created a VEGF gradient by rupturing capsules to one side of the channel, a homogenous distribution of VEGF-A/C, supplied by incubation with media, can be used to promote vessel sprouting throughout the gel and form vascular networks[64]. While soluble VEGF was demonstrated in multiple studies to enable BEC and LEC vessel sprouting, immobilization of growth factors onto the surface of matrices by covalent binding has been shown to improve their stability and function[85]. Helm et al. achieved this by utilizing an engineered VEGF variant that binds

covalently to fibrin[63]. The formation of new vasculature by both BECs and LECs could be observed by fluorescence microscopy at multiple focal depths and assessed for vessel density, lumen diameter, and general morphology.

4.6 Functional assays are required to show the clinical relevance of an integrated tissue model

After solving the problems introduced in the previous sections of this discussion, namely vascularization, optimal fibrin hydrogel conditions, ECM incorporation, cytokine supplementation, and stromal cell support, all of these elements could be combined into a working model and maintained with a bioreactor system (see Fig. 4.1). Media flow could be facilitated by a peristaltic pump, such that the pressure difference across the system would drive flow through the endothelialized channels and sprouted vessels contained in the hydrogel. If needed, an in-line oxygenation membrane could supply additional oxygen to the media upstream of the chambers. Cytokines, antibodies, and migratory cells could be collected from the outflow chamber.

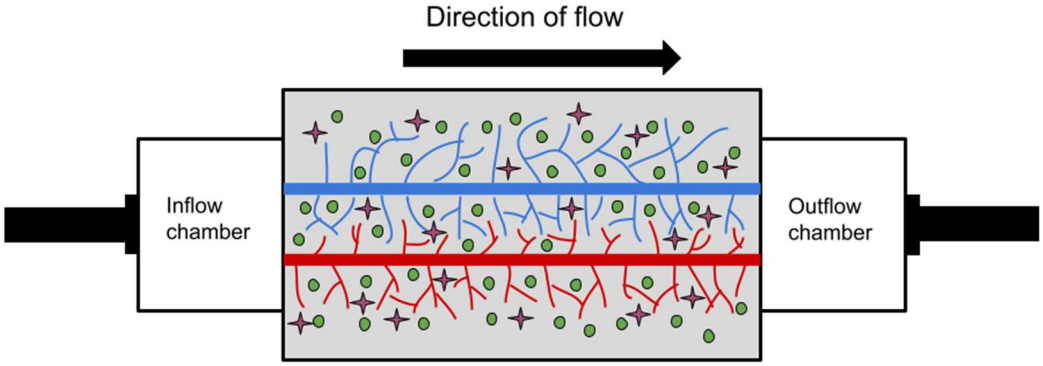

Figure 4.1 This diagram illustrates a potential design for a vascularized fibrin hydrogel containing immune cell populations and supplied with culture media and antigen by tubing connected to a pump system. Gray background indicates fibrin hydrogel containing decellularized, processed ECM. Larger, straight lines indicate endothelialized pin mold channels from which fluid enters and exits the hydrogel (blue = lymphatics, red = blood vessels). Green and purple shapes are representative of immune cells of varying types.

This construct could be used to perform *in vitro* diagnostic tests of drug immunoreactivity and vaccine efficacy or study the interactions of cancer cells with the immune system. The hydrogel scaffold and encapsulated cell populations could also be matured *in vitro* and then removed from the bioreactor for implantation to potentially combat lymphedema and immune deficiencies. For any of this to be plausible, it would first need to be validated that this model shares similar basic functionality with lymph nodes in the body.

To initiate an immune reaction by the cells contained in the hydrogel, a chosen antigen can be introduced into the vasculature through the inflow chamber along with lipopolysaccharide (LPS), a bacterial endotoxin that is commonly used as an inflammatory stimulus[86]. The outflow chamber would be used to collect inflammatory cytokines that might be released upon later restimulation in response to immune cell activation. These cytokines could then be identified by use of a multiplex immunoassay. Giese et al. performed a similar experiment and observed the inflammatory secretion profile, looking at concentrations of IL-2, IL-4, IL-6, interferon gamma (IFN-γ), and TNF-α, among others[47,87].

Long-term viability and the development of populations of functionally relevant immune cell phenotypes could also be observed by degrading the fibrin matrix with nattokinase, collecting the cells, staining them with marker-specific, fluorochrome-conjugated antibodies, and separating them by flow cytometry. Using a similar approach, Kuzin et al. identified CD3+ T cells isolated from 3D culture and grouped them by effector function (CD4+/CD8+) and naivety (CD45RA+/CD45RO+)[86]. B cells were identified by the CD19 marker and organized into further subtypes (naive B cells, pre-GC B cells, GC B cells, plasma cells, and memory B cells) by their combinations of IgD, CD27, and CD38 expression[86]. Purwada et al., on the other hand, identified GC cells by the surface marker GL7, and separated them into GC dark zone and light zone phenotypes by looking at their CXCR4 and CD83 expression levels[40]. Kuzin et al. also identified plasmacytoid and myeloid DCs by a combination of several surface markers and separated them from monocytes by the lack of CD14 expression[86]. The expansion of various cell types can be determined by cytometric counting, while the viability of each

separated cell population can be assessed with a L/D stain and fluorescence microscopy. To understand the distribution and proliferative dynamics of cell populations within the matrix, the hydrogel can be removed from the bioreactor, fixed, sectioned, and stained with antibodies for specific surface markers. Kuzin et al. stained for CD3 and CD19 markers to differentiate T and B cell zones, while Giese et al identified proliferating cells (Ki67+) and differentiated plasma cells (CD138+)[86,87]. Purwada et al. visualized GC formation by staining for GL7[40].

As a final addition to *in vitro* characterization, antibodies could be collected from the outflow chamber a few days after antigen stimulation. An enzyme-linked immunosorbent assay (ELISA) can be used to measure antigen-specific antibodies. It can also be used to observe affinity maturation as it can determine the relative affinities of antibodies collected at different time points to the antigen of interest[88]. Furthermore, as Kuzin et al. demonstrate, class switching can be detected by performing an ELISA in which antibodies against human IgM and IgG are used[86]. Since naive B cells can produce only IgM and IgD antibodies, the detection of IgG, IgA, or IgE antibodies would indicate that class switching had occurred[3].

5. Conclusion

There is a need for a tissue-engineered, 3D model of a human lymph node to perform *in vitro* screening of drugs and vaccines in a more physiologically relevant microenvironment. While there do exist such *in vitro* models, they are limited in the extent to which they recreate the microenvironment of the lymph node. They can be improved by the addition of decellularized lymph node ECM, as it has the potential to provide encapsulated immune cells with a wide variety of highly relevant, bioactive peptides. Furthermore, there is a need for these tissue-engineered models to be implantable to deliver therapeutic cells and structure *in vivo* to address a variety of pathologies including cancer, auto-immune disease, and lymphedema. As of yet, lymph node models with proven functionality are not lymphatically or otherwise vascularized and therefore not ideally prepared for implantation and therapeutic efficacy. This problem can be addressed by applying a previously existing approach for vascularizing fibrin hydrogels by the introduction of endothelialized channels and subsequent *in vitro* angiogenesis.

Fibrin hydrogels were found to be a good candidate for 3D scaffolding in a lymph node model because they maintain high PBMC/PBC viability in culture and have been used in several studies as a platform for angiogenesis and lymphangiogenesis. Porcine lymph node tissue was successfully decellularized and shown to retain high amounts of collagen and laminin ECM after this process, indicating that it can be used to provide leukocytes with many of the binding motifs that they encounter in the lymph node microenvironment. However, fibronectin was not shown to be retained and further work could be done to ascertain which isoforms of collagen and laminin were present. Some immunologically relevant, soluble cytokines were detected even after decellularization of lymph node tissue, but these results would benefit from an expanded analyte panel and greater number of trials in order to get a strong sense of which important molecules are present and which may need to be supplemented. Further processing of the ECM is required to fully solubilize it for incorporation into hydrogels. The approach for introducing channels in fibrin hydrogels was reproducible but needs to become more

consistent through improvements to experimental technique or hydrogel composition. At such a point, it would need to be determined whether endothelialization and capillary sprouting of BECs and LECs in response to VEGF signaling can be achieved in this platform. A bioreactor system is needed to support the model *in vitro.* Finally, functional assays would be required to demonstrate proliferation, the production of inflammatory cytokines and antigen-specific antibodies, GC formation, and the development of important effector cell populations in response to an antigen challenge.

Bibliography

1. Ruddle, N. H., & Akirav, E. M. (2009). Secondary Lymphoid Organs: Responding to Genetic and Environmental Cues in Ontogeny and the Immune Response. *The Journal of Immunology*, *183*(4), 2205–2212. https://doi.org/10.4049/jimmunol.0804324
2. Randolph, G. J., Ivanov, S., Zinselmeyer, B. H., & Scallan, J. P. (2017). The Lymphatic System: Integral Roles in Immunity. *Annual Review of Immunology*, *35*(1), 31–52. https://doi.org/10.1146/annurev-immunol-041015-055354
3. Murphy, K., & Weaver, C. (2017). *Janeway's Immunobiology* (9th ed.). Garland Science, Taylor & Francis Group, LLC.
4. Willard-Mack, C. L. (2006). Normal Structure, Function, and Histology of Lymph Nodes. *Toxicologic Pathruology*, *34*(5), 409–424. https://doi.org/10.1080/01926230600867727
5. Abdulkhaleq, L. A., Assi, M. A., Abdullah, R., Zamri-Saad, M., Taufiq-Yap, Y. H., & Hezmee, M. N. M. (2018). The crucial roles of inflammatory mediators in inflammation: A review. *Veterinary World*, *11*(5), 627–635. https://doi.org/10.14202/vetworld.2018.627-635
6. Eckert, N., Permanyer, M., Yu, K., Werth, K., & Förster, R. (2019). Chemokines and other mediators in the development and functional organization of lymph nodes. *Immunological Reviews*, *289*(1), 62–83. https://doi.org/10.1111/imr.12746
7. Acton, S. E., & Reis e Sousa, C. (2016). Dendritic cells in remodeling of lymph nodes during immune responses. *Immunological Reviews*, *271*(1), 221–229. https://doi.org/10.1111/imr.12414
8. Stein, J. V., & Nombela-Arrieta, C. (2005). Chemokine control of lymphocyte trafficking: A general overview. *Immunology*, *116*(1), 1–12. https://doi.org/10.1111/j.1365-2567.2005.02183.x
9. Nosenko, M. A., Drutskaya, M. S., Moisenovich, M. M., & Nedospasov, S. A. (2016). Bioengineering of artificial lymphoid organs. *Acta Naturae*, *8*(2), 10–23.
10. Gray, E. E., & Cyster, J. G. (2012). Lymph node macrophages. *Journal of Innate Immunity*, *4*(5–6), 424–436. https://doi.org/10.1159/000337007
11. Gasteiger, G., Ataide, M., & Kastenmüller, W. (2016). Lymph node - An organ for T-cell activation and pathogen defense. *Immunological Reviews*, *271*(1), 200–220. https://doi.org/10.1111/imr.12399
12. De Silva, N. S., & Klein, U. (2015). Dynamics of B cells in germinal centres. *Nature Reviews Immunology*, *15*(3), 137–148. https://doi.org/10.1038/nri3804
13. Chang, J. E., & Turley, S. J. (2015). Stromal infrastructure of the lymph node and coordination of immunity. *Trends in Immunology*, *36*(1), 30–39. https://doi.org/10.1016/j.it.2014.11.003
14. Jackson, D. G. (2019). Leucocyte trafficking via the lymphatic vasculature-mechanisms and consequences. *Frontiers in Immunology*, *10*(MAR), 1–19. https://doi.org/10.3389/fimmu.2019.00471
15. Petrova, T. V., & Koh, G. Y. (2018). Organ-specific lymphatic vasculature: From development to pathophysiology. *Journal of Experimental Medicine*, *215*(1), 35–49. https://doi.org/10.1084/jem.20171868
16. Rauniyar, K., Jha, S. K., & Jeltsch, M. (2018). Biology of vascular endothelial growth factor C in the morphogenesis of lymphatic vessels. *Frontiers in Bioengineering and Biotechnology*, *6*(FEB). https://doi.org/10.3389/fbioe.2018.00007

17. Gorfu, G., Virtanen, I., Hukkanen, M., Lehto, V.-P., Rousselle, P., Kenne, E., … Patarroyo, M. (2008). Laminin isoforms of lymph nodes and predominant role of α5-laminin(s) in adhesion and migration of blood lymphocytes. *Journal of Leukocyte Biology*, *84*(3), 701–712. https://doi.org/10.1189/jlb.0108048
18. Kaldjian, E. P., Elizabeth Gretz, J., Anderson, A. O., Shi, Y., & Shaw, S. (2001). Spatial and molecular organization of lymph node T cell cortex: A labyrinthine cavity bounded by an epithelium-like monolayer of fibroblastic reticular cells anchored to basement membrane-like extracellular matrix. *International Immunology*, *13*(10), 1243–1253. https://doi.org/10.1093/intimm/13.10.1243
19. Simon, T., & Bromberg, J. S. (2017). Regulation of the Immune System by Laminins. *Trends in Immunology*, *38*(11), 858–871. https://doi.org/10.1016/j.it.2017.06.002
20. Li, L., Shirkey, M. W., Zhang, T., Xiong, Y., Piao, W., Saxena, V., … Bromberg, J. S. (2020). The lymph node stromal laminin α5 shapes alloimmunity. *Journal of Clinical Investigation*, *130*(5), 2602–2619. https://doi.org/10.1172/JCI135099
21. Shannon, L. A., Calloway, P. A., Welch, T. P., & Vines, C. M. (2010). CCR7/CCL21 migration on fibronectin is mediated by phospholipase Cγ1 and ERK1/2 in primary T lymphocytes. *Journal of Biological Chemistry*, *285*(50), 38781–38787. https://doi.org/10.1074/jbc.M110.152173
22. Fodor, W. L. (2003). Tissue engineering and cell based therapies, from the bench to the clinic: the potential to replace, repair and regenerate. *Reproductive Biology and Endocrinology : RB&E*, *1*, 102. https://doi.org/10.1186/1477-7827-1-102
23. El-Sherbiny, I. M., & Yacoub, M. H. (2013). Hydrogel scaffolds for tissue engineering: Progress and challenges. *Global Cardiology Science and Practice*, *2013*(3), 38. https://doi.org/10.5339/gcsp.2013.38
24. Xiao, S., Zhao, T., Wang, J., Wang, C., Du, J., Ying, L., … Xu, K. (2019). Gelatin Methacrylate (GelMA)-Based Hydrogels for Cell Transplantation: an Effective Strategy for Tissue Engineering. *Stem Cell Reviews and Reports*, *15*(5), 664–679. https://doi.org/10.1007/s12015-019-09893-4
25. Ahmed, T. A. E., Dare, E. V., & Hincke, M. (2008). Fibrin: A versatile scaffold for tissue engineering applications. *Tissue Engineering - Part B: Reviews*, *14*(2), 199–215. https://doi.org/10.1089/ten.teb.2007.0435
26. Vijayavenkataraman, S., Yan, W. C., Lu, W. F., Wang, C. H., & Fuh, J. Y. H. (2018). 3D bioprinting of tissues and organs for regenerative medicine. *Advanced Drug Delivery Reviews*, *132*, 296–332. https://doi.org/10.1016/j.addr.2018.07.004
27. Bar-Ephraim, Y. E., Kretzschmar, K., & Clevers, H. (2019). Organoids in immunological research. *Nature Reviews Immunology*. https://doi.org/10.1038/s41577-019-0248-y
28. Polini, A., del Mercato, L. L., Barra, A., Zhang, Y. S., Calabi, F., & Gigli, G. (2019). Towards the development of human immune-system-on-a-chip platforms. *Drug Discovery Today*, Vol. 24, pp. 517–525. https://doi.org/10.1016/j.drudis.2018.10.003
29. Gilpin, A., & Yang, Y. (2017). Decellularization Strategies for Regenerative Medicine: From Processing Techniques to Applications. *BioMed Research International*, *2017*. https://doi.org/10.1155/2017/9831534
30. Price, A. P., Godin, L. M., Domek, A., Cotter, T., D'Cunha, J., Taylor, D. A., & Panoskaltsis-Mortari, A. (2015). Automated decellularization of intact, human-sized lungs for tissue engineering. *Tissue Engineering - Part C: Methods*, *21*(1), 94–103. https://doi.org/10.1089/ten.tec.2013.0756
31. Mendibil, U., Ruiz-Hernandez, R., Retegi-Carrion, S., Garcia-Urquia, N., Olalde-Graells, B., & Abarrategi, A. (2020). Tissue-specific decellularization methods: Rationale and

strategies to achieve regenerative compounds. *International Journal of Molecular Sciences*, *21*(15), 1–29. https://doi.org/10.3390/ijms21155447

32. Zhu, J., & Marchant, R. E. (2011). Design properties of hydrogel tissue-engineering scaffolds. *Expert Review of Medical Devices*, *8*(5), 607–626. https://doi.org/10.1586/erd.11.27
33. Catoira, M. C., Fusaro, L., Di Francesco, D., Ramella, M., & Boccafoschi, F. (2019). Overview of natural hydrogels for regenerative medicine applications. *Journal of Materials Science: Materials in Medicine*, *30*(10). https://doi.org/10.1007/s10856-019-6318-7
34. Shanti, A., Teo, J., & Stefanini, C. (2018). In vitro immune organs-on-chip for drug development: A review. *Pharmaceutics*, *10*(4). https://doi.org/10.3390/pharmaceutics10040278
35. Sun, W., Luo, Z., Lee, J., Kim, H. J., Lee, K. J., Tebon, P., … Khademhosseini, A. (2019). Organ-on-a-Chip for Cancer and Immune Organs Modeling. *Advanced Healthcare Materials*, *8*(4), 1–12. https://doi.org/10.1002/adhm.201801363
36. Shah, S. B., & Singh, A. (2017). Creating artificial lymphoid tissues to study immunity and hematological malignancies. *Current Opinion in Hematology*, *24*(4), 377–383. https://doi.org/10.1097/MOH.0000000000000356
37. Kim, S., Shah, S. B., Graney, P. L., & Singh, A. (2019). Multiscale engineering of immune cells and lymphoid organs. *Nature Reviews Materials*, *4*(6), 355–378. https://doi.org/10.1038/s41578-019-0100-9
38. Gosselin, E. A., Eppler, H. B., Bromberg, J. S., & Jewell, C. M. (2018). Designing natural and synthetic immune tissues. *Nature Materials*, *17*(6), 484–498. https://doi.org/10.1038/s41563-018-0077-6
39. Alderfer, L., Wei, A., & Hanjaya-Putra, D. (2018). Lymphatic Tissue Engineering and Regeneration. *Journal of Biological Engineering*, *12*(1), 1–26. https://doi.org/10.1186/s13036-018-0122-7
40. Purwada, A., Jaiswal, M. K., Ahn, H., Nojima, T., Kitamura, D., Gaharwar, A. K., … Singh, A. (2015). Ex vivo engineered immune organoids for controlled germinal center reactions. *Biomaterials*, *63*(2015), 24–34. https://doi.org/10.1016/j.biomaterials.2015.06.002
41. Purwada, A., Shah, S. B., Béguelin, W., August, A., Melnick, A. M., & Singh, A. (2019). Ex vivo synthetic immune tissues with T cell signals for differentiating antigen-specific, high affinity germinal center B cells. *Biomaterials*, *198*, 27–36. https://doi.org/10.1016/j.biomaterials.2018.06.034
42. Moura Rosa, P., Gopalakrishnan, N., Ibrahim, H., Haug, M., & Halaas, Ø. (2016). The intercell dynamics of T cells and dendritic cells in a lymph node-on-a-chip flow device. *Lab on a Chip*, *16*(19), 3728–3740. https://doi.org/10.1039/c6lc00702c
43. Pérez Del Río, E., Martinez Miguel, M., Veciana, J., Ratera, I., & Guasch, J. (2018). Artificial 3D Culture Systems for T Cell Expansion. *ACS Omega*, *3*(5), 5273–5280. https://doi.org/10.1021/acsomega.8b00521
44. Cheung, A. S., Zhang, D. K. Y., Koshy, S. T., & Mooney, D. J. (2018). Scaffolds that mimic antigen-presenting cells enable ex vivo expansion of primary T cells. *Nature Biotechnology*, *36*(2), 160–169. https://doi.org/10.1038/nbt.4047
45. Stephan, S. B., Taber, A. M., Jileaeva, I., Pegues, E. P., Sentman, C. L., & Stephan, M. T. (2015). Biopolymer implants enhance the efficacy of adoptive T-cell therapy. *Nature Biotechnology*, *33*(1), 97–101. https://doi.org/10.1038/nbt.3104
46. Weiden, J., Voerman, D., Dölen, Y., Das, R. K., Van Duffelen, A., Hammink, R., … Figdor, C. G. (2018). Injectable biomimetic hydrogels as tools for efficient T Cell

expansion and delivery. *Frontiers in Immunology*, *9*(NOV), 1–15. https://doi.org/10.3389/fimmu.2018.02798

47. Kraus, T., Lubitz, A., Schließer, U., Giese, C., Reuschel, J., Brecht, R., … Winter, G. (2019). Evaluation of a 3D Human Artificial Lymph Node as Test Model for the Assessment of Immunogenicity of Protein Aggregates. *Journal of Pharmaceutical Sciences*, *108*(7), 2358–2366. https://doi.org/10.1016/j.xphs.2019.02.011
48. Suematsu, S., & Watanabe, T. (2004). Generation of a synthetic lymphoid tissue-like organoid in mice. *Nature Biotechnology*, *22*(12), 1539–1545. https://doi.org/10.1038/nbt1039
49. Okamoto, N., Chihara, R., Shimizu, C., Nishimoto, S., & Watanabe, T. (2007). Artificial lymph nodes induce potent secondary immune responses in naive and immunodeficient mice. *Journal of Clinical Investigation*, *117*(4), 997–1007. https://doi.org/10.1172/JCI30379
50. Lin, H. J., Wang, W., Huang, Y. Y., Liao, W. T., Lin, T. Y., Lin, S. Y., & Liu, D. Z. (2019). Decellularized lymph node scaffolding as a carrier for dendritic cells to induce anti-tumor immunity. *Pharmaceutics*, *11*(11), 1–16. https://doi.org/10.3390/pharmaceutics11110553
51. Galliger, Z., & Panoskaltsis-Mortari, A. (2018). Tracheal cartilage isolation and decellularization. *Methods in Molecular Biology*, *1577*(July 2017), 155–160. https://doi.org/10.1007/7651_2017_52
52. Skolasinski, S., & Panoskaltsis-Mortari, A. (2017). Decellularization of Intact Lung Tissue Through Vasculature and Airways Using Negative and Positive Pressure. In *Methods Mol Biol.* (pp. 307–315). https://doi.org/10.1007/7651_2017_32
53. Edmondson, R., Broglie, J. J., Adcock, A. F., & Yang, L. (2014). Three-dimensional cell culture systems and their applications in drug discovery and cell-based biosensors. *Assay and Drug Development Technologies*, *12*(4), 207–218. https://doi.org/10.1089/adt.2014.573
54. Lin, Y., Louie, D., Ganguly, A., Wu, D., Huang, P., & Liao, S. (2018). Elastin Shapes Small Molecule Distribution in Lymph Node Conduits. *The Journal of Immunology*, *200*(9), 3142–3150. https://doi.org/10.4049/jimmunol.1800074
55. Aumailley, M. (2013). The laminin family. *Cell Adhesion and Migration*, *7*(1), 48–55. https://doi.org/10.4161/cam.22826
56. Tarnowski, B. I., Spinale, F. G., & Nicholson, J. H. (1991). DAPI as a useful stain for nuclear quantitation. *Biotechnic and Histochemistry*, *66*(6), 296–302. https://doi.org/10.3109/10520299109109990
57. Meng, F., Meyer, C. M., Joung, D., Vallera, D. A., McAlpine, M. C., & Panoskaltsis-Mortari, A. (2019). 3D Bioprinted In Vitro Metastatic Models via Reconstruction of Tumor Microenvironments. *Advanced Materials*, *31*(10), 1–10. https://doi.org/10.1002/adma.201806899
58. Flick, M. J., Du, X. L., Witte, D. P., Jirousková, M., Soloviev, D. A., Busuttil, S. J., … Degen, J. L. (2004). Leukocyte engagement of fibrin(ogen) via the integrin receptor αMβ2/Mac-1 is critical for host inflammatory response in vivo. *Journal of Clinical Investigation*, *113*(11), 1596–1606. https://doi.org/10.1172/JCI20741
59. Hastings, W. D., Gurdak, S. M., Tumang, J. R., & Rothstein, T. L. (2006). CD5+/Mac-1- peritoneal B cells: A novel B cell subset that exhibits characteristics of B-1 cells. *Immunology Letters*, *105*(1), 90–96. https://doi.org/10.1016/j.imlet.2006.01.002
60. Bednarczyk, M., Stege, H., Grabbe, S., & Bros, M. (2020). β2 Integrins—Multi-Functional Leukocyte Receptors in Health and Disease. *International Journal of Molecular Sciences*, *21*(4), 1–43. https://doi.org/10.3390/ijms21041402

61. Salsmann, A., Schaffner-Reckinger, E., Kabile, F., Plançon, S., & Kieffer, N. (2005). A new functional role of the fibrinogen RGD motif as the molecular switch that selectively triggers integrin αIIbβ3-dependent RhoA activation during cell spreading. *Journal of Biological Chemistry*, *280*(39), 33610–33619. https://doi.org/10.1074/jbc.M500146200
62. Ventura Ferreira, M. S., Jahnen-Dechent, W., Labude, N., Bovi, M., Hieronymus, T., Zenke, M., … Neuss, S. (2012). Cord Blood-Hematopoietic Stem Cell Expansion in 3D Fibrin Scaffolds with Stromal Support. *Biomaterials*, *33*(35), 9165. https://doi.org/10.1016/j.biomaterials.2012.09.004
63. Helm, Cara-Lynn E.; Zisch, Andreas; Swartz, M. A. (2006). Engineered Blood and Lymphatic Capillaries in 3-D VEGF-Fibrin-Collagen Matrices With Interstitial Flow. *Biotechnology and Bioengineering*, *96*(1), 167–176. https://doi.org/10.1002/bit.21185
64. Knezevic, L., Schaupper, M., Mühleder, S., Schimek, K., Hasenberg, T., Marx, U., … Holnthoner, W. (2017). Engineering Blood and Lymphatic Microvascular Networks in Fibrin Matrices. *Frontiers in Bioengineering and Biotechnology*, *5*(April), 1–12. https://doi.org/10.3389/fbioe.2017.00025
65. Marino, D., Luginbuhl, J., Scola, S., Meuli, M., & Reichmann, E. (2014). Bioengineering Dermo-Epidermal Skin Grafts with Blood and Lymphatic Capillaries. *Science Translational Medicine*, *6*(221), 221ra14-221ra14. https://doi.org/10.1126/scitranslmed.3006894
66. Soares, A., Govender, L., Hughes, J., Mavakla, W., de Kock, M., Barnard, C., … Hanekom, W. A. (2010). Novel application of Ki67 to quantify antigen-specific in vitro lymphoproliferation. *Journal of Immunological Methods*, *362*(1–2), 43–50. https://doi.org/10.1016/j.jim.2010.08.007
67. Place, T. L., Domann, F. E., & Case, A. J. (2017). Limitations of oxygen delivery to cells in culture: An underappreciated problem in basic and translational research. *Free Radical Biology and Medicine*, *113*, 311–322. https://doi.org/10.1016/j.freeradbiomed.2017.10.003
68. Sardi, M., Lubitz, A., & Giese, C. (2016). Modeling Human Immunity In Vitro : Improving Artificial Lymph Node Physiology by Stromal Cells. *Applied In Vitro Toxicology*, *2*(3), 143–150. https://doi.org/10.1089/aivt.2016.0004
69. Cuzzone, D. A., Albano, N. J., Aschen, S. Z., Ghanta, S., & Mehrara, B. J. (2015). Decellularized lymph nodes as scaffolds for tissue engineered lymph nodes. *Lymphatic Research and Biology*, *13*(3), 186–194. https://doi.org/10.1089/lrb.2013.0054
70. Hussels, M., Engel, S., & Bock, N. (2019). Investigation of direct counting and sizing of DNA fragments in flow applying an improved data analysis and correction method. *Biomolecular Detection and Quantification*, Vol. 17. https://doi.org/10.1016/j.bdq.2019.100083
71. Knight, C. G., Morton, L. F., Peachey, A. R., Tuckwell, D. S., Farndale, R. W., & Barnes, M. J. (2000). The collagen-binding a-domains of integrins α1/β1 and α2/β1 recognize the same specific amino acid sequence, GFOGER, in native (triple- helical) collagens. *Journal of Biological Chemistry*, *275*(1), 35–40. https://doi.org/10.1074/jbc.275.1.35
72. Speziale, P., Arciola, C. R., & Pietrocola, G. (2019). Fibronectin and Its Role in Human Infective Diseases. *Cells*, *8*(12). https://doi.org/10.3390/cells8121516
73. SKORSTENGAARD, K., JENSEN, M. S., SAHL, P., PETERSEN, T. E., & MAGNUSSON, S. (1986). Complete primary structure of bovine plasma fibronectin. *European Journal of Biochemistry*, *161*(2), 441–453. https://doi.org/10.1111/j.1432-1033.1986.tb10464.x

74. Theodore, P. R., Simon, A. R., Warrens, A. N., Sackstein, R., & Sykes, M. (2002). Porcine mononuclear cells adhere to human fibronectin independently of very late antigen-5: Implications for donor-specific tolerance induction in xenotransplantation. *Xenotransplantation*, *9*(4), 277–289. https://doi.org/10.1034/j.1399-3089.2002.01086.x
75. Mitra, B., Jindal, R., Lee, S., Dong, D. X., Li, L., Sharma, N., … Yarmush, M. L. (2013). Microdevice integrating innate and adaptive immune responses associated with antigen presentation by dendritic cells. *RSC Advances*, *3*(36), 16002–16010. https://doi.org/10.1039/c3ra41308j
76. Stachowiak, A. N., & Irvine, D. J. (2008). Inverse opal hydrogel-collagen composite scaffolds as a supportive microenvironment for immune cell migration. *Journal of Biomedical Materials Research Part A*, *85A*(3), 815–828. https://doi.org/10.1002/jbm.a.31661
77. Caralt, M., Uzarski, J. S., Iacob, S., Obergfell, K. P., Berg, N., Bijonowski, B. M., … Wertheim, J. A. (2015). Optimization and Critical Evaluation of Decellularization Strategies to Develop Renal Extracellular Matrix Scaffolds as Biological Templates for Organ Engineering and Transplantation. *American Journal of Transplantation*, *15*(1), 64–75. https://doi.org/10.1111/ajt.12999
78. Olausson, M., Kuna, V. K., Travnikova, G., Bäckdahl, H., Patil, P. B., Saalman, R., … Sumitran-Holgersson, S. (2014). In vivo application of tissue-engineered veins using autologous peripheral whole blood: A proof of concept study. *EBioMedicine*, *1*(1), 72–79. https://doi.org/10.1016/j.ebiom.2014.09.001
79. Fletcher, A. L., Malhotra, D., Acton, S. E., Lukacs-Kornek, V., Bellemare-Pelletier, A., Curry, M., … Turley, S. J. (2011). Reproducible isolation of lymph node stromal cells reveals site-dependent differences in fibroblastic reticular cells. *Frontiers in Immunology*, *2*(SEP), 1–15. https://doi.org/10.3389/fimmu.2011.00035
80. Khattak, S. F., Spatara, M., Roberts, L., & Roberts, S. C. (2006). Application of colorimetric assays to assess viability, growth and metabolism of hydrogel-encapsulated cells. *Biotechnology Letters*, *28*(17), 1361–1370. https://doi.org/10.1007/s10529-006-9104-9
81. Carrion, B., Janson, I. A., Kong, Y. P., & Putnam, A. J. (2014). A safe and efficient method to retrieve mesenchymal stem cells from three-dimensional fibrin gels. *Tissue Engineering - Part C: Methods*, *20*(3), 252–263. https://doi.org/10.1089/ten.tec.2013.0051
82. Yang, G., Mahadik, B., Choi, J. Y., & Fisher, J. P. (2020). Vascularization in tissue engineering: fundamentals and state-of-art. *Progress in Biomedical Engineering*, *2*(1), 012002. https://doi.org/10.1088/2516-1091/ab5637
83. Singh, S., Dodt, J., Volkers, P., Hethershaw, E., Philippou, H., Ivaskevicius, V., … Biswas, A. (2019). Structure functional insights into calcium binding during the activation of coagulation factor XIII A. *Scientific Reports*, *9*(1), 1–18. https://doi.org/10.1038/s41598-019-47815-z
84. Dare, E. V., Griffith, M., Poitras, P., Kaupp, J. A., Waldman, S. D., Carlsson, D. J., … Hincke, M. T. (2009). Genipin cross-linked fibrin hydrogels for in vitro human articular cartilage tissue-engineered regeneration. *Cells Tissues Organs*, *190*(6), 313–325. https://doi.org/10.1159/000209230
85. Guex, A. G., Hegemann, D., Giraud, M. N., Tevaearai, H. T., Popa, A. M., Rossi, R. M., & Fortunato, G. (2014). Covalent immobilisation of VEGF on plasma-coated electrospun scaffolds for tissue engineering applications. *Colloids and Surfaces B: Biointerfaces*, *123*, 724–733. https://doi.org/10.1016/j.colsurfb.2014.10.016

86. Kuzin, I., Sun, H., Moshkani, S., Feng, C., Mantalaris, A., Wu, J. H. D., & Bottaro, A. (2011). Long-term immunologically competent human peripheral lymphoid tissue cultures in a 3D bioreactor. *Biotechnology and Bioengineering*, *108*(6), 1430–1440. https://doi.org/10.1002/bit.23055
87. Giese, C., Lubitz, A., Demmler, C. D., Reuschel, J., Bergner, K., & Marx, U. (2010). Immunological substance testing on human lymphatic micro-organoids in vitro. *Journal of Biotechnology*, *148*(1), 38–45. https://doi.org/10.1016/j.jbiotec.2010.03.001
88. Klasse, P. J. (2016). How to assess the binding strength of antibodies elicited by vaccination against HIV and other viruses. *Expert Review of Vaccines*, *15*(3), 295–311. https://doi.org/10.1586/14760584.2016.1128831

Appendices

Appendix A.1 List of all analytes included in the Luminex multiplex immunoassay and Bradford assay

Endothelial growth factor
Fibroblast growth factor 2
Eotaxin
Transforming growth factor alpha
Granulocyte colony-stimulating factor
FMS-like tyrosine kinase 3 ligand
Granulocyte-macrophage colony-stimulating factor
Fractalkine
Interferon alpha-2
Interferon gamma
Chemokine (C-X-C motif) ligand 1
Interleukin-10
Chemokine (C-C motif) ligand 7
Interleukin-12 subunit beta
C-C motif chemokine 22
Interleukin-12
Interleukin-13
Interleukin-15
Soluble CD40-ligand
Interleukin-17A
Interleukin-1 receptor antagonist
Interleukin-1 alpha
Interleukin-9
Interleukin-1 beta
Interleukin-2
Interleukin-3
Interleukin-4
Interleukin-5
Interleukin-6
Interleukin-7
Interleukin-8
C-X-C motif chemokine ligand 10
Chemokine (C-C motif) ligand 2
Chemokine (C-C motif) ligand 3
Chemokine (C-C motif) ligand 4
Tumor necrosis factor alpha
Tumor necrosis factor beta
Vascular endothelial growth factor

Appendix A.2 Full IHC IF compared to secondary-only and autofluorescence controls

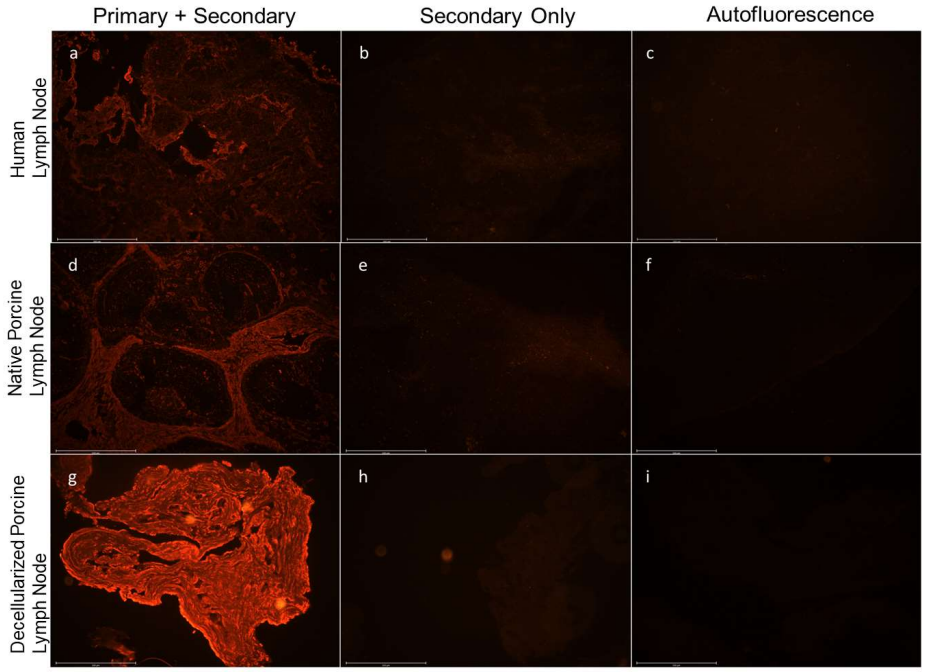

Figure A.2.1 The results of full staining, secondary-only staining, and no staining of tissue sections with anti-laminin antibodies. The type of tissue section is displayed on the left and the stain type on the top of the image. All scale bars = 500 μm.

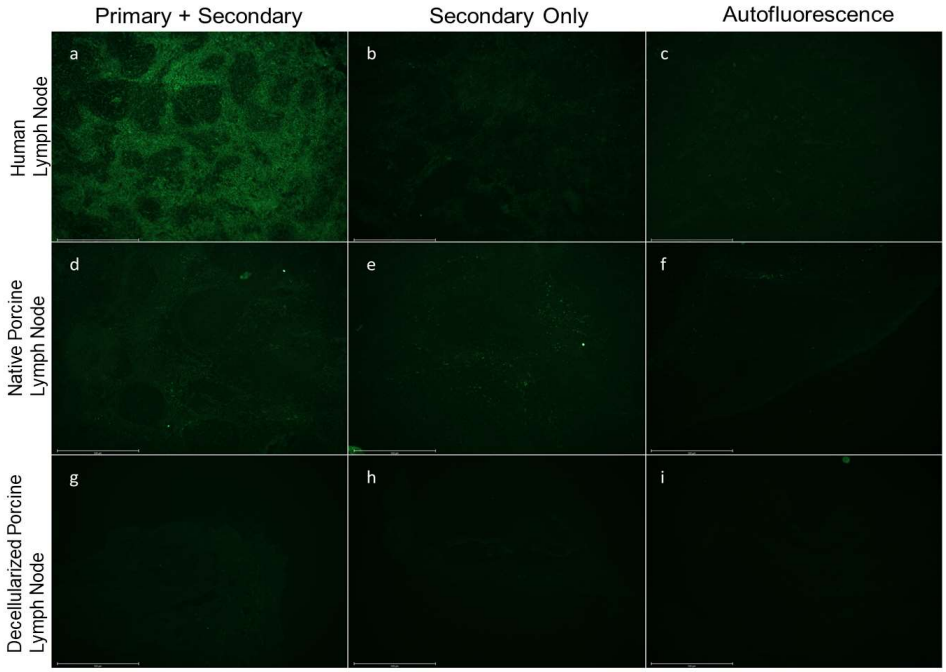

Figure A.2.2 The results of full staining, secondary-only staining, and no staining of tissue sections with anti-fibronectin antibodies. The type of tissue section is displayed on the left and the stain type on the top of the image. All scale bars = 500 μm.

Appendix A.3 Lymphoid tissue engineering review submitted to the Journal of Immunology and Regenerative Medicine

Tissue Engineering of the Lymphoid Organs

Caleb Harff[1] and Angela Panoskaltsis-Mortari[1,2 *]

[1]Biomedical Engineering Graduate Program, [2]Department of Pediatrics, Division of Blood and Marrow Transplantation & Cell Therapy, University of Minnesota, Minneapolis, MN, 55455

*Corresponding author: Division of Blood and Marrow Transplantation & Cell Therapy, Department of Pediatrics, University of Minnesota, 420 Delaware St. SE, Minneapolis, MN 55455, USA.

Email address: panos001@umn.edu

Abstract

The lymphoid system protects the body from pathogens through organs that produce immune cells and facilitate immune surveillance. The study and treatment of a variety of pathologies affecting or interacting with the immune system can benefit from tissue engineering strategies. These designs can be implemented *in vitro* and *in vivo* through a variety of fabrication methods. Here we describe structure, cell types, and signaling found in the bone marrow niche, thymus, peripheral lymphoid organs, and lymphatic vasculature. We then summarize lymphoid tissue engineering studies from recent reports, and choice of design components including scaffolds, stromal cells, and chemical or physical signals. Finally, we discuss the current limitations and future of this field.

*Keywords:*Tissue engineering, Lymphoid organs, Lymphatic system, 3D culture, Scaffold, Bioreactor

Introduction

The purpose of the immune system is to defend the body from pathogens while maintaining tolerance of the body's own tissues and avoiding adverse reactions to non-pathogenic external sources of antigens (i.e. commensal bacteria, food, etc.). The requisite functions for the achievement of this purpose are divided between different subsets of immune organs. The primary lymphoid organs, namely the thymus and bone marrow, are the sites for production and differentiation of hematopoietic progenitors into lymphoid and myeloid cells which provide the adaptive and innate branches of the immune response. They also provide an environment conducive to the selection of the aforementioned lymphocytes which are functional yet do not display pathogenic autoreactivity. The secondary lymphoid organ subsystem is comprised of the spleen, lymph nodes, tonsils, Peyer's patches, adenoids, and other lymphoid formations, which are found in a variety of tissues and referred to as the mucosa-associated lymphoid tissues[1]. These organs survey the body (primarily through the lymphatics) for antigens and are responsible for mounting an adaptive immune response by selectively activating B and T cells whose receptors are specific to the threat. Alternate forms of the antigen-specific receptors on B cells are secreted as antibodies. Tertiary lymphoid organs form in tissues experiencing chronic inflammation, and perform many of the same functions as secondary lymphoid organs. Finally, the lymphatic vasculature, although not placed in any of these three categories, plays a vital role in the transportation of immune cells and pathogens. In addition, the lymphatic endothelial cells of the vasculature support secondary lymphoid organs by enabling immune cell chemotaxis and antigen presentation[2]. Within the lymphatic organs, lymphocytes are supported by a variety of

stromal cells that provide them with signals needed for survival, growth, development, and migration.

The design of biomimetic constructs or models, grounded in an understanding of biology and engineering principles, has made significant contributions to the field of regenerative medicine and resulted in a supply of commercially available products that are used to develop approaches to replace injured or dysfunctional tissues. This endeavor, known as tissue engineering, makes use of cells, scaffolds, and a variety of chemical or physical signals to replicate the structure and function of natural tissues [Figure 1]. For the purposes of immune tolerance, it is often most efficacious to use autologous cells from the intended recipient of a tissue engineered construct[3]. These cells may be taken from a patient to be expanded and seeded in a scaffold *ex vivo* or they may simply be recruited to a site of implantation of a scaffold to be incorporated into a design *in vivo*. Stem cells are another useful resource since they are self-renewing and capable of differentiation. The term scaffold refers to a variety of three-dimensional structures, often hydrogels, which can be used to contain and provide signals to cells. These may be derived from natural materials or from synthetic sources and generally have pores or channels that allow the movement and interaction of one or more cell types within the construct. It is imperative that these materials not be cytotoxic and that, if they are intended to be implanted, display full compatibility with the recipient animal model or human patient. Signals that are used in tissue engineered designs may include chemical signals such as growth factors, cell adhesion peptides, chemokines, and other relevant molecules that promote viability, proliferation, migration, or specific functions of a target cell population. Physical signals may be provided by the material used for scaffolding, as

is the case for factors such as stiffness or surface topography. External physical signals such as fluid flow, tensile or compressive loading, and even electrical stimulation can play an important role in the development of an intended cellular phenotype or function.

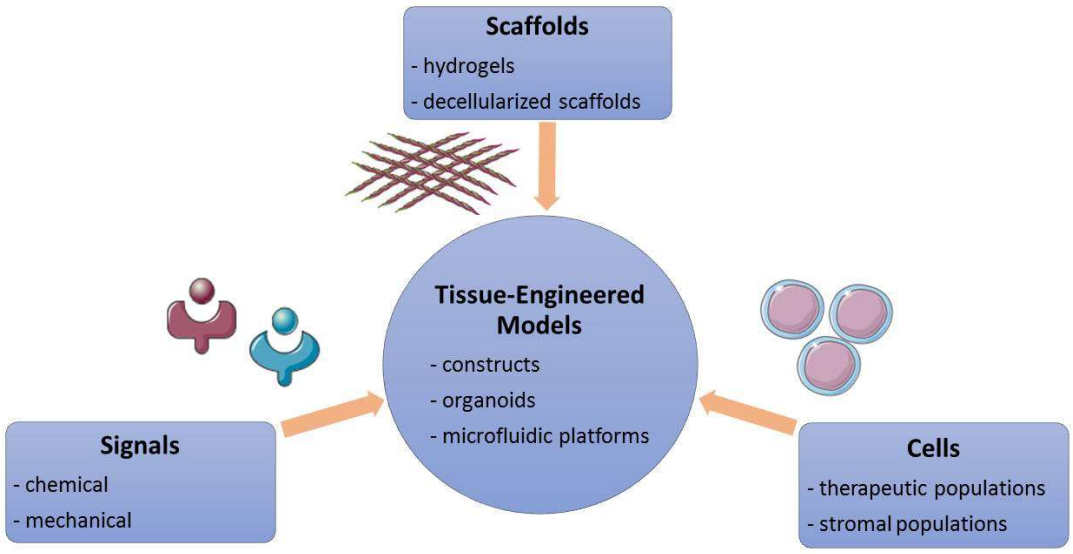

Fig. 1. Tissue engineering design often utilizes a combination of scaffold materials, cell types, and environmental signals to replicate natural function and achieve desired outcomes. Reproduction of the artwork: "Ligand", "Receptor", "Lymphocyte", and "Collagen" by Servier Medical Art at https://smart.servier.com/ is permitted under the terms of the Creative Commons Attribution Unported 3.0 license.

The design of a tissue engineered construct generally falls into one of a set of distinct approaches. One standard approach involves the seeding of cells into a porous scaffold. Such a design may be constructed by the casting or bioprinting of a polymeric material or hydrogel. Bioprinting provides a means of creating a complex spatial organization that may not be possible with simpler methods but requires the use of materials whose properties allow them to be effectively printed[4]. When stem cells are placed in 3D clusters that self-organize and differentiate into requisite somatic cell types, it is known as organoid formation[5]. The latter approach is often supported by placement of the cells within a scaffold material but it is also possible for these cells to secrete their

own extracellular matrix. In order to provide cells within a tissue engineered construct that is maintained *in vitro* with nutrients and waste removal, scaffolds are often placed within a perfused housing known as a bioreactor. Bioreactors can also be used to provide chemical or physical signals with or without temporal variation. Alternatively, a construct can be implanted into an animal model for *in vivo* maturation or designed to simply exert its effect directly upon implantation within a patient, as is the case with many injectable scaffold approaches. Advances in microfluidic technology have led to its combination with 3D cell culture to create organ-on-a-chip models. An advantage of this approach is the high degree of control over architecture and perfusion that it imparts[6]. Another technology, which permits use of the body's own structural design, is decellularization: removal of cellular content from an organ or tissue leaving behind the natural scaffold provided by its extracellular matrix. In addition to consideration of the scaffold type and method used, the material itself is an important factor. Many synthetic materials are easily and consistently producible and can be modified with natural peptides or other bioactive molecules to impart biological function. These modifications can be forgone if a naturally derived material is chosen but these are generally more expensive, harder to manipulate and process, and can be more vulnerable to batch variability.

Lymphatic bioengineering involves the use of cells and biological factors in an appropriate medium or scaffold to reconstruct or mimic the function of some part of the lymphoid organ system. This endeavor has the potential to provide the medical sector with a variety of services. For example, it could better establish the efficacy and safety of pharmaceutical drugs that can be limited by their interaction with the immune system and the resultant, potentially immunotoxic, response. The advent of highly biomimetic, three-

dimensional engineered models of each organ of the immune system could provide the industry with a reliable, reproducible, cost-effective, and ethical alternative to the pre-clinical trials which are performed on animal models and whose results often translate poorly to the clinical phase[6,7,8]. Some other experimentally-related concerns with the use of animal models include the presence of fundamental differences in the immune systems of different species and the inability to fully measure or control the complex cellular interactions in a test subject[5,6]. Additionally, *in vitro* models provide a multitude of experimental benefits including the ability to manipulate signaling pathways, engineer tissue niches, and introduce epigenetic or genomic alterations to cell lines[9]. Of these, the ability to recreate the appropriate, 3-dimensional tissue niche in terms of extracellular matrix components, chemical gradients, scaffold stiffness, and other mechanical gradients is especially vital for immune cell function, giving a bioengineered tissue model an advantage over oversimplified, 2-dimensional culture systems[6,9]. Furthermore, *in vitro* models provide an improved system for imaging or performing molecular analyses at multiple timepoints in an experiment, thereby allowing observation of temporal dynamics[5,10]. Finally, bioengineered models have the potential to encapsulate individual specificity within therapeutic screening tests by isolating, expanding, and seeding the patient's own cells in the scaffold or construct. This could serve to capture the traits of their specific disease by using affected cell populations, avoid adverse immune responses to allogeneic cells, and characterize their personalized reaction to a drug or immunotherapy[6,8,11].

Alongside providing *in vitro* systems for drug and immunotherapy screening, bioengineered lymphatic tissue models can provide a means of studying the dynamics of

auto-immune disease and cancer within lymphoid organ-specific microenvironments[7,12]. This could elucidate the evolution of these pathologies and give insight on potential immunotherapeutic approaches based on the interactions of diseased cells with surrounding immune cells. Furthermore, the recreation of tissue-specific niches involving hematopoietic stem and progenitor cells may allow observations of lineage development and the expansion of rare, potentially therapeutic cell populations[9,13].

Another beneficial outcome of the progression of lymphatic tissue engineering would be the implantation of secondary lymphoid organ constructs to replace or bolster inadequate natural immune function. Such an approach could be used as a vehicle for immunotherapy by implanting immune cells in a physiologically and pathologically relevant location. These cells could be pre-primed against an antigen particular to the infectious disease vector or to the cancer type of interest. They can also be provided with the appropriate microenvironment by the scaffold they are seeded in, allowing *in vivo* expansion and improved viability. Furthermore, this tactic could be used to combat pathological inflammation and auto-immune disease by providing a population of regulatory immune cells to control these adverse immune responses[11]. Additionally, the negative effects of genetic disorders involving an inhibition of lymphatic organ development or lack of function such as DiGeorge syndrome, severe combined immune deficiencies (SCID) or Fanconi anemia could be circumvented by implantation of an appropriate lymphatic tissue construct to restore function. As a final application, the implantation of a tissue-engineered secondary lymphoid organ construct (alongside engineered lymphatic vasculature, as needed) could be used as a direct tissue replacement to treat inherited or acquired lymphedema, the accumulation of interstitial fluid resulting

from insufficient lymphatic drainage. Acquired lymphedema is often a result of radiation therapy or tumor removal[14]. An additional benefit of such a replacement would be the restoration of immune surveillance provided by the lost lymphatic organs and vasculature.

Engineering the Bone Marrow Niche

The bone marrow is the primary home of the hematopoietic stem cell (HSC) that has the potential for both self-renewal and differentiation into the immune cells of the myeloid and lymphoid lineages. Regulation of HSCs in the bone marrow is dependent on the signaling dynamics of local tissue microenvironments called niches [Figure 2]. There are two distinct HSC niches; those of the first type (the vascular niche) are localized around sinusoid vessels, near endothelial cells[11]. A second type (the endosteal niche) exists within the endosteum, in the presence of osteoblasts[11]. The first supports expansion and differentiation whereas the second maintains a reservoir of long-term progenitors in a quiescent state[11]. The maintenance of these niches is influenced directly and indirectly by several local cell types including endothelial cells, mesenchymal and perivascular stromal cells, osteoblasts, osteoclasts, macrophages, and cells of the sympathetic nervous system[15]. Furthermore, a number of extracellular matrix proteins contribute to the structure and function of the niche, including fibronectin, tenascin, thrombospondin, elastin, laminin, collagen, and a variety of proteoglycans[16]. Finally, the hematopoietic niche is hypoxic, an attribute that may promote local signaling, which contributes to the function of the niche[17].

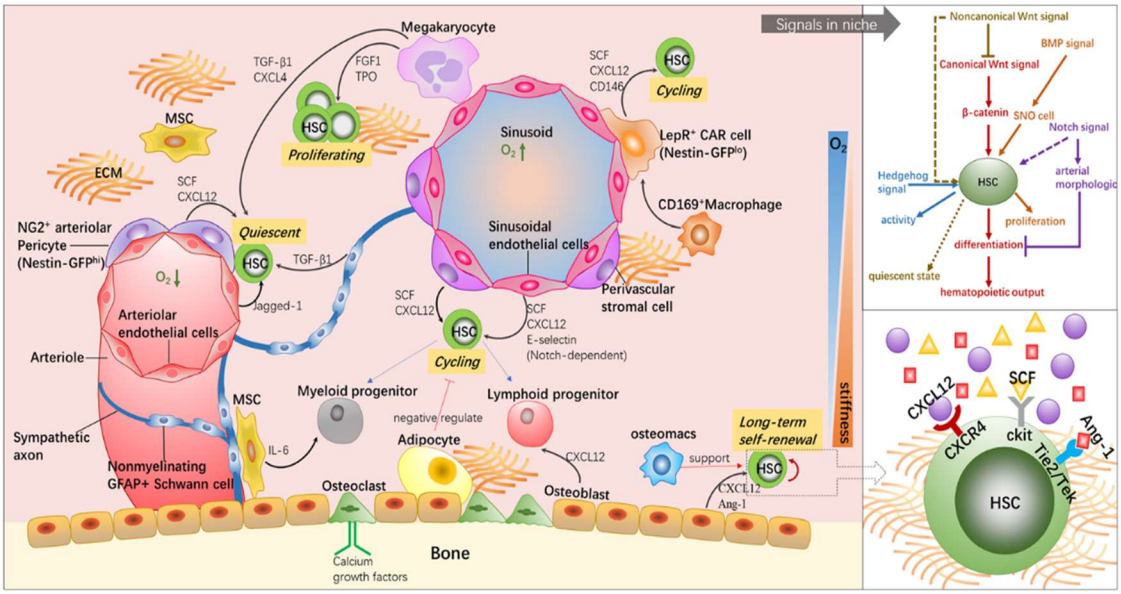

Fig. 2. The bone marrow stem cell niche contains stromal cells and provides a variety of signals to resident HSPCs. Adapted from Zhang et al., 2019[18]. Reproduction is permitted under the terms of the Creative Commons Attribution 4.0 International license.

The ability to recreate the bone marrow niche *in vitro* opens the door to improved expansion of hematopoietic stem and progenitor cell (HSPC) populations that are valuable for treating a variety of hematological disorders in which blood cell presence or function is lost[19]. It also provides a platform for *ex vivo* drug screening and for the study of hematopoietic biology and lineage commitment[20]. Furthermore, it can be used to promote the commitment of hematopoietic progenitors to a lymphoid lineage to produce B or T cells that combat infection and provide a means of suppressing the initiation and development of cancer[21,22].

Given the complexity of the bone marrow niche, the challenge of tissue engineering a model to recreate its functions includes choosing an appropriate set of cell types in a sufficiently biomimetic scaffold to provide necessary chemical, mechanical, and physical-spatial cues. This has been attempted by several different research groups, generally by seeding HSPCs within a 3D scaffold of natural or synthetic polymers

alongside a supportive stromal cell population. While early studies simply provided an undefined stromal population from bone marrow cell cultures, more recent studies have used mesenchymal stromal cells isolated from the bone marrow, placenta, or cord blood. Furthermore, a 2019 study by Braham et al. included mesenchymal stem/stromal cells (MSCs) committed toward an osteogenic or adipogenic lineage as well as endothelial progenitor cells with the rationale that adipocytes and endothelial cells are key stromal cells in the hematopoietic niche[17]. The use of multiple stromal cell types to better recreate the bone marrow niche may gain popularity going forward.

The scaffold-with-stromal-cell approach often requires the inclusion of additional soluble, chemical signals, which indicates that a sufficiently biomimetic cellular and structural design has not yet been developed to induce the full portfolio of chemical signaling found in the niche. Common supplementary cytokines to encourage the maintenance and proliferation of HSPCs in these tissue-engineered scaffolds include stem cell factor, Fms-like tyrosine kinase 3 ligand, thrombopoietin, and various interleukins. Furthermore, the choice of a synthetic polymer-based scaffold often requires modifications with natural molecules to promote cell adhesion and viability but can provide greater control over its mechanical properties. Another, different method to provide a scaffold construct with cells and chemical signals is to incubate it *in vivo*. An example of this strategy is given by a study by Torisawa et al. in which a microfluidic chip combined with a collagen and demineralized bone powder scaffold containing pro-osteogenic factors was seeded *in vivo* by cells recruited after implantation within a murine host[20]. A summary of experimental designs and key results are presented in Figure 3 below.

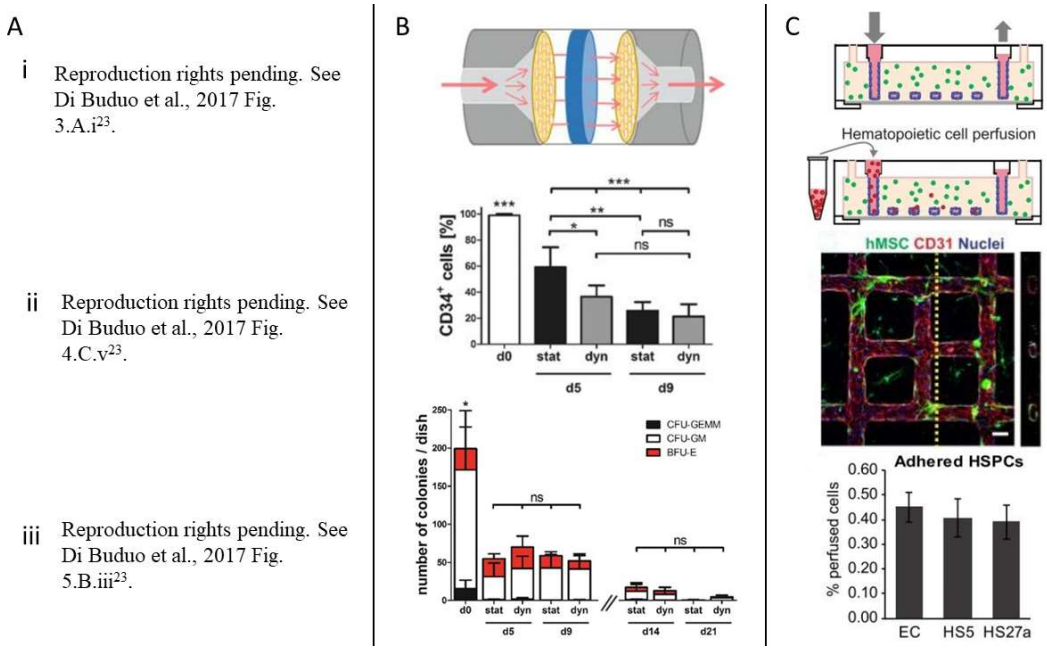

Fig. 3. Experimental setups and key results for a selection of bone marrow niche engineering studies. **A** i) A perfused silk sponge functionalized with fibronectin is ii) seeded with megakaryocytes (green = cells, blue = silk, scale bar = 100 μm) and iii) forms and releases platelets (scale bar = 50 μm). **B** Flow dynamics contribute to HSPC culture in a bioreactor with a perfused hydrogel. **C** HSPCs are perfused into a collagen-based microvessel platform to study migration and stromal cell interactions. HSPC adherence is influenced by stromal cell interactions. Panel **A** is adapted from Di Buduo et al.[23], **B** from Rödling et al.[24], **C** from Kotha et al.[25]. Panel **A** figures are reprinted with permission from Elsevier. Reproduction of the figures in **B** and **C** is permitted under the terms of the Creative Commons Attribution 4.0 International license.

Other design aspects that have been explored within the last decade include the use of active perfusion to supply nutrients and provide physiologically mimetic, supportive mechanical signals from fluid flow while removing waste[26]. Perfusion can be achieved within the context of a microfluidic device, also known as the bone-marrow-on-a-chip approach, or within a larger scale bioreactor. While microfluidic devices provide high throughput and precise control, the limitation on the volume of the system may restrict its complexity which, in the case of attempting to replicate the bone marrow niche, has been seen by some as a drawback[26]. Additionally, a number of studies have characterized hypoxic conditions within their constructs and found this state able to improve the viability and proliferation of the seeded cells while promoting gene

expression characteristic of the hypoxic bone marrow niche[17,27,28]. Brief descriptions of bone marrow niche engineering studies from various research groups are given in Table 1, below.

Table 1. Recent approaches to engineering the bone marrow niche for the expansion of HSPCs

Type	Scaffold	Stromal Cells	Exogenous Cytokines	Additional Objectives	Reference
In vitro, synthetic matrix	PET film or Fibra-Cel mesh conjugated with fibronectin or collagen	None	SCF, Flt-3 ligand, TPO, IL-3	HSPC engraftment	29
	Silicate or polyacrylamide hydrogel with clay nanoparticle + PDDA coating	HS-5 BM stromal cells and fetal osteoblasts	IL-2, IL-3, IL-7, Flt-3 ligand, SCF, BMP-4	HSPC differentiation to B lymphocytes	21
	PVF resin	Those present in BMC population	None	HSPC differentiation to erythroid cells	27
	PuraMatrix	MSCs	SCF, IL-3, IL-6	HSPC engraftment	28
	PEGDA- *co*-A6ACA	From BMC population or recruited *in vivo*	None	*In vivo* osteogenesis	30
In vitro, hybrid matrix	PLGA/PU and collagen type I	From CBMNC population	None	MSC expansion	31
	β-TCP with Matrigel or collagen type I/III	MSCs	SCF, TPO, Flt-3 ligand, IL-6	Osteogenesis	32
In vitro, natural matrix	Alginate or Matrigel	MSCs, O-MSCs, A-MSCs, endothelial progenitor cells, MS5 feeder layer	None	None	17

	Collagen I	None	GM-CSF	HSPC differentiation into DCs	33
In vitro, microfluidic chip or perfused bioreactor with natural matrix	Collagen type I, DBP	Those expressing CXCL12, recruited *in vivo*	BMP-2, BMP-4, SCF, IL-11, Flt-3 ligand, LDL, G-CSF	Study radiation toxicity effect on HSPCs	20
	Type I collagen	MSCs, BM fibroblasts, ECs	None	Study HSPC migration and interactions with stromal cells	25
	Silk fibroin modified with fibronectin	None	TPO, IL-11	Megakaryocyte differentiation into platelets	23
In vitro, microfluidic chip or perfused bioreactor with synthetic matrix	Hydroxyapatite	MSCs	TPO, SCF, Flt-3 ligand	MSC osteogenic differentiation	26
	Hydroxyapatite and zirconium oxide	MSCs	TPO, Flt-3 ligand	None	34
	PEG modified with RGD peptide	MSCs	TPO, SCF, Flt-3 ligand, IL-3	None	24
In vivo, injectable hybrid hydrogel	Alginate and PEG modified with DLL-4	Any recruited in the host	BMP-2	HSPC differentiation into T cells	22

Engineering the Thymus

The thymus is the site of T cell maturation. Lymphocyte progenitor cells from the bone marrow are recruited to the thymus by homing signals and there encounter a tissue-specific niche which promotes their differentiation into mature T cells[35]. The thymus contains two distinct regions, the cortex and the medulla [Figure 4]. Each one contains its own specific type of thymic epithelial cells (TECs) that provide essential trophic signals

alongside other stromal cell types, which include mesenchymal fibroblasts, macrophages, and dendritic cells (DCs)[36,37]. In particular, Notch ligand signaling provided by TECs is crucial for T cell development[38]. Furthermore, they provide the signals necessary for positive and negative selection of thymocytes, which occur in the cortex and medulla, respectively[37]. These stages of development result in a population of mature T cells with potent yet non-autoreactive T cell receptors. The three-dimensional organization of TECs in the thymus is a requirement for their function; monolayer culture of these cells results in a loss of expression of key genes[36].

Reproduction rights pending. See Singh, 2017 Fig. 2.A (upper portion)[39].

Fig. 4. The thymus is divided into two main areas, the medulla and cortex, and is responsible for the production of mature T cells and maintenance of central tolerance. Adapted from Singh et al., 2017[39]. Reprinted with permission from Elsevier.

The thymus is particularly susceptible to the loss of its TEC population and a subsequent deficiency in T cell production, which compromises the immune system[35]. This organ naturally degenerates over the course of the human lifetime, with peak cellularity and function occurring around nine months after birth and decreasing with age[37]. An additional concern that could be addressed by thymic tissue engineering is the existence of genetic defects that result in diseases such as Di George syndrome in which the thymus fails to develop and there is an innate lack of T cell production[38]. External insults that can compromise the function of the thymus include atrophy through acute infection, chemotherapy, and therapeutic irradiation[37]. These problems can potentially be solved by *in vitro* production and subsequent administration to the patient of therapeutic

cell populations (TECs and/or mature T cells) or by the implantation of a functional, tissue engineered thymic graft. Additionally, central immune tolerance to allografts could be induced for donor-specific tissues by use of a thymic construct[35].

The thymic niche is similar to that found in the bone marrow in the sense that its complexity is imparted by 3D stromal cell organization, signaling, and extracellular matrix (ECM) components that provide physical anchors and harbor chemical factors. However, this niche is less well understood and fewer attempts have been made to determine what combination of scaffold, stromal cells, and cytokines are minimally necessary for an effectively biomimetic model. Commonly used exogenous factors to promote T cell production include Flt-3 ligand, SCF, and IL-7. A study by Poznansky et al. attempted this goal by seeding HSPCs and a mixture of thymic stromal cells (TSCs) into a 3D synthetic scaffold, resulting in a greater proliferation of mature T cells than in a simple co-culture[40]. Other traditional, scaffold-using studies include a study in which Matrigel® and thymic tissue were placed in a silicone construct, and a study in which PCL and collagen were used to provide a hybrid matrix for HSPCs and supportive stromal cells[36,41]. In both of these cases, however, *in vivo* maturation was required for the desired T cell production, indicating that a sufficiently biomimetic scaffold model remains to be constructed *in vitro*. Most recent approaches instead utilize organoid formation or a decellularized thymus matrix and many of them use implantation to achieve maturation and T cell production *in vivo.* Organoid formation has been approached by combining HSPCs with medullary TECs and thymic mesenchyme on a gelfoam base[38]. A simplification of this stromal cell population requirement was achieved by Seet et al. through the use of a DLL1-transduced stromal cell line to form organoids

with a mature T cell production. Another advantage of the aforementioned design is its ability to obtain this result *in vitro* and without exogenous growth factors[42].

Decellularization of the thymus for use in tissue engineering has gained recent popularity. This approach was demonstrated by Fan et al. Decellularized thymic ECM was reseeded with TSCs and HSPCs, provided with exogenous IL-7, and used to produce mature T cells *in vitro*[35]. Another research group augmented this approach by first incubating TECs in a composite hydrogel with growth factor and stromal cell support, seeding the decellularized thymus with these and other stromal cells, and finally implanting the construct to produce mature T cells *in vivo*[43]. A summary of experimental designs and key results are presented in Figure 5, below. Brief descriptions of thymus engineering studies from various research groups are given in Table 2.

A

i Reproduction rights pending. See Tajima et al., 2015 Fig. 1.A[37].

ii Reproduction rights pending. See Tajima et al., 2015 Fig. 1.D[37].

iii Reproduction rights pending. See Tajima et al., 2015 Fig. 2.A[37].

B

i Reproduction rights pending. See Hun et al., 2017 Fig. 3.C[43].

ii Reproduction rights pending. See Hun et al., 2017 Fig. 4.H[43].

Fig. 5. Experimental setups and key results for a selection of thymus engineering studies. **A** i) Amphiphilic peptides and adaptor complexes modified with antibodies form self-assembling hydrogels with embedded TECs. These gels ii) maintain TEC viability (green = live, red = dead) and iii) support T cell production when implanted in B6.nude mice. **B** Decellularized thymic scaffolds were reseeded with TECs and implanted in the kidney capsule of athymic nude mice (scale bar = 100 μm). This approach was compared to reaggregation thymic organ culture in its ability to produce T cells upon engraftment. Panel **A** figures are adapted from Tajima et al.[37] and **B** from Hun et al.[43] . Reprinted with permission from Elsevier.

Table 2. Recent approaches to engineering the thymus to produce mature T cells from HSPCs

Type	Scaffold	Stromal Cells	Exogenous Cytokines	Additional Objectives	Reference
In vitro, synthetic matrix	Tantalum-coated carbon matrix	TSCs	None	None	40
	DLL4-functionalized magnetic polystyrene microbeads	OP9 bone marrow stromal cells	IL-7, SCF	None	44
In vivo, hybrid matrix	Silicone chamber containing Matrigel and thymic tissue	From thymic stroma	FGF-2	None	36
	3D co-culture on fibrin and Jettex-3D	Medullary TECs, human skin fibroblasts	TGFβ-1, RANKL, KGF, CD40L	Medullary TEC maturation and proliferation	45
In vivo, natural matrix	EAK peptide hydrogel	TECs	None	None	37
In vitro, organoid	None	Medullary TECs and thymic mesenchyme	Flt-3 ligand, IL-7, SCF	None	38
	None	MS5 DLL1-transduced bone marrow stromal cells	None	None	42
In vitro, decellularized scaffold	Decellularized thymus	TSCs	IL-7	None	35
	Decellularized thymus (TECs incubated in gelatin-PEG hybrid matrix)	TECs, thymic fibroblasts (TECs supported by embryonic	BMP-4 (used in TEC incubation)	None	43

		fibroblasts during initial incubation)			

Engineering the Peripheral Lymphoid Organs

The peripheral lymphoid system includes the spleen and lymph nodes as well as other mucosa-associated lymphoid tissues, such as the tonsils and Peyer's patches, which are distributed throughout the body[46]. The purpose of these organs and tissues is to enhance immune surveillance by filtering extracellular fluids, provide an environment for effective antigen capture and presentation, and facilitate adaptive immune responses[46]. Extracellular fluid called lymph drains from tissue and flows into the lymph nodes via afferent lymphatic vessels and brings with it antigens produced by infection or malignancy[46] [Figure 6]. Furthermore, antigen-bearing dendritic cells are actively recruited to the lymph nodes by chemokine gradients[46]. B and T lymphocytes are present in designated, separate areas in the lymph node[46]. The architecture of the lymph node promotes the exposure of naive T cells to antigen-presenting macrophages and dendritic cells[46]. Upon activation, T cells migrate to the edges of their zones to encounter B cells and provide helper signals[46]. Activated lymphocytes proliferate and differentiate in the lymph node and leave via the efferent vessels to perform their effector functions. Leukocytes in the paracortex (T cell zone) of the node are surrounded by stroma referred to as reticular meshwork that is composed of fibroblastic reticular cells and the extracellular matrix fibers (also known as reticular fibers) that they secrete[47]. This meshwork enables lymphocyte migration and forms conduits for the transportation of

soluble antigen and inflammatory cytokines. In the lymph node, B cell zones are home to the germinal center (GC) reaction, a key process that results in B cell antibody class switching and affinity maturation[48] [Figure 6, upper right].

The white pulp of the spleen carries out a similar function to the lymph nodes but does so with bloodborne antigens rather than those collected by the lymph. Akin to the lymph nodes, the spleen has designated B and T cell zones, populations of antigen presenting cells, and the capacity for germinal center formation[49]. In addition to those carried in the blood and lymph, antigen is able to contact the lymphatic system through mucosal surfaces in the gastrointestinal and respiratory tracts. They are collected by microfold cells, specialized epithelial cells which are present in a variety of mucosa-associated lymphoid tissues[50]. All of the aforementioned peripheral lymphoid organs and tissues share a similar basic organization that allows them to collect antigen and have it presented to circulating lymphocytes. These secondary structures are inherently dynamic. For example, the lymph nodes are remodeled and enlarged upon nearby infection[51].

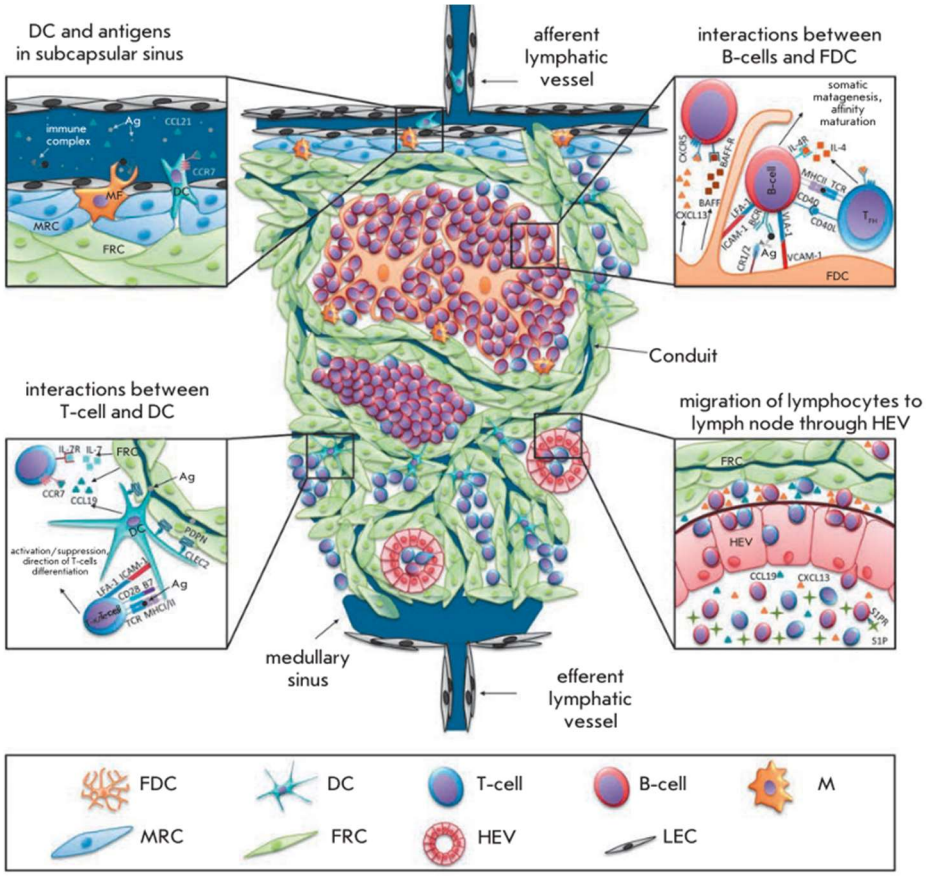

Fig. 6. The lymph nodes facilitate interactions between stromal cells and lymphocytes which allow activation and the progression of the adaptive immune response. Adapted from Nosenko et al.[11]. Reproduction is permitted under the terms of the Creative Commons Attribution 4.0 International license.

The loss of lymph nodes to radiation therapy or surgical resection can result in lymphedema and susceptibility to infection or further malignancy[52]. The construction of functional peripheral lymphoid organ models could replace lost function and treat lymphedema under these conditions. Besides tissue replacement, these models could also be used *in vitro* to test the immunogenicity of pharmaceutical drugs, develop vaccines in preclinical stages, and generate highly specific plasma cells for adoptive immunotherapy[53,54,55].

Many of the peripheral lymphoid organ tissue-engineering studies of the last two decades were focused on either the production of a germinal center reaction (using only B cells) or on the formation of more efficient immunological synapses (T cells and APCs)

in 3D. Of the former, studies by Purwada et al. show promising results. In the first of these publications, a gelatin and silicate nanoparticle hydrogel was used to incubate B cells in the presence of a transgenic stromal cell line and exogenous IL-4[56]. The stromal cells in this study produced CD40L and BAFF to replicate the function of the T follicular helper (TFH) cells and follicular dendritic cells (FDCs) found naturally in the lymph node. The latter study replaced the modified gelatin matrix with a PEG-maleimide scaffold conjugated with adhesion peptides and was able to achieve GC-like B cell phenotypes, antibody class switching, and the production of antigen-specific B cells[54].

With regard to those studies focused on the formation of immunological synapses and T cell activation, microfluidic devices provide a highly controllable format with which to study specific behaviors, as demonstrated by Rosa et al. in a study that looked at T cell and DC interactions under controlled flow conditions[57]. The use of artificial APCs for the activation of T cells in 3D culture conditions has been recently investigated by research groups out of Barcelona and Harvard and found to have an advantage over traditional 2D culture approaches[58,59]. The study by Cheung et al. found success in the complementary use of soluble mitogenic signals and liposome membrane-bound T cell receptor (TCR) stimulation ligands co-delivered by matrix-forming silica microrods to achieve rapid expansion of T cells[59]. Finally, injectable gels have proven their use in the delivery and expansion of T cells *in vivo*. This was accomplished using an alginate gel functionalized with GFOGER peptide, and through a polyisocyanopeptide hydrogel functionalized with GRGDS[60,61]. This approach can be applied to the immunotherapeutic treatment of cancer by delivering and expanding T cells that can recognize tumor-specific antigens at the location of a tumor or tumor resection site[60]. These studies included an

integrin-binding peptide to enable cell migration and egress from the gel into the site of interest[60,61].

Of the studies that involve both T and B lymphocytes, long term research by Giese et al. has resulted in a bioreactor with RGD-Dextran gel discs that is able to support a lymphocytic immune response to protein aggregates, and maintain separated T and B cell zones, mimicking secondary lymphoid organ structure[53]. While this series of publications focused on *in vitro* functionality, other studies implemented *in vivo* recruitment of immune cells to seed implanted collagen sponges supported by thymus-derived stromal cells[62,63]. These efforts resulted in the induction of distinct B and T cell areas, antigen-specific antibody production, and even some evidence of a secondary immune response upon further stimulation. There have also been recent attempts to utilize decellularized lymph nodes as a scaffold for the *in vivo* production of potentially therapeutic cell populations. One example is the work of Lin et al. demonstrating the use of this approach to produce anti-tumor DCs in a biologically relevant microenvironment[52]. A summary of experimental designs and key results are presented in Figure 7, below. Brief descriptions of peripheral lymphoid organ engineering studies from various research groups are given in Table 3.

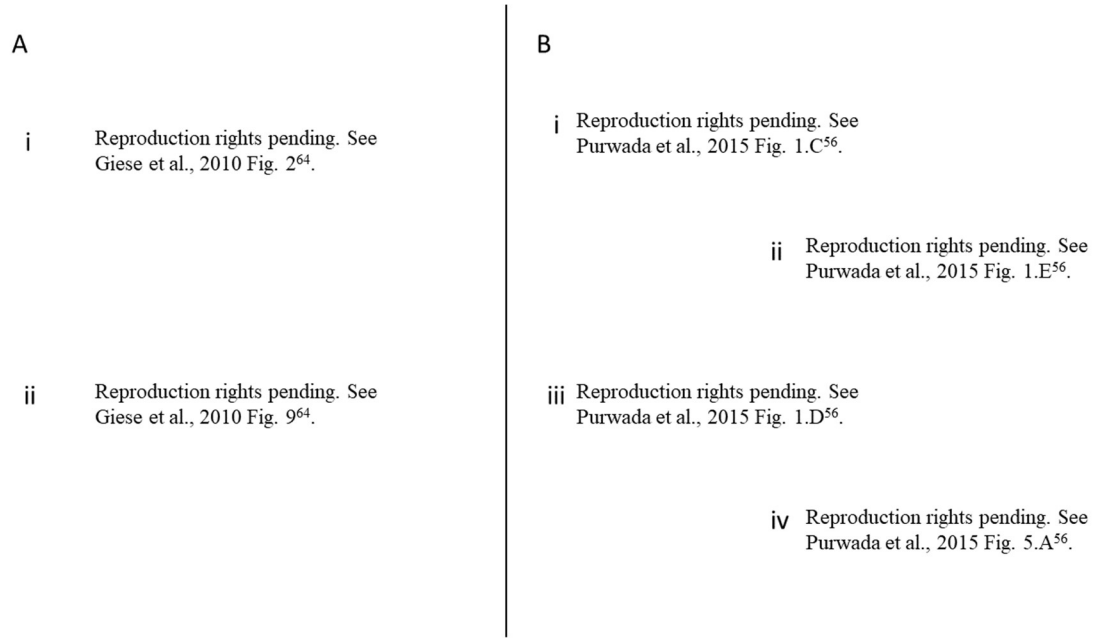

Fig. 7. Experimental setups and key results for a selection of peripheral lymphoid organ engineering studies. **A** (upper panel) A bioreactor that is supplied with cell media and oxygen contains a hydrogel matrix seeded with lymphocytes and stromal cells. (lower panel) Inflammatory cytokines are secreted in response to specific antigen challenges. **B** Crosslinked Gelatin-SiNP hydrogels containing naïve B cells and engineered stromal cells produce GC B cells (scale bar = 10 mm). Panel **A** figures are adapted from Giese et al.[64] and **B** from Purwada et al.[56]. Reprinted with permission from Elsevier.

Table 3. Recent approaches to engineering the peripheral lymphoid organs to mount an adaptive immune response to antigen challenge

Type	Scaffold	Stromal Cells and APCs	Exogenous Cytokines	Other Objectives	Reference
In vitro, microfluidic chip or perfused bioreactor	Agarose or polyamide hydrogel	DCs, MSCs, lymph node stromal cells	None	Study immune modulation by MSCs	64, 65, 66
	RGD-Dextran hydrogel	LN stromal-like cells differentiated from MSCs, DCs	TNFα, LTα1β2	Study the effect of LN-like stromal cells on immune response, evaluate protein aggregate immunogenicity	55, 67
	Macroporous cellulose microspheres	Tonsil stromal cells	None	None	68
	None	DCs	CCL19	Study of DC migration, T cell activation	69

	None, but channels coated with collagen or fibronectin	DCs derived from spleen tumors	None	Study DC:T cell binding strength and interactions under varied flow conditions	57
	"Live" slice of a LN	Those present in LN stroma	None	Peptide delivery to specific LN slice zones	70
In vivo, natural matrix	Collagen scaffold	DCs, LTα-transfected thymus-derived stromal cells, those recruited *in vivo*	None	B and T cells area formation, study of cell recruitment kinetics	62, 63
	Alginate functionalized with GFOGER peptide	None, but lipid-coated silica microspheres in matrix contain activation ligands (anti-CD3/CD28/CD137)	IL-15/IL-15Rα fusion protein	Expand and deliver tumor-specific T cells	60
In vivo, synthetic matrix	Polyisocyanopeptide hydrogel functionalized with GRGDS peptide	None	IL-2, IL-6	Expand T cells and deliver *in vivo*	61
In vitro, natural matrix	Gelatin crosslinked with silicate nanoparticles	40LB transgenic cell line, expresses BAFF and CD40L	IL-4	None	56
In vitro, hybrid matrix	PEG-collagen hydrogel	DCs	CCL21 (bound to PEG)	T cell and DC migration	71
	PU-collagen/Matrigel sponge	None	None	Study impact of interstitial flow on TRC phenotype	72
In vitro, natural or synthetic matrix	Matrigel or polystyrene scaffold	Dynabeads acted as artificial APCs	None	CD4+ T cell activation and proliferation	58

In vitro, synthetic matrix	Maleimide-PEG functionalized with RGD or REDV	40LB transgenic cell line, expresses BAFF and CD40L	IL-4	None	54
	Silica microrods which assemble into 3D matrix	None, but matrix functionalized with T cell stimulation ligands (anti-CD3/CD8)	IL-2	T cell expansion and antigen-specific enrichment	59
In vivo, decellularized scaffold	Decellularized murine lymph nodes	Those present in splenic stroma	None	Delivery of splenocytes to murine model	73
	Decellularized rat lymph nodes	Murine bone marrow DCs	None	BMDC delivery for tumor-specific immunity	52

Engineering the Lymphatic Vasculature

Recent studies of the functions of lymphatic vessels and the expression profiles of lymphatic endothelial cells (LECs) have uncovered a rich and dynamic role for this component of the lymphatic system. Lymphatic vessels spread out into the skin and mucosal membranes, draining lymph from tissues that contain sufficient interstitial fluid[74]. The LECs surrounding the lymphatic capillaries form discontinuous cell junctions, which can respond to changes in interstitial pressure to allow fluid entry via specialized valves[74]. Lymphatic vessels contain intraluminal valves to maintain unidirectional flow of the lymph; the contraction of smooth muscle surrounding the vessels also serves this purpose[74][Figure 8]. A 2019 study by Berendam et al. revealed that LECs have different expression profiles than blood endothelial cells for proteins influencing extracellular matrix production, cell adhesion, and chemotaxis[75].

Furthermore, the expression profiles of lymph node LECs vary from those of LECs in other tissues[75]. CCL21 is produced by LECs to recruit DCs and promote directional crawling[74]. Additionally, the CCL21 gradient produced by subcapsular sinus LECs enables migration of DCs into the lymph node paracortex to interact with T cells[74]. Inflammation causes the expression of VCAM-1 on LECs, which promotes T cell and DC entry into lymphatic vessels while sphingosine-1-phosphate (S1P) plays an important role in T cell migration and survival in the lymph node[74]. Furthermore, lymph node LECs produce IL-7, which supports lymphocyte expansion during lymph node remodeling[74].

In addition to functions that support an immune response, LN LECs have an immunomodulatory role. These cells produce a variety of TGF-β superfamily proteins, which have immunosuppressive effects[75]. Lymph node LECs can also directly express self-antigen to maintain peripheral tolerance via CD8 T cell deletion or transfer it to DCs that use it to cause CD4 T cell anergy through MHC-II presentation[75]. A final function of the lymphatic vasculature, which is not directly related to immune activity, is the transport of dietary lipids from the gut[76]. Lymphatic vessels in the villi called lacteals are responsible for the uptake and transport of triacylglycerols from the small intestine[76].

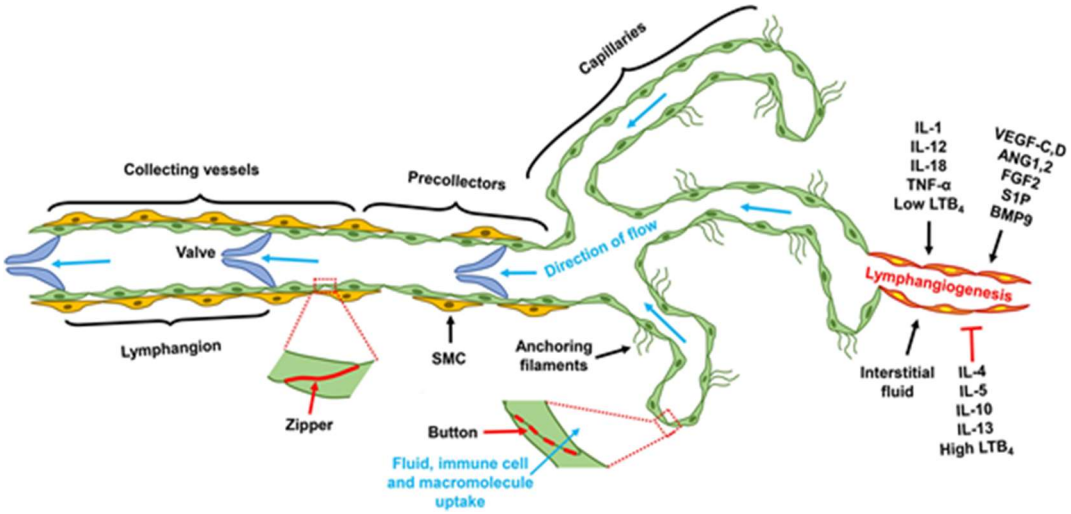

Fig. 8. The lymphatic vasculature drains interstitial fluid from the tissues, enabling the transport of antigen and immune cells to the peripheral lymphoid organs. Adapted from Jiang et al., 2019[77]. Reproduction is permitted under the terms of the Creative Commons Attribution 4.0 International license.

There are several motivations for the development of tissue engineered lymphatic vasculature. Lymphedema is a symptom of congenital or acquired lymphatic impairment; the second form is often a result of radiotherapy or surgery for the treatment of cancer[78,79]. Reconstruction of the lymphatic vasculature using tissue engineered constructs can alleviate lymphedema and provide an advantage over traditional surgical repair or lymph node engraftment, two current solutions that have yielded limited success[79,80]. Furthermore, skin grafts and other tissues or organs intended for transplantation can benefit from inclusion of lymphatic vasculature through the provision of lymphatic drainage and immune accessibility[81,82]. Finally, *in vitro* models of the lymphatic vasculature can provide a means of studying the functions of LECs with regards to fluid flow, immune cell interactions, or the transport of dietary lipids[76,83].

A look at studies attempting to tissue-engineer lymphatic vessels reveals a variety of approaches. Some of the earliest efforts were pioneered by Swartz and colleagues; these feature collagen or fibrin gels set in a perfused bioreactor alongside blood endothelial cells[83,84]. Their study used a collagen and fibrin combination gel modified

with a vascular endothelial growth factor (VEGF) fusion protein bound to the fibrin component[84]. This approach resulted in the *in vitro* formation of lymphatic capillaries and was used to study the effect of fluid flow and shear stress on LEC morphology[83,84]. A later study took a different direction with the creation of a LEC-enterocyte transwell interface model to study the transport of lipids from the gut to the lymphatics[76]. Dai et al. studied an *in vivo* approach, forming a polyglycolic acid (PGA) scaffold seeded with LECs in a silicone tube for implantation and maturation of a lymphatic vessel in a murine model[80]. A number of growth factors including VEGF were used to support this design during an initial *in vitro* incubation phase[80]. Marino et al. returned to the use of fibrin and collagen, supplemented with VEGF-A and VEGF-C to form blood and lymphatic capillaries both *in vitro* and within an implanted skin graft model[81]. Fibroblasts acted as supportive stromal cells, and keratinocytes formed an integral part of the skin model in this study[81]. Another publication revealed that lymphatic vasculature can be formed without an exogenous scaffold as fibroblasts can produce ECM and form vessels when cultured with LECs[78]. The authors also showed that similar results can be achieved in a collagen gel and that hepatocyte growth factor (HGF) and VEGF-C promote lymphangiogenesis. Hadamitzky et al. attempted a similar strategy using a natural matrix, seeding LECs within a nanofibrillar collagen scaffold with conjugated VEGF-C[79]. Implantation in a porcine model led to promising histological results and an improvement in bioimpedance readings, indicating interstitial fluid drainage. Most recently, Knezevic et al. used adipose-derived stromal cells to support the development of lymphatic vasculature *in vitro*, supported by a fibrin hydrogel[82]. The use of these stromal cells had a positive impact on LEC migration and proliferation, resulting in better vasculogenesis. A

summary of experimental designs and key results are presented in Figure 9, below. Brief descriptions of thymus engineering studies from various research groups are given in Table 4.

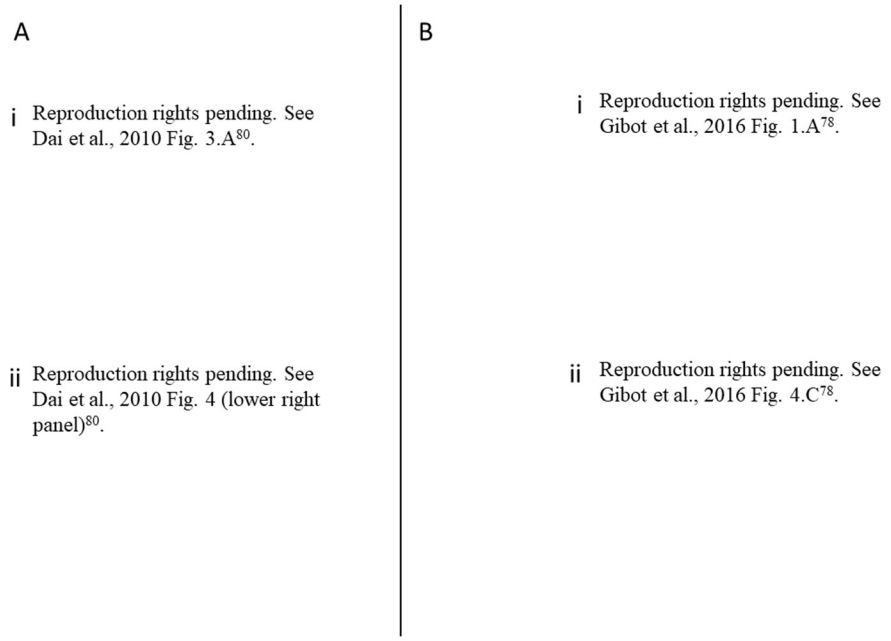

Fig. 9. Experimental setups and key results for a selection of lymphatic vessel engineering studies. **A** PGA sheets containing LECs are wrapped around silicone tubes and form lymphatic vessels after implantation in nude mice for 6 weeks. **B** Stacked sheets of fibroblasts and LECs form vascular networks (scale bar = 5 mm). When LECs are layered between collagen gels, the degree of tube formation is dependent on HGF and VEGF-C. Panel **A** figures are adapted from Dai et al.[80] and **B** from Gibot et al.[78]. Reprinted with permission from Elsevier.

Table 4. Recent approaches to engineering lymphatic vessels

Type	Scaffold	Stromal Cells and/or BECs	Exogenous Cytokines	Other Objectives	Reference
In vitro, perfused bioreactor	Collagen gel	BECs	Phorbol 12-miristate 13-acetate (PMA)	Study morphogenetic response of LECs to fluid dynamics	83

	Collagen and fibrin gel	BECs	Matrix-bound VEGF fusion protein	None	84
In vivo, transwell	Collagen coating on transwell	Caco-2 cells to replicate enterocyte function	None	Replicate the LEC-enterocyte interface, study the transport of lipids from Caco-2 cells to LECs	76
In vivo, synthetic matrix	PGA sheets in a silicone tube	None	VEGF, FGF, IGF, EGF	None	80
In vitro and *in vivo,* natural matrix	Fibrin or collagen gel	BECs, fibroblasts, keratinocytes (when used with skin model)	VEGF-A, VEGF-C, TGF-β1 (used as a repressive factor)	None	81
In vitro, natural matrix	Collagen gel or ECM secreted by fibroblasts	Fibroblasts	HGF or VEGF-C when in exogenous collagen gel	Study effects of HGF/VEGF-C on lymph-angiogenesis	78
	Nanofibrillar collagen scaffold	None	VEGF-C conjugated to scaffold	Improvement of bioimpedance in porcine model	79
	Fibrin gel	ASCs, BECs	VEGF-C	None	82

Summary, Challenges, and Future Directions

The field of lymphoid tissue engineering has seen notable accomplishments over the last few decades. Bone marrow niche models have been used to expand HSPC populations and guide their differentiation into a variety of lineages. These studies have also recreated other facets of the niche including hypoxia and stromal cell matrix deposition. Furthermore, the human blood compartment has been reconstituted in depleted murine models. Thymic constructs have produced mature T cells from HSPCs

and restored thymic T cell production in animal models. Tissue-engineered constructs mimicking some functions of peripheral lymphoid organs have shown an improvement over 2D cell culture with respect to T cell expansion and activation. They have also achieved germinal center reactions, resulting in high affinity, class-switched antibody production. Additionally, DC and T cell migration and interactions have been studied closely through microfluidic devices partially recreating the environment of these tissues. Finally, attempts to engineer lymphatic vasculature have achieved a degree of lymphangiogenesis *in vitro* and vessels that display natural function *in vivo*.

There are a number of visible trends in recent studies of lymphoid tissue engineering. Decellularization has become a popular method for producing highly biomimetic natural scaffolds that allow reseeding and delivery of cells. This approach has been implemented for lymphoid organs whose structures lend themselves to effective decellularization, namely the thymus and lymph nodes. Current bone marrow models use MSCs for stromal support and in many cases are still dependent on a set of exogenous cytokines although recreation of the niche has also been achieved without these. Continuing to ascertain what subsets of stromal cells best support the bone marrow niche will likely be advantageous for advances to these models. Thymic constructs are likewise dependent on support by TECs, although a recent study by Seet et al. used a custom stromal line instead of primary stromal cells that require extra costs associated with isolation, are susceptible to experimental variability, and may be limited by supply [42]. These cells may be engineered to express specific cytokines needed for the microenvironment. With regards to the engineering of peripheral lymphoid tissues, T cell activation designs have benefited from the use of silica microparticles. These can be

coated with lipids for functionalization with activation ligands, carry soluble cytokines, and even self-assemble into 3D structures. Several studies that have implemented hydrogel scaffolds not containing natural cell adhesion peptide sequences have functionalized their matrices with said ligands since integrin binding provides a key mechanism for lymphocyte migration. Attempts to create lymphatic vasculature mostly utilize natural hydrogels such as collagen or fibrin as a scaffold, fibroblasts or adipose stem cells (ASCs) as supportive stromal cells, and incorporate VEGF-C either as a bound or soluble signal. Little has been done to demonstrate the clinically relevant, functional potential of these vessels although a study by Hadamitzky measured the effect of their implanted construct on bioimpedance in a porcine lymphedema model[79].

There are many challenges and unanswered questions that present themselves to those seeking to advance the field. The bone marrow niche has been shown to contain stiffness gradients and complex ECM patterning that may affect resident cell behavior[85]. Although methods for the mechanical characterization of tissue-engineered constructs exist, little has been done in the field of lymphatic engineering to explore these properties. Furthermore, attempts at engineering the niche have been primarily focused on the expansion of HSPCs for the purpose of producing lymphocyte populations, which have readily apparent clinical uses. However, there may also be reasons to use such a platform for the production of innate immune cell populations. One such reason may be the production of anti-inflammatory or “M2” macrophage subtypes, which promote wound healing and support the incorporation of implanted lymphatic constructs[86]. Microfluidic platforms have been used to directly observe immune cell migration and interactions in the context of bone marrow and peripheral lymphoid organ models. As of

yet, this approach has not been applied to thymic models and has the potential to elucidate key behaviors of the immune and stromal cells in this organ.

Attempts to engineer a germinal center in peripheral lymphoid organ constructs have not yet demonstrated formation of dark and light zones, two distinct germinal center areas that are regulated by the expression of chemokine receptors on their resident B cells and may contribute significantly to efficient affinity maturation[48]. Furthermore, although high affinity antibodies have been generated for hapten antigens in these models, their ability to generate antibodies for more complex antigens has not yet been tested.

Tissue engineered models of the lymphatic vasculature have focused primarily on the use of VEGF-C to promote vessel sprouting but full development of mature vessels may depend on other chemical factors such as Notch ligands[87]. Furthermore, the design of VEGF-C gradients, instead of a more homogeneous inclusion seen in recent studies would be more biomimetic and may contribute to improved development of the vasculature[87,88]. It may also be beneficial to implement and characterize smooth muscle cell and pericyte coverage as well as valve structures in future studies as these are key components of mature, functional lymphatic vessels.

Interstitial flow is an important factor that has been shown to contribute to the behavior of cells in the lymphatic vasculature, lymph nodes, and bone marrow[18,69,89]. While flow dynamics and shear stresses have been incorporated in a variety of studies using microfluidic devices or other bioreactor platforms, these parameters will likely need to be fine-tuned to physiological values to provide the most effective microenvironment for immune cell survival and function.

The field of lymphoid tissue engineering has much to contribute to regenerative medicine and immunotherapies. As the manufacturing techniques improve and the designs home in on the combinations of scaffolds, cells, and signals that are crucial for desired functional outcomes, lymphoid tissue models will attain clinical relevance and impact development of therapeutic modalities for a variety of pathologies.

Competing Interests

The authors declare that they have no competing interests.

REFERENCES

[1] Ruddle, N. H., & Akirav, E. M. (2009). Secondary Lymphoid Organs: Responding to Genetic and Environmental Cues in Ontogeny and the Immune Response. The Journal of Immunology, 183(4), 2205–2212. https://doi.org/10.4049/jimmunol.0804324

[2] Randolph, G. J., Ivanov, S., Zinselmeyer, B. H., & Scallan, J. P. (2017). The Lymphatic System: Integral Roles in Immunity. Annual Review of Immunology, 35(1), 31–52. https://doi.org/10.1146/annurev-immunol-041015-055354

[3] Fodor, W. L. (2003). Tissue engineering and cell based therapies, from the bench to the clinic: the potential to replace, repair and regenerate. Reproductive Biology and Endocrinology : RB&E, 1, 102. https://doi.org/10.1186/1477-7827-1-102

[4] Vijayavenkataraman, S., Yan, W. C., Lu, W. F., Wang, C. H., & Fuh, J. Y. H. (2018). 3D bioprinting of tissues and organs for regenerative medicine. Advanced Drug Delivery Reviews, 132, 296–332. https://doi.org/10.1016/j.addr.2018.07.004

[5] Bar-Ephraim, Y. E., Kretzschmar, K., & Clevers, H. (2019). Organoids in immunological research. Nature Reviews Immunology. https://doi.org/10.1038/s41577-019-0248-y

[6] Polini, A., del Mercato, L. L., Barra, A., Zhang, Y. S., Calabi, F., & Gigli, G. (2019). Towards the development of human immune-system-on-a-chip platforms. Drug Discovery Today, Vol. 24, pp. 517–525. https://doi.org/10.1016/j.drudis.2018.10.003

[7] Shanti, A., Teo, J., & Stefanini, C. (2018). In vitro immune organs-on-chip for drug development: A review. Pharmaceutics, 10(4). https://doi.org/10.3390/pharmaceutics10040278

[8] Sun, W., Luo, Z., Lee, J., Kim, H. J., Lee, K. J., Tebon, P., … Khademhosseini, A. (2019). Organ-on-a-Chip for Cancer and Immune Organs Modeling. Advanced Healthcare Materials, 8(4), 1–12. https://doi.org/10.1002/adhm.201801363

[9] Shah, S. B., & Singh, A. (2017). Creating artificial lymphoid tissues to study immunity and hematological malignancies. Current Opinion in Hematology, 24(4), 377–383. https://doi.org/10.1097/MOH.0000000000000356

[10] Kim, S., Shah, S. B., Graney, P. L., & Singh, A. (2019). Multiscale engineering of immune cells and lymphoid organs. Nature Reviews Materials, 4(6), 355–378. https://doi.org/10.1038/s41578-019-0100-9

[11] Gosselin, E. A., Eppler, H. B., Bromberg, J. S., & Jewell, C. M. (2018). Designing natural and synthetic immune tissues. Nature Materials, 17(6), 484–498. https://doi.org/10.1038/s41563-018-0077-6

[12] Nosenko, M. A., Drutskaya, M. S., Moisenovich, M. M., & Nedospasov, S. A. (2016). Bioengineering of artificial lymphoid organs. Acta Naturae, 8(2), 10–23.

[13] Bello, A. B., Park, H., & Lee, S. H. (2018). Current approaches in biomaterial-based hematopoietic stem cell niches. Acta Biomaterialia, 72, 1–15. https://doi.org/10.1016/j.actbio.2018.03.028

[14] Alderfer, L., Wei, A., & Hanjaya-Putra, D. (2018). Lymphatic Tissue Engineering and Regeneration. Journal of Biological Engineering, 12(1), 1–26. https://doi.org/10.1186/s13036-018-0122-7

[15] Morrison, S. J., & Scadden, D. T. (2014). The bone marrow niche for haematopoietic stem cells. Nature, 505(7483), 327–334. https://doi.org/10.1038/nature12984

[16] Klamer, S., & Voermans, C. (2014). The role of novel and known extracellular matrix and adhesion molecules in the homeostatic and regenerative bone marrow microenvironment. Cell Adhesion and Migration, 8(6), 563–577. https://doi.org/10.4161/19336918.2014.968501

[17] Braham, M. V. J., Li Yim, A. S. P., Garcia Mateos, J., Minnema, M. C., Dhert, W. J. A., Öner, F. C., … Alblas, J. (2019). A Human Hematopoietic Niche Model Supporting Hematopoietic Stem and Progenitor Cells In Vitro. Advanced Healthcare Materials, 8(10), 1–14. https://doi.org/10.1002/adhm.201801444

[18] Zhang, P., Zhang, C., Li, J., Han, J., Liu, X., & Yang, H. (2019). The physical microenvironment of hematopoietic stem cells and its emerging roles in engineering applications. Stem Cell Research and Therapy, 10(1), 1–13. https://doi.org/10.1186/s13287-019-1422-7
[19] Raic, A., Rödling, L., Kalbacher, H., & Lee-Thedieck, C. (2014). Biomimetic macroporous PEG hydrogels as 3D scaffolds for the multiplication of human hematopoietic stem and progenitor cells. Biomaterials, 35(3), 929–940. https://doi.org/10.1016/j.biomaterials.2013.10.038
[20] Torisawa, Y. S., Spina, C. S., Mammoto, T., Mammoto, A., Weaver, J. C., Tat, T., … Ingber, D. E. (2014). Bone marrow-on-a-chip replicates hematopoietic niche physiology in vitro. Nature Methods, 11(6), 663–669. https://doi.org/10.1038/nmeth.2938
[21] Nichols, J. E., Cortiella, J., Lee, J., Niles, J. A., Cuddihy, M., Wang, S., … Kotov, N. A. (2009). In vitro analog of human bone marrow from 3D scaffolds with biomimetic inverted colloidal crystal geometry. Biomaterials, 30(6), 1071–1079. https://doi.org/10.1016/j.biomaterials.2008.10.041
[22] Shah, N. J., Mao, A. S., Shih, T.-Y., Kerr, M. D., Sharda, A., Raimondo, T. M., … Scadden, D. T. (2019). An injectable bone marrow–like scaffold enhances T cell immunity after hematopoietic stem cell transplantation. Nature Biotechnology, 37(3), 293–302. https://doi.org/10.1038/s41587-019-0017-2
[23] Di Buduo, C. A., Soprano, P. M., Tozzi, L., Marconi, S., Auricchio, F., Kaplan, D. L., & Balduini, A. (2017). Modular flow chamber for engineering bone marrow architecture and function. Biomaterials, 146(2017), 60–71. https://doi.org/10.1016/j.biomaterials.2017.08.006
[24] Rödling, L., Schwedhelm, I., Kraus, S., Bieback, K., Hansmann, J., & Lee-Thedieck, C. (2017). 3D models of the hematopoietic stem cell niche under steady-state and active conditions. Scientific Reports, 7(1), 1–15. https://doi.org/10.1038/s41598-017-04808-0
[25] Kotha, S. S., Hayes, B. J., Phong, K. T., Redd, M. A., Bomsztyk, K., Ramakrishnan, A., … Zheng, Y. (2018). Engineering a multicellular vascular niche to model hematopoietic cell trafficking. Stem Cell Research and Therapy, 9(1), 1–14. https://doi.org/10.1186/s13287-018-0808-2
[26] Bourgine, P. E., Klein, T., Paczulla, A. M., Shimizu, T., Kunz, L., Kokkaliaris, K. D., … Martin, I. (2018). In vitro biomimetic engineering of a human hematopoietic niche with functional properties. Proceedings of the National Academy of Sciences of the United States of America, 115(25), E5688–E5695. https://doi.org/10.1073/pnas.1805440115
[27] Miyoshi, H., Murao, M., Ohshima, N., & Tun, T. (2011). Three-dimensional culture of mouse bone marrow cells within a porous polymer scaffold: effects of oxygen concentration and stromal layer on expansion of haematopoietic progenitor cells. Journal of Tissue Engineering and Regenerative Medicine, 5(2), 112–118. https://doi.org/10.1002/term.295
[28] Sharma, M. B., Limaye, L. S., & Kale, V. P. (2012). Mimicking the functional hematopoietic stem cell niche in vitro: Recapitulation of marrow physiology by hydrogel-based three-dimensional cultures of mesenchymal stromal cells. Haematologica, 97(5), 651–660. https://doi.org/10.3324/haematol.2011.050500
[29] Feng, Q., Chai, C., Jiang, X.-S., Leong, K. W., & Mao, H.-Q. (2006). Expansion of engrafting human hematopoietic stem/progenitor cells in three-dimensional scaffolds with surface-immobilized fibronectin. Journal of Biomedical Materials Research Part A, 78A(4), 781–791. https://doi.org/10.1002/jbm.a.30829
[30] Shih, Y. R., Kang, H., Rao, V., Chiu, Y. J., Kwon, S. K., & Varghese, S. (2017). In vivo engineering of bone tissues with hematopoietic functions and mixed chimerism. Proceedings of the National Academy of Sciences of the United States of America, 114(21), 5419–5424. https://doi.org/10.1073/pnas.1702576114
[31] Mortera-Blanco, T., Mantalaris, A., Bismarck, A., Aqel, N., & Panoskaltsis, N. (2011). Long-term cytokine-free expansion of cord blood mononuclear cells in three-dimensional scaffolds. Biomaterials,

32(35), 9263–9270. https://doi.org/10.1016/j.biomaterials.2011.08.051
[32] Ventura Ferreira, M. S., Bergmann, C., Bodensiek, I., Peukert, K., Abert, J., Kramann, R., … Schneider, R. K. (2016). An engineered multicomponent bone marrow niche for the recapitulation of hematopoiesis at ectopic transplantation sites. Journal of Hematology and Oncology, 9(1), 1–14. https://doi.org/10.1186/s13045-016-0234-9
[33] Fang, Y., Wang, B., Zhao, Y., Xiao, Z., Li, J., Cui, Y., … Jing, Z. (2017). Collagen scaffold microenvironments modulate cell lineage commitment for differentiation of bone marrow cells into regulatory dendritic cells. Scientific Reports, 7(January), 1–12. https://doi.org/10.1038/srep42049
[34] Sieber, S., Wirth, L., Cavak, N., Koenigsmark, M., Marx, U., Lauster, R., & Rosowski, M. (2018). Bone marrow-on-a-chip: Long-term culture of human haematopoietic stem cells in a three-dimensional microfluidic environment. Journal of Tissue Engineering and Regenerative Medicine, 12(2), 479–489. https://doi.org/10.1002/term.2507
[35] Fan, Y., Tajima, A., Goh, S. K., Geng, X., Gualtierotti, G., Grupillo, M., … Trucco, M. (2015). Bioengineering thymus organoids to restore thymic function and induce donor-specific immune tolerance to allografts. Molecular Therapy, 23(7), 1262–1277. https://doi.org/10.1038/mt.2015.77
[36] Seach, N., Mattesich, M., Abberton, K., Matsuda, K., Tilkorn, D. J., Rophael, J., … Morrison, W. A. (2010). Vascularized Tissue Engineering Mouse Chamber Model Supports Thymopoiesis of Ectopic Thymus Tissue Grafts. Tissue Engineering Part C: Methods, 16(3), 543–551. https://doi.org/10.1089/ten.tec.2009.0135
[37] Tajima, A., Pradhan, I., Trucco, M., & Fan, Y. (2016). Restoration of Thymus Function with Bioengineered Thymus Organoids. Current Stem Cell Reports, 2(2), 128–139. https://doi.org/10.1007/s40778-016-0040-x
[38] Chung, B., Montel-Hagen, A., Ge, S., Blumberg, G., Kim, K., Klein, S., … Crooks, G. M. (2014). Engineering the human thymic microenvironment to support thymopoiesis in vivo. Stem Cells, 32(9), 2386–2396. https://doi.org/10.1002/stem.1731
[39] Singh, A. (2017). Biomaterials innovation for next generation ex vivo immune tissue engineering. Biomaterials, 130(2017), 104–110. https://doi.org/10.1016/j.biomaterials.2017.03.015
[40] Poznansky, M. C., Evans, R. H., Foxall, R. B., Olszak, I. T., Piascik, A. H., Hartman, K. E., … Scadden, D. T. (2000). Efficient generation of human T cells from a tissue-engineered thymic organoid. Nature Biotechnology, 18(7), 729–734. https://doi.org/10.1038/77288
[41] Tuckett, A. Z., Yang, X., Wang, L., Wang, H., van den Brink, M. R. M., & Zakrzewski, J. L. (2013). In Vivo Generation of Thymus-Independent T Cells in a Tissue-Engineered T Cell Development Supporting Microenvironment. Biology of Blood and Marrow Transplantation, 19(2), S208–S209. https://doi.org/10.1016/j.bbmt.2012.11.235
[42] Seet, C. S., He, C., Bethune, M. T., Li, S., Chick, B., Gschweng, E. H., … Montel-Hagen, A. (2017). Generation of mature T cells from human hematopoietic stem and progenitor cells in artificial thymic organoids. Nature Methods, 14(5), 521–530. https://doi.org/10.1038/nmeth.4237
[43] Hun, M., Barsanti, M., Wong, K., Ramshaw, J., Werkmeister, J., & Chidgey, A. P. (2017). Native thymic extracellular matrix improves in vivo thymic organoid T cell output, and drives in vitro thymic epithelial cell differentiation. Biomaterials, 118(2017), 1–15. https://doi.org/10.1016/j.biomaterials.2016.11.054
[44] Pinto, S., Schmidt, K., Egle, S., Stark, H.-J., Boukamp, P., & Kyewski, B. (2013). An Organotypic Coculture Model Supporting Proliferation and Differentiation of Medullary Thymic Epithelial Cells and Promiscuous Gene Expression. The Journal of Immunology, 190(3), 1085–1093. https://doi.org/10.4049/jimmunol.1201843
[45] Taqvi, S., Dixit, L., & Roy, K. (2006). Biomaterial-based notch signaling for the differentiation of hematopoietic stem cells into T cells. Journal of Biomedical Materials Research Part A, 79A(3), 689–697. https://doi.org/10.1002/jbm.a.30916

[46] Ruddle, N. H., & Akirav, E. M. (2009). Secondary Lymphoid Organs: Responding to Genetic and Environmental Cues in Ontogeny and the Immune Response. The Journal of Immunology, 183(4), 2205–2212. https://doi.org/10.4049/jimmunol.0804324
[47] Willard-Mack, C. L. (2006). Normal Structure, Function, and Histology of Lymph Nodes. Toxicologic Pathology, 34(5), 409–424. https://doi.org/10.1080/01926230600867727
[48] De Silva, N. S., & Klein, U. (2015). Dynamics of B cells in germinal centres. Nature Reviews Immunology, 15(3), 137–148. https://doi.org/10.1038/nri3804
[49] Mebius, R. E., & Kraal, G. (2005). Structure and function of the spleen. Nature Reviews Immunology, 5(8), 606–616. https://doi.org/10.1038/nri1669
[50] Dillon, A., & Lo, D. D. (2019). M cells: Intelligent engineering of mucosal immune surveillance. Frontiers in Immunology, 10(JUL), 1–13. https://doi.org/10.3389/fimmu.2019.01499
[51] Acton, S. E., & Reis e Sousa, C. (2016). Dendritic cells in remodeling of lymph nodes during immune responses. Immunological Reviews, 271(1), 221–229. https://doi.org/10.1111/imr.12414
[52] Lin, H. J., Wang, W., Huang, Y. Y., Liao, W. T., Lin, T. Y., Lin, S. Y., & Liu, D. Z. (2019). Decellularized lymph node scaffolding as a carrier for dendritic cells to induce anti-tumor immunity. Pharmaceutics, 11(11), 1–16. https://doi.org/10.3390/pharmaceutics11110553
[53] Kraus, T., Lubitz, A., Schließer, U., Giese, C., Reuschel, J., Brecht, R., … Winter, G. (2019). Evaluation of a 3D Human Artificial Lymph Node as Test Model for the Assessment of Immunogenicity of Protein Aggregates. Journal of Pharmaceutical Sciences, 108(7), 2358–2366. https://doi.org/10.1016/j.xphs.2019.02.011
[54] Purwada, A., Shah, S. B., Béguelin, W., August, A., Melnick, A. M., & Singh, A. (2019). Ex vivo synthetic immune tissues with T cell signals for differentiating antigen-specific, high affinity germinal center B cells. Biomaterials, 198, 27–36. https://doi.org/10.1016/j.biomaterials.2018.06.034
[55] Roh, K. H., Song, H. W., Pradhan, P., Bai, K., Bohannon, C. D., Dale, G., … Roy, K. (2018). A synthetic stroma-free germinal center niche for efficient generation of humoral immunity ex vivo. Biomaterials, 164, 106–120. https://doi.org/10.1016/j.biomaterials.2018.02.039
[56] Purwada, A., Jaiswal, M. K., Ahn, H., Nojima, T., Kitamura, D., Gaharwar, A. K., … Singh, A. (2015). Ex vivo engineered immune organoids for controlled germinal center reactions. Biomaterials, 63(2015), 24–34. https://doi.org/10.1016/j.biomaterials.2015.06.002
[57] Moura Rosa, P., Gopalakrishnan, N., Ibrahim, H., Haug, M., & Halaas, Ø. (2016). The intercell dynamics of T cells and dendritic cells in a lymph node-on-a-chip flow device. Lab on a Chip, 16(19), 3728–3740. https://doi.org/10.1039/c6lc00702c
[58] Pérez Del Río, E., Martinez Miguel, M., Veciana, J., Ratera, I., & Guasch, J. (2018). Artificial 3D Culture Systems for T Cell Expansion. ACS Omega, 3(5), 5273–5280. https://doi.org/10.1021/acsomega.8b00521
[59] Cheung, A. S., Zhang, D. K. Y., Koshy, S. T., & Mooney, D. J. (2018). Scaffolds that mimic antigen-presenting cells enable ex vivo expansion of primary T cells. Nature Biotechnology, 36(2), 160–169. https://doi.org/10.1038/nbt.4047
[60] Stephan, S. B., Taber, A. M., Jileaeva, I., Pegues, E. P., Sentman, C. L., & Stephan, M. T. (2015). Biopolymer implants enhance the efficacy of adoptive T-cell therapy. Nature Biotechnology, 33(1), 97–101. https://doi.org/10.1038/nbt.3104
[61] Weiden, J., Voerman, D., Dölen, Y., Das, R. K., Van Duffelen, A., Hammink, R., … Figdor, C. G. (2018). Injectable biomimetic hydrogels as tools for efficient T Cell expansion and delivery. Frontiers in Immunology, 9(NOV), 1–15. https://doi.org/10.3389/fimmu.2018.02798
[62] Suematsu, S., & Watanabe, T. (2004). Generation of a synthetic lymphoid tissue-like organoid in mice. Nature Biotechnology, 22(12), 1539–1545. https://doi.org/10.1038/nbt1039
[63] Okamoto, N., Chihara, R., Shimizu, C., Nishimoto, S., & Watanabe, T. (2007). Artificial lymph nodes induce potent secondary immune

responses in naive and immunodeficient mice. Journal of Clinical Investigation, 117(4), 997–1007. https://doi.org/10.1172/JCI30379
[64] Giese, C., Lubitz, A., Demmler, C. D., Reuschel, J., Bergner, K., & Marx, U. (2010). Immunological substance testing on human lymphatic micro-organoids in vitro. Journal of Biotechnology, 148(1), 38–45.
[65] Giese, C., Demmler, C. D., Ammer, R., Hartmann, S., Lubitz, A., Miller, L., … Marx, U. (2006). A human lymph node in vitro - Challenges and progress. Artificial Organs, 30(10), 803–808. https://doi.org/10.1111/j.1525-1594.2006.00303.x https://doi.org/10.1016/j.jbiotec.2010.03.001
[66] Seifert, M., Lubitz, A., Trommer, J., Könnig, D., Korus, G., Marx, U., … Giese, C. (2012). Crosstalk between immune cells and mesenchymal stromal cells in a 3D bioreactor system. International Journal of Artificial Organs, 35(11), 986–995. https://doi.org/10.5301/ijao.5000118
[67] Sardi, M., Lubitz, A., & Giese, C. (2016). Modeling Human Immunity In Vitro : Improving Artificial Lymph Node Physiology by Stromal Cells. Applied In Vitro Toxicology, 2(3), 143–150. https://doi.org/10.1089/aivt.2016.0004
[68] Kuzin, I., Sun, H., Moshkani, S., Feng, C., Mantalaris, A., Wu, J. H. D., & Bottaro, A. (2011). Long-term immunologically competent human peripheral lymphoid tissue cultures in a 3D bioreactor. Biotechnology and Bioengineering, 108(6), 1430–1440. https://doi.org/10.1002/bit.23055
[69] Mitra, B., Jindal, R., Lee, S., Dong, D. X., Li, L., Sharma, N., … Yarmush, M. L. (2013). Microdevice integrating innate and adaptive immune responses associated with antigen presentation by dendritic cells. RSC Advances, 3(36), 16002–16010. https://doi.org/10.1039/c3ra41308j
[70] Ross, A. E., Belanger, M. C., Woodroof, J. F., & Pompano, R. R. (2017). Spatially resolved microfluidic stimulation of lymphoid tissue: Ex vivo. Analyst, 142(4), 649–659. https://doi.org/10.1039/c6an02042a
[71] Stachowiak, A. N., & Irvine, D. J. (2008). Inverse opal hydrogel-collagen composite scaffolds as a supportive microenvironment for immune cell migration. Journal of Biomedical Materials Research Part A, 85A(3), 815–828. https://doi.org/10.1002/jbm.a.31661
[72] Tomei, A. A., Siegert, S., Britschgi, M. R., Luther, S. A., & Swartz, M. A. (2009). Fluid Flow Regulates Stromal Cell Organization and CCL21 Expression in a Tissue-Engineered Lymph Node Microenvironment. The Journal of Immunology, 183(7), 4273–4283. https://doi.org/10.4049/jimmunol.0900835
[73] Cuzzone, D. A., Albano, N. J., Aschen, S. Z., Ghanta, S., & Mehrara, B. J. (2015). Decellularized lymph nodes as scaffolds for tissue engineered lymph nodes. Lymphatic Research and Biology, 13(3), 186–194. https://doi.org/10.1089/lrb.2013.0054
[74] Petrova, T. V., & Koh, G. Y. (2018). Organ-specific lymphatic vasculature: From development to pathophysiology. Journal of Experimental Medicine, 215(1), 35–49. https://doi.org/10.1084/jem.20171868
[75] Berendam, S. J., Koeppel, A. F., Godfrey, N. R., Rouhani, S. J., Woods, A. N., Rodriguez, A. B., … Engelhard, V. H. (2019). Comparative transcriptomic analysis identifies a range of immunologically related functional elaborations of lymph node associated lymphatic and blood endothelial cells. Frontiers in Immunology, 10(MAR), 1–17. https://doi.org/10.3389/fimmu.2019.00816
[76] Dixon, J. B., Raghunathan, S., & Swartz, M. A. (2009). A tissue-engineered model of the intestinal lacteal for evaluating lipid transport by lymphatics. Biotechnology and Bioengineering, 103(6), 1224–1235. https://doi.org/10.1002/bit.22337
[77] Jiang, X., Tian, W., Nicolls, M. R., & Rockson, S. G. (2019). The Lymphatic System in Obesity, Insulin Resistance, and Cardiovascular Diseases. Frontiers in Physiology, 10(November), 1–10. https://doi.org/10.3389/fphys.2019.01402
[78] Gibot, L., Galbraith, T., Kloos, B., Das, S., Lacroix, D. A., Auger, F. A., & Skobe, M. (2016). Cell-based approach for 3D reconstruction of lymphatic capillaries in vitro reveals distinct functions of HGF and VEGF-C in lymphangiogenesis. Biomaterials, 78, 129–139. https://doi.org/10.1016/j.biomaterials.2015.11.027

[79] Hadamitzky, C., Zaitseva, T. S., Bazalova-Carter, M., Paukshto, M. V., Hou, L., Strassberg, Z., … Huang, N. F. (2016). Aligned nanofibrillar collagen scaffolds – Guiding lymphangiogenesis for treatment of acquired lymphedema. Biomaterials, 102(2016), 259–267. https://doi.org/10.1016/j.biomaterials.2016.05.040

[80] Dai, T. ting, Jiang, Z. hua, Li, S. li, Zhou, G. dong, Kretlow, J. D., Cao, W. Gang, … Cao, Y. lin. (2010). Reconstruction of lymph vessel by lymphatic endothelial cells combined with polyglycolic acid scaffolds: A pilot study. Journal of Biotechnology, 150(1), 182–189. https://doi.org/10.1016/j.jbiotec.2010.07.028

[81] Marino, D., Luginbuhl, J., Scola, S., Meuli, M., & Reichmann, E. (2014). Bioengineering Dermo-Epidermal Skin Grafts with Blood and Lymphatic Capillaries. Science Translational Medicine, 6(221), 221ra14-221ra14. https://doi.org/10.1126/scitranslmed.3006894

[82] Knezevic, L., Schaupper, M., Mühleder, S., Schimek, K., Hasenberg, T., Marx, U., … Holnthoner, W. (2017). Engineering Blood and Lymphatic Microvascular Networks in Fibrin Matrices. Frontiers in Bioengineering and Biotechnology, 5(April), 1–12. https://doi.org/10.3389/fbioe.2017.00025

[83] Ng, C. P., Helm, C. E., & Swartz, M. A. (2004). Interstitial flow differentially stimulates blood and lymphatic endothelial cell morphogenesis in vitro. Microvascular Research, 68(3), 258–264. https://doi.org/10.1016/j.mvr.2004.08.002

[84] Helm, Cara-Lynn E.; Zisch, Andreas; Swartz, M. A. (2006). Engineered Blood and Lymphatic Capillaries in 3-D VEGF-Fibrin-Collagen Matrices With Interstitial Flow. Biotechnology and Bioengineering, 96(1), 167–176. https://doi.org/10.1002/bit.21185

[85] Ivanovska, I. L., Shin, J.-W., Swift, J., & Discher, D. E. (2015). Stem cell mechanobiology: diverse lessons from bone marrow. Trends in Cell Biology, 25(9), 523–532. https://doi.org/10.1016/j.tcb.2015.04.003

[86] Barthes, J., Dollinger, C., Muller, C. B., Liivas, U., Dupret-Bories, A., Knopf-Marques, H., & Vrana, N. E. (2018). Immune assisted tissue engineering via incorporation of macrophages in cell-laden hydrogels under cytokine stimulation. Frontiers in Bioengineering and Biotechnology, 6(AUG), 1–17. https://doi.org/10.3389/fbioe.2018.00108

[87] Semo, J., Nicenboim, J., & Yaniv, K. (2016). Development of the lymphatic system: New questions and paradigms. Development (Cambridge), 143(6), 924–935. https://doi.org/10.1242/dev.132431

[88] Meng, F., Meyer, C.M., Joung, D., Vallera, D.A., McAlpine, M.C., Panoskaltsis-Mortari, A. (2019). 3D bioprinted in vitro metastatic models via reconstruction of tumor microenvironments. Advanced Materials, 31(10):e1806899. Doi:10.1002/adma.201806899.

[89] Schaupper, M., Jeltsch, M., Rohringer, S., Redl, H., & Holnthoner, W. (2016). Lymphatic Vessels in Regenerative Medicine and Tissue Engineering. Tissue Engineering - Part B: Reviews, 22(5), 395–407. https://doi.org/10.1089/ten.teb.2016.0034